Theoretical Investigation of Ion Hydration in Clusters and Solutions

Soran Jahangiri

A Thesis in

The Department of

Chemistry and Biochemistry

Presented in Partial Fulfillment of the Requirements

For the Degree of

Doctor of Philosophy (Chemistry) at

Concordia University

Montreal, Quebec, Canada

September 2013

CONCORDIA UNIVERSITY
SCHOOL OF GRADUATE STUDIES

This is to certify that the thesis prepared

By: **Soran Jahangiri**

Entitled: **Theoretical Investigation of Ion Hydration in Clusters and Solutions**

and submitted in partial fulfillment of the requirements for the degree of

DOCTOR OF PHILOSOPHY (Chemistry)

complies with the regulations of the University and meets the accepted standards with respect to originality and quality.

Signed by the final examining committee:

_____ Chair
Dr. U. Shalev

_____ External Examiner
Dr. P.-N. Roy

_____ External to Program
Dr. R. Wuthrich

_____ Examiner
Dr. A. English

_____ Examiner
Dr. G. Lamoureux

_____ Thesis Supervisor
Dr. G. Peslherbe

Approved by _____
Chair of Department or Graduate Program Director
Dr. H. Muchall, Graduate Program Director

September 19, 2013 _____
Interim Dean J. Locke, Faculty of Arts and Science

ABSTRACT

Theoretical Investigation of Ion Hydration in Clusters and Solutions

Soran Jahangiri, Ph.D.

Concordia University, 2013

The aim of this work is to develop and implement efficient theoretical approaches based on first-principles to investigate key features of ion hydration in clusters and solutions. For this purpose, the parameter set of the self-consistent-charge density-functional tight-binding (SCC-DFTB) model, an approximate version of (first-principles) density-functional theory, has been extended to include halogen atoms and used to describe the interatomic interactions in molecular dynamics (MD) simulations performed to investigate the hydration features of halides. The results of these first-principles-based simulations unambiguously demonstrate the higher affinity of the larger halides for the cluster surface, hence resolving a long-standing controversy. Given the accuracy and computational efficiency of SCC-DFTB in describing halide cluster hydration, the model was further validated against high-level quantum-chemistry data and employed to investigate ionic clusters containing the polyatomic anions of the Hofmeister series: different hydration extents were found for the anions investigated, consistent with their order in the series. For instance, kosmotropic ions, i.e. those favoring water structure, tend to adopt fully hydrated structures, while chaotropic ions, i.e. those that disrupt hydrogen-bonded water networks, tend to be expelled from the water droplet and adopt surface hydration structures. Turning our attention to cations, the hydration

behavior of alkyl diammonium of varying alkyl chain length was also investigated in clusters by MD simulations with empirical force fields validated against SCC-DFTB. In light of the increased surface propensity of longer dications found in water clusters, the relationship between the hydration extent of these ions and their effect on the salting out of organic molecules in aqueous solvent mixtures was also investigated: while fully hydrated shorter dications promote phase separation, partially hydrated longer dications have a stabilizing effect on organic aggregates in the mixture. These findings helped rationalize previous experimental data on environmentally-friendly "switchable" solvents, the design of which could be greatly assisted by further such simulations. The methodology developed, based on first-principles, not only allowed studies that helped unveil a possible relationship between the hydration extent of ions and their specific effect in solutions, but should also find a broad range of applications.

Acknowledgements

I would like to thank my supervisor, Dr. Gilles Peslherbe, for his guidance and support and the members of my research committee, Drs. Ann English and Guillaume Lamoureux, for their evaluation and advice. I am also thankful to Dr. Grygoriy Dolgonos for his valuable help and Dr. Thomas Frauenheim as well for providing me the opportunity of performing part of the work at the Bremen Center for Computational Materials Science. I am also grateful to Drs. Philip Jessop and Sean Mercer for their critical evaluation and feedback. I also wish to acknowledge the financial supports I received from Concordia University and Natural Sciences and Engineering Research Council of Canada as well as access to the computational resources from Calcul Quebec. Finally, I wish to thank my friends and colleagues at the Centre for Research in Molecular Modeling, particularly, Sima, Maria, Xijun, Chun, and Dr. Denise Koch.

Contribution of Authors

The work presented in this thesis has been performed by Soran Jahangiri and supervised by Dr. Gilles Peslherbe. The *ab initio* calculations in Chapter 4 have been performed based on the structures optimized by Lemin Cai. The molecular dynamics simulations in Chapter 6 (for clusters containing up to 40 water molecules) have been performed based on the input files and structures created by Valery Legris-Falardeau. Chapter 2 has been edited by Dr. Grygoriy Dolgonos and Chapter 7 has been edited by Drs. Philip Jessop and Sean Mercer. All Chapters have been edited by Dr. Gilles Peslherbe.

Table of Contents

List of Figures

List of Tables

Chapter 1

Introduction

1.1. Preamble

Ions are ubiquitous chemical compounds with a widespread presence ranging from the atmosphere to human cells. Because of this prevalent availability, ions are involved in many chemical processes in nature and profoundly affect a broad range of phenomena that are essential to life. In the atmosphere, ion-induced nucleation has been considered as the first step in the formation of atmospheric aerosols.[1-3] Presence of ionic groups in the structure of biological macromolecules is essential for their conformational stability and function in biological systems.[4-7] Ions play important roles in chemical separation processes, such as aqueous/organic phase separation which are broadly used in industry.[8] Effect of ions on the rate of chemical reactions in salt solutions has also been reported.[9]

In all of the systems mentioned above, despite the obvious diversity, ions exert their effects in the presence of water molecules. This is true in the sense that chemical reactions in nature mainly take place in the aqueous phase. In this respect, a comprehensive knowledge about the behavior of ions in aqueous solutions is necessary to understand the role they play in various natural phenomena.

The hydration of ions in ionic water clusters has been broadly investigated to shed light on their hydration behavior at molecular level.[10-12] In particular, inspection of the hydration properties of ions upon sequential addition of water molecules in water clusters provides insight into the relative strength of the ion–water and water–water interactions which is necessary to understand the behavior of ions in aqueous solutions. In this respect, ionic water clusters are appropriate paradigms for investigating the basic features of the hydrated ions, such as their hydration extent and their effect on the water structure, that have been used to explain the *specific effect* of ions on various properties of ionic

solutions.[13,14] Presence of ionic water clusters in the atmosphere and their role in the atmospheric reactions and formation of larger atmospheric droplets has also motivated various investigations.[2] Moreover, the hydration of model biomolecules in water clusters has been investigated to provide detailed information about the water binding sites and binding energies as well as the effect of water on the structure of biomolecules.[15,16] In this thesis, our aim is to develop, validate and apply computational models to investigate the hydration behavior of ions at molecular level.

1.2. The specific effect of ions in aqueous solutions

It has been known for long that the relative effect of ions on a variety of solution properties follows a specific trend, regardless of the properties on which ionic effects are investigated, which for anions is usually represented as follows:[17,18]

$$CO_3^{2-} > SO_4^{2-} > HPO_4^{2-} > F^- > CH_3COO^- > Cl^- > Br^- > NO_3^- > I^- > ClO_4^- > SCN^-.$$

This particular behavior of ions, which is usually referred to as the ion specific effect, was initially discovered by Franz Hofmeister and co-workers based on the effect of ions on the solubility of proteins.[19,20] Accordingly, the specific ion effect and the ranking presented above are also referred to as the Hofmeister effect and the Hofmeister series, respectively. An analogous series has been reported for cations although it has been shown that the anionic effects are usually more pronounced compared to that of cations. The specific ion effect and its underlying mechanism have attracted considerable attention in the recent years.[17]

Initial attempts at rationalizing the specific ion effect were made by relating it to the ability of hydrated ions in modulating the water structure.[21,22] According to this

mechanism, hydrated ions exert their specific effect indirectly – through water molecules – according to their ability to "enhance" or "break" the water structure. This led to the introduction of structure-maker and structure-breaker ions (also referred to as kosmotropic and chaotropic ions) which has been widely used to explain behavior of ions in aqueous solutions.[22] It should be noted that, the level at which solvated ions affect the water structure has been the subject of extensive debates in the literature.[23] In particular, Bakker and co-workers have recently reported that the effect of ions on the hydrogen-bond structure of water, beyond the first solvation shell of the ions, is negligible.[24] In this respect, detailed investigation of the effect of hydrated ions on the water structure in clusters and particularly the level at which ions affect the water structure – in the absence of bulk and counter-ion effects – might provide valuable insights into this issue.[14]

The hydration extent of ions is another factor that has been recently considered to shed light on the mechanism of the specific ion effect.[18,25] It has been shown that the direct interactions between ions and organic molecules or the immediate presence of ions at the interface are essential to explain the specific ion effects on the solubility of organic molecules and surface tension of the solvent.[26] Results of such investigations are particularly important as presence of ions at interfaces is in contradiction to the classical theories that assumes an ion-free layer of water molecules at the surface of ionic solutions.[27] However, the results of recent investigations, which were initially triggered by the computational investigations of ionic water clusters, showed that some ions are highly stabilized at aqueous interfaces and therefore might exert their specific effect – in part – from direct interactions.[28] The surface propensity of ions might also have significant consequences on their chemistry in aqueous solutions.[29] In this respect,

behavior of ions in atmospheric droplets and biological systems and also effects of ions on aqueous/organic phase separation, protein precipitation and chemical reactions might be better explained by considering their hydration extents.[17] However, despite its importance, this subject has not been comprehensively investigated. In this respect, detailed investigation of the hydration extent of various ions in water clusters might provide molecular level insights to further understand this important feature of the hydrated ions.

1.3. Experimental investigations of ionic water clusters

Extensive information about the structural, thermodynamic, and spectroscopic properties of hydrated ions has been obtained from experimental investigations of ionic water clusters. These investigations were initiated to determine the thermodynamic properties of ionic water clusters by employing mass spectrometry.[30] In this respect, experimental investigations of the ion–water equilibria in the gas phase have provided sequential hydration properties, such as free energy, enthalpy and entropy of hydration, for a broad variety of ions.[31-34] From these investigations, indirect information about the structure of ionic water clusters, in particular the hydration shells of water molecules around the ions, could be also obtained.[35]

Structural features of the ionic water clusters have been investigated experimentally by infrared (IR) spectroscopy.[10,11] In particular, such investigations provide information about the local environment of the hydrated ions by inspecting the frequency of the water O–H stretching mode. From these investigations, information about the type of hydrogen bonds (e.g. water–water, ion–water) in the clusters could be

obtained. For instance, IR spectroscopy of halide–water clusters demonstrated that the halide anions form single hydrogen bonds with water molecules.[36] Photoelectron spectroscopy has been also used to provide structural information about the water hydration shells around ions and indirect evidences about the hydration extent of ions in clusters.[37] In particular, it has been shown that doubly-charged anions such as sulfate are fully hydrated in water clusters while singly-charged anions such as nitrate are only partially hydrated at the cluster surface.[38,39]

1.4. Theoretical investigations of ionic water clusters

Theoretical methods have been broadly used to provide supplementary information to experimental results and to investigate systems for which experimental data are not available. In particular, methods based on first-principles (i.e. *ab initio* quantum-chemistry and density functional theory (DFT) methods) and empirical force fields have been employed in such investigations.

1.4.1. First-principles methods

Small ionic water clusters containing ~10 water molecules have been comprehensively investigated by *ab initio* quantum-chemistry and DFT methods. In particular, low-energy structures, stepwise hydration energies as well as spectroscopic features of a wide range of ionic water clusters have been determined from these investigations.[40-46] These methods have been also employed to describe the interatomic interactions in molecular dynamics (MD) simulations.[47,48] However, despite the expected accuracy of first-principles based methods in describing chemical systems, their respective calculations are

usually very expensive and can not be easily carried out for large systems and long simulations.

1.4.2. Empirical force fields

Empirical force fields have been also widely employed to investigate ion hydration in clusters.[28] As mentioned earlier, our current knowledge about the interfacial presence of ions is mainly originated from the results of molecular simulations and particularly those performed on ionic water clusters. Berkowitz, Dang, Peslherbe and co-workers were among the first who demonstrated that larger halide anions prefer to be asymmetrically hydrated in water clusters.[49-54] The results of these investigations were extended to solutions by Jungwirth and Tobias[55,56] and were further confirmed by experimental studies employing surface sensitive spectroscopic techniques.[57] However, the accuracy of the results obtained with these methods needs to be validated with higher level quantum-chemistry models particularly when experimental data are not available for validation.

1.4.3. The DFTB model

In light of the limitations discussed above, approximate quantum-chemistry and semiempirical methods might be considered as appropriate tools to investigate medium-sized ionic water clusters. In particular, density-functional tight-binding (DFTB) model, which is an approximate quantum-chemistry method based on density-functional theory and tight-binding method, has shown great promise in describing various chemical systems.[58]

The energy term in DFTB model is represented as:[59]

$$E^{DFTB} = \sum_{i}^{occ} \langle \Psi_i | \hat{H}_0 | \Psi_i \rangle + E^{rep} , \qquad (1.1)$$

where the Hamiltonian operator ($\hat{H}_0$) is constructed based on a reference electron density which is usually considered to be the electron density of neutral atom and the single-electron wave functions (Ψ_i) are represented as a linear combination of Slater-type orbitals and the repulsive term (E^{rep}) is considered as a sum over short range diatomic repulsion potentials.

In DFTB formalism the calculation of energy is simplifying according to the following procedure. First, only valence electrons are explicitly included in the energy calculations and the effects of core electrons are taken into account with effective potentials. Furthermore, the Hamiltonian and overlap matrix elements for any given orientation of atomic orbitals (depending on the positions of atoms in the system) are represented in terms of few reference elements (corresponding to σ, π, and δ overlaps between atomic orbitals) by using the Slater and Koster formalism.[60] In this way, the number of Hamiltonian and overlap matrix elements that need to be calculated for a system that contains s and p orbitals in the valence shell is reduced to 4 (ssσ, spσ, ppσ, ppπ). These reference elements might be obtained from DFT, one time, and tabulated for future calculations. It should be noted that in the advanced versions of the DFTB model, some extra energy terms are added to the DFTB energy to better describe atomic charge distributions.[61] The DFTB model with its recent extensions has been employed to investigate various chemical systems although the method has not yet been parameterized for all elements of the periodic table.[62]

1.5. Objectives and outline

The primary objective of this thesis is to extend, validate and apply accurate and transferable computational methods to comprehensively investigate the hydration behavior of a broad range of ions with different charge, size, and geometry with a particular attention to their surface vs. interface propensity. For this purpose, the self-consistent charge density-functional tight-binding (SCC-DFTB)[58] model with its third-order extension (DFTB3),[61] which is an approximate quantum-chemistry model based on density functional theory, will be parameterized, validated and applied to investigate the hydration of the anions of the Hofmeister series in water clusters. Furthermore, in order to provide insights into the relation between the hydration extent of ions and their specific effect in solutions, comprehensive simulations with empirical force fields will be performed to investigate the hydration of α,ω-alkyl diammonium chlorides, as model compounds, and their effects on phase separation in tetrahydrofuran/water mixture. These model systems have been particularly chosen as presence of both hydrophobic and hydrophilic domains in α,ω-alkyl diammonium cations allows systematic change of their hydration properties such that empirical force fields, which their application is necessary for the corresponding bulk simulations, are able to accurately predict their hydration behaviour. Moreover, the accuracy of the force fields employed in these simulations will be validated with results of DFTB3 simulations and experimental data.

In Chapter 2 of this thesis, the parameter set of the DFTB3 model will be extended to include halogen atoms and their interactions with oxygen and hydrogen on the basis of a standard procedure that includes generation of the parameters from DFT calculations. The new parameters will be stored in a particular format to be used by the

DFTB+ computer code[63] which is routinely used to perform DFTB3 calculations. The accuracy of the newly generated parameters in predicting geometries, atomization energies and harmonic vibrational frequency of small halogen containing molecules will be validated against results of higher level quantum-chemistry models and available experimental data. Moreover, the structural and energetic properties and also vibrational frequencies of $X^-(H_2O)_{1-4}$, (X = Cl, Br, I) clusters calculated from DFTB3 will be compared with results of high-level electron correlation quantum-chemistry calculations to examine the accuracy of the parameters in predicting the hydration properties of halide anions in small water clusters.

In Chapter 3, the DFTB3 parameters generated for halides will be used to describe interatomic interactions in MD simulations to investigate the hydration behaviour of halide anions in aqueous clusters. Replica exchange MD simulations will be performed to validate the efficiency of sampling in the simulations and selected number of results will be refined with higher order first-principles calculations for further validation. Results of this chapter could be used as a benchmark to validate results of previous computational investigations.

In Chapter 4, the accuracy of various DFTB models in predicting the hydration properties of polyatomic anions of the Hofmeister series in small water clusters will be benchmarked against high-level *ab initio* quantum-chemistry calculations. Analogous to what was mentioned earlier for halide–water clusters, the structural and energetic properties as well as vibrational frequencies of clusters containing up to 4 water molecules and each of carbonate, sulphate, hydrogen phosphate, acetate, nitrate, perchlorate and thiocyanate will be calculated by DFTB and results will be compared

with those of *ab initio* calculations. Results of this part will provide comprehensive information about the capability of DFTB models in describing anion–water interactions.

In Chapter 5, DFTB3 model will be implemented in MD simulations to investigate the hydration behaviour of the polyatomic anions of the Hofmeister series. For this purpose, accurate potential of mean force calculations will be carried out to characterize the hydration extent of the ions. It should be pointed out that our simulations will be the first comprehensive molecular simulations of these systems that are performed with a full quantum chemical description of the interatomic interactions. Accordingly, we expect our results to provide valuable insights about the factors that determine the solvation behaviour of ions in aqueous systems.

In Chapter 6, the hydration of α,ω-alkyl diammonium cations of varying alkyl chain length in water clusters will be comprehensively investigated by MD simulations to characterize their hydration extent as well as their conformational change upon hydration. For this purpose, the OPLS[64] model will be validated against *ab initio* quantum-chemistry and DFTB3 methods and experimental data and will be subsequently used to describe interatomic interactions in the simulations.

In Chapter 7, the hydration properties of alkyl diammonium chlorides in solution and their specific effect on phase separation in tetrahydrofuran/water mixtures will be investigated by MD simulations. It should be noted that the hydration extent of these ions could be accurately described by empirical force fields as quantum effects such as polarizability and charge transfer – which have been shown to be important in characterizing the hydration extent of small anions – do not play an important role. Moreover, the accuracy of the force field in predicting the tetrahydrofuran/water mixing

properties will be carefully evaluated. Results of this chapter are expected to provide insights into the relation between the hydration extent of ions and their specific effect in solutions.

Chapter 2

Parameterization of Halogens for the Density-Functional Tight-Binding Description of Halide Hydration

Published as:

S. Jahangiri, G. Dolgonos, T. Frauenheim, G. H. Peslherbe, *J. Chem. Theory Comput.*

DOI: 10.1021/ct300919h

2.1. Introduction

The hydration of ions has been the subject of extensive investigations in recent years.[12,23,28,65,66] In particular, the propensity of large and polarizable anions to locate towards air-water interfaces has garnered increasing attention and a variety of experimental and theoretical studies have shown unambiguously a systematic increase of the surface concentration of such soft anions.[13,55,57,67,68] These observations can be used to provide evidence for the molecular determinants of the behavior of solvated ions such as the specific ion effect.[22,25] This warrants a comprehensive molecular-level understanding of the underlying mechanisms that govern ion solvation.

Halogen anions, *i.e.* halides, have long been a paradigm for investigating the behavior of solvated ions,[49,52-54,69-72] as the effects of size, charge density and polarizability on the ion solvation structures, the ion-solvent interactions and the spectroscopic signature of hydrogen bonding can be investigated comparatively across the halide series. The presence of halides in atmospheric droplets or clouds over the marine boundary layer has also motivated a large body of experimental and theoretical investigations.[28,57,68] In this respect, electronic structure theory methods can be used to investigate ion-solvent interactions through accurate evaluation of structural, energetic, and spectroscopic properties of halide-containing water clusters. However, application of these methods, and in particular the high-level electron correlation ones, is restricted to small systems because of high computational cost. As an alternative, semiempirical and approximate methods with affordable computational costs could be used to overcome this deficiency and to facilitate electronic structure calculations for larger systems.

Accordingly, the development and validation of practical approximate methods are essential to extend the applicability of theoretical investigations to larger systems.

The density-functional tight-binding (DFTB) model[59] is an approximate method based on density-functional theory (DFT) and the tight-binding method with a computational cost up to 3 orders of magnitude lower than that of conventional DFT.[73] Therefore, the efficiency of the DFTB model makes it an appropriate approach for investigating systems for which DFT and *ab initio* quantum-chemistry calculations are prohibitively time-consuming. Similarly to semi-empirical molecular orbital methods, this efficiency is achieved by considering explicitly only the valence electrons in the system and by evaluating Hamiltonian and overlap matrix elements as predetermined parameterized quantities. But in contrast to most semi-empirical methods, matrix elements are not considered as adjustable parameters and are evaluated directly from reference DFT calculations for each pair of atoms as a function of interatomic distance. The main advantage of this approach lies in the generation of parameters that are not dependent on reference systems used as a basis for parameterization and are presumably more transferable. It has been shown that for systems containing atoms with different electronegativities the accuracy of the DFTB model is significantly improved by adjusting atomic charge distributions through adding a self-consistent-charge term to the DFTB energy.[58] DFTB and its self-consistent-charge version (often referred to as DFTB2) have been successfully applied to various systems and the validity of the model in predicting structural and energetic properties as well as vibrational frequencies has been previously demonstrated.[74-82] Moreover, DFTB2 has been further extended to a

model known as DFTB3 that even better describes systems containing charged species.[61,83]

In this work, DFTB2 and DFTB3 parameters have been generated for the description of H−X and O−X (X = Cl, Br, I) interactions, following a procedure that has revealed highly successful before for systems containing organic and biological molecules,[58,61,83,84] zinc,[85] titanium,[86] cadmium, selenium, tellurium,[87] and boron,[88] amongst other works of similar scope. The accuracy of the newly parameterized model has been validated for selected systems and properties against results of DFT and *ab initio* quantum-chemistry calculations. Particular attention was paid to the equilibrium geometries, atomization energies and harmonic vibrational frequencies of hydrogen halides and halogen oxoacids, as well as the geometries, binding energies and vibrational frequencies of halide-containing water clusters. The outline of this article is as follows: the computational methodology and the details of the parameterization are given in Section 2.2, the results obtained with the newly parameterized model for halogen-containing molecules and halide-water clusters are presented and discussed in Section 2.3, and concluding remarks follow in Section 2.4.

2.2. Computational methodology

2.2.1. DFTB models

The expansion of the DFT energy in terms of charge density fluctuations over a reference electron density is the basic framework of various DFTB models. The reference density is chosen as the localized (or compressed) electron density of neutral atoms in order to

mimic the behavior of interacting atoms in molecular (or periodic) systems, for which atomic densities expand to a lesser extent than for isolated atoms. Based on this framework, the standard DFTB energy is obtained from a zeroth-order expansion as:[74]

$$E^{DFTB0} = \sum_{i}^{occ} \langle \Psi_i | \hat{H}_0 | \Psi_i \rangle + E_{rep} \,, \tag{2.1}$$

where the first term is the so-called band-structure energy, which is the sum over one-electron orbital energies given a reference Kohn-Sham Hamiltonian $\hat{H}_0$, and the second term represents the repulsion energy. The DFTB2 energy is constructed by expanding the DFT energy up to second-order, which amounts to adding a self-consistent charge correction:[58]

$$E^{DFTB2} = E^{DFTB0} + E^{2nd\ order} = E^{DFTB0} + \frac{1}{2}\sum_{ab} \Delta q_a \Delta q_b \gamma_{ab} \,, \tag{2.2}$$

where Δq_A and Δq_B are induced atomic charges derived from Mulliken charges that are solved for self-consistently and γ_{ab} is a function of chemical hardness. The DFTB3 model is obtained by including a third order term to the energy expansion:[61]

$$E^{DFTB3} = E^{DFTB2} + E^{3rd\ order} = E^{DFTB2} + \frac{1}{3}\sum_{ab} \Delta q_a^2 \Delta q_b \Gamma_{ab} \,, \tag{2.3}$$

where Γ_{ab} represents the change of γ_{ab} with respect to charge.

The one-electron orbital energies in equation 2.1 are obtained by solving Kohn-Sham equations ($\hat{H}_0 \Psi_i = \varepsilon_i \Psi_i$) in which each orbital Ψ_i is represented as a linear combination of pseudoatomic Slater-type basis functions initially optimized from DFT calculations using an effective potential augmented by a harmonic term of the form $(r/r_0)^n$ to compress the orbitals on the nucleus.[58,59] The exponent *n* is usually chosen as 2 and the radius r_0 taken as twice the covalent radius (r_c) for all atom types.[89] Along with

the optimized exponents of the Slater-type functions, such DFT calculations also provide reference atomic electron densities, which are used in the effective potential of the Hamiltonian $\hat{H}_0$, making the Kohn-Sham equations no longer iterative in the DFTB model (but not in the DFTB2 and DFTB3 versions since the Hamiltonian is modified to account for the induced charges). The Hamiltonian and overlap matrix integrals in the localized atomic basis are evaluated as a function of interatomic distance for each pair of atom types, and the Slater-Koster formalism[60] allows to restrict their evaluation to a limited number of specific orientations of atomic orbitals. Such calculations are performed once and the resulting values are tabulated so that these quantities can be simply evaluated by interpolation of the tabulated data in future calculations.

The repulsion term is represented as a sum over pair-wise, short-range, diatomic repulsion potentials.[74] These potentials are calculated as a function of interatomic distance by subtracting the electronic DFTB energy from the DFT energy for any type of atom pair. Similarly to the Hamiltonian and overlap matrix elements, reference diatomic repulsion potentials are evaluated once and tabulated for future calculations. The evaluation of repulsion potentials from DFT calculations compensates (at least in part) for the errors due to the approximations made in evaluating the DFTB electronic energies.

As mentioned earlier, the second-order term in equation 2.2 is obtained from the calculation of Mulliken atomic charges of two interacting atoms in a self-consistent manner. The γ_{ab} function in equation 2.2 represents the extent of charge interaction as a function of distance and can be formulated by assuming the following two limits.[58,61] At long distances, the charge interaction can be considered as a Coulomb interaction

between two separated point charges, which makes the γ_{ab} function simply the inverse of the distance between the charges. At zero distance, the γ_{ab} function represents the self-interaction and can be approximately related to the second-order derivative of the energy with respect to the occupation number of the highest occupied atomic orbital, the so-called Hubbard parameter, which is related to the ionization potential and the electron affinity. Based on these two limits, and assuming an exponential decay for charge densities, an analytical expression has been obtained for γ_{ab} as a function of interatomic distance, which depends on the Hubbard parameter of each atom.[58] The values of the Hubbard parameters can be calculated by DFT for each atom type and tabulated together with the matrix elements and diatomic repulsion potentials. It should be noted that inclusion of a modified γ_{ab} function for H−X interactions (γ^h) leads to a better description of hydrogen bond energies.[90,91]

In DFTB3, the dependence of the γ_{ab} function on atomic charges is also taken into account by introducing the Γ_{ab} function, $\Gamma_{ab} = \partial\gamma_{ab} / \partial q_a |_{q_a^0}$. The latter can be obtained from the chain rule as the product of the derivative of the γ_{ab} function with respect to the Hubbard parameter $(\partial\gamma_{ab} / \partial U_a)$ and the derivative of the Hubbard parameter with respect to charge $(\partial U_a / \partial q_a)|_{q_a^0}$.[61] The former term is obtained analytically and the latter one, which represents the third order derivative of the total atomic energy with respect to charge, is calculated from the values of the Hubbard parameter obtained in different charged states.[61] Inclusion of the third-order energy term allows a better treatment of systems containing negatively charged ions.[61,83]

In summary, the parameterization of DFTB involves calculating and tabulating the reference matrix elements and pair-wise repulsion terms as a function of interatomic distance for any desired pair of atom types. In this way the DFTB model is solely parameterized on the basis of DFT data without including any adjustable empirical parameter.

2.2.2. Computational details

Reference electron densities and pseudoatomic wave functions have been obtained by solving atomic Kohn-Sham equations with the Perdew, Burke and Ernzerhof (PBE)[92] exchange-correlation functional. As mentioned earlier, the effective potential also includes a $(r/r_0)^2$ term where the choice of r_0 is based on the covalent radius of each atom type. In this work, two different values of r_0 were used for generating reference densities and optimizing basis functions, in agreement with the procedure previously implemented to obtain the *parameters for **m**aterials and b**io**logical systems (MIO)* [58]and *DFTB**3** parameters for **o**rganic and **b**iological applications (3OB)*.[83] The oxygen and hydrogen radii were chosen as those used to generate the MIO and 3OB parameters and analogous criteria were employed for generating the halogen radii. However, the latter were slightly adjusted to better reproduce the energy gap between the highest occupied and the lowest unoccupied atomic orbitals predicted by DFT calculations with the hybrid exchange-correlation functional of PBE and Adamo.[92,93] The resulting r_0 values for halogen atoms are $8r_c$ and $1.5r_c$ for generating the reference densities and optimizing the basis functions, respectively, which are within the range employed in earlier works.[88] It should be noted that the choice of the confinement radii does not have a significant

influence on the resulting molecular properties, as pointed out in earlier investigations.[89] The Hamiltonian and overlap matrix elements have been obtained by considering an *s* orbital for hydrogen, *s* and *p* orbitals for oxygen and *s*, *p* and *d* orbitals for halogen atoms. The diagonal elements of the Hamiltonian matrix are the eigenvalues of the Hamiltonians for the free atoms and the off-diagonal elements are obtained from a two-center approximation.[58] The Hubbard derivatives were found to be –0.06, –0.05 and –0.04 au for chlorine, bromine and iodine, respectively, and the adjustable parameter of the γ^h function was set to 4.0 for consistency with the 3OB set.[83]

Pairwise repulsion potentials have been obtained on the basis of DFT results obtained with the Becke 3-parameter Lee-Yang-Parr (B3LYP)[94-96] functional for X_2, HX and HOX molecules as reference systems for characterizing X−X, H−X and O−X interactions (X = Cl, Br, I), respectively. The DFTB2 parameterization was performed on the basis of all-electron basis set reference data obtained with the 6-31G(d) basis set for chlorine[97] and bromine[98] containing molecules and the 6-311G(d) basis set for iodine[99-101] containing molecules to keep the parameters consistent with the MIO[58] set developed previously. A larger basis set was found to be necessary to describe the highly polarizable iodine. The DFTB3 parameters were obtained on the basis of reference data obtained with the cc-pVTZ[102] basis set for consistency with the 3OB[83] set developed more recently. For systems containing bromine and iodine, effective core potentials (cc-pVTZ-PP basis set)[100,101,103,104] were used to partially include relativistic effects. However, it should be noted that previous investigations[105,106] of heavier halide hydration have employed all-electron basis set methods, since relativistic effects appear unimportant for these systems.

In order to predict accurate bond dissociation energies, the resulting repulsion curves have been adjusted by shifting them up to reproduce the DFT bond dissociation energies for the reference systems.[86] The shifted curves were then exponentially extended to zero. For H−X interactions, instead of using such exponentially decaying functions, repulsion curves were connected to the tail of the curve obtained for the $X^-(H_2O)$ system. A similar procedure was originally employed for carbon-carbon interactions where different molecules with different bond orders were used to generate different regions of the carbon-carbon repulsion curve.[89]

All PBE calculations used to generate the reference electron densities and optimizing the basis functions, as well as generating Hamiltonian and overlap matrix elements, were performed with an in-house code called Twocnt. The DFTB+ code[63] was used for DFTB calculations, while all DFT and *ab initio* quantum-chemistry calculations were performed using the Gaussian09 suite of programs. The conjugate-gradient method (with a force threshold of 10^{-5} au) was used for DFTB geometry optimizations, and all necessary parameters for hydrogen and oxygen were taken from the MIO-1-1[58] and 3OB-1-1 sets.[83] Atomization energies (AEs) were calculated for halogen-containing molecules as the difference between the energy of the molecule and the sum of those of its dissociated atoms. All values were corrected for zero-point energy. The reference halogen, oxygen and hydrogen atoms were considered as spin-polarized systems in DFTB calculations[107] (the respective spin constants for halogen atoms are listed in Table S1 of the Supporting Information) and the corresponding DFT calculations were performed within the unrestricted-spin formalism (UB3LYP). All *ab initio* quantum-chemistry calculations for halide–water clusters were performed with frozen-core second-

order Møller-Plesset (MP2) theory[108] using Dunning's correlation-consistent aug-cc-pVTZ basis set for chlorine[102] and the aug-cc-pVTZ-PP basis set for bromine[103] and iodine.[100,101,104] Stepwise binding energies of halide-water clusters were calculated as:

$$\Delta E_{n,n-1} = E[X^-(H_2O)_n] - E[X^-(H_2O)_{n-1}] - E[H_2O], \quad (2.4)$$

where $E[\ ]$ denotes the total energy of the species in brackets. All DFT and *ab initio* cluster binding energies were further corrected for basis set superposition error (BSSE) using the counterpoise procedure of Boys and Bernardi.[109] We note that such corrections can not be properly implemented in DFTB calculations, which employ predetermined matrix elements to calculate energies. However, since the model employs a minimal basis set of localized function to construct the molecular wave function, DFTB is not expected to suffer from BSSE. Moreover, inclusion of a modified γ_{ab} function with an empirical adjustable parameter for hydrogen-bonded systems might also partially compensate for BSSE in evaluating cluster binding energies.

2.3. Results and discussion

In order to validate the accuracy of the newly generated DFTB parameters and benchmark their reliability for investigating halide hydration, structural, energetic and vibrational properties have been calculated for small covalent molecules containing halogen atoms and water clusters containing halides, and the results have been compared with those predicted by DFT and with available experimental data. Cluster properties have also been compared with the results of high-level MP2 calculations. In the following, the discussion will focus primarily on DFTB3 results, with reference to DFTB2 results occasionally for comparison.

2.3.1. Covalent systems

A test set of 18 molecules, namely X_2, HX and HXO_{1-4} (X = Cl, Br, I), has been examined. The structures of the molecules are shown in Figure 2.1, while selected geometrical and energetic properties are collected in Tables 1.1 to 1.3 for each molecule, and all molecular vibrational frequencies (reported in more detail as Supporting Information in Tables S2 to S4) are compared in Figure 2.2.

2.3.1.1. Chlorine-containing molecules

All optimized DFTB3 molecular geometries for chlorine-containing molecules coincide with their DFT counterparts (*cf.* Figure 2.1), with the exception of $HClO_3$ which exhibits some slight differences. The DFTB3 energy difference between the $HClO_3$ DFT-optimized structure and the global-minimum-energy structure is only 3.8 kcal/mol, which is negligible in light of the energetics discussed below. Inspection of Table 2.1 indicates that DFTB3 bond lengths are accurately predicted compared to DFT and experimental values. Generally, DFTB3 Cl−O single-bond lengths are larger than their DFT counterparts (with a maximum absolute deviation of 0.053 Å obtained for $HClO_3$), whereas DFTB3 Cl=O double-bond lengths are usually smaller than their DFT counterparts (by no more than 0.02 Å). Similarly, calculated Cl−O−H bond angles are also overestimated by DFTB3, with an average deviation of about 7–9° from reference DFT and experimental values.

As for the energetics of bond breaking, DFTB3 reproduces the Cl_2, HCl and HOCl AEs predicted by DFT, which are underestimated relative to experimental data. This is not

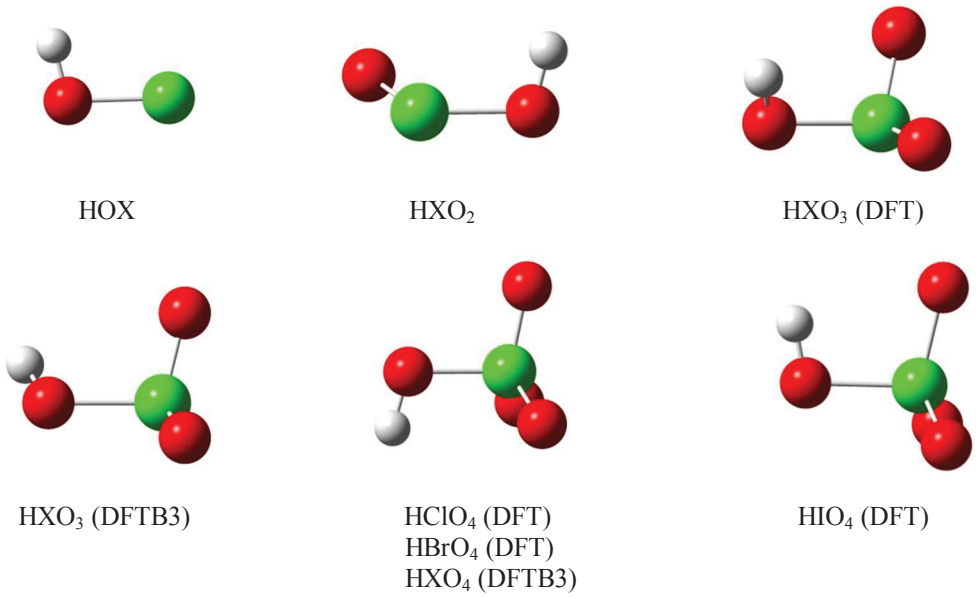

Figure 2.1. Optimized structures of HXO_{1-4} (X = Cl, Br, I) molecules.

surprising, since this DFT data is the basis for the parameterization of DFTB3. In the larger $HClO_{2-4}$ molecules, the deviations of the AEs increase by about 20 kcal/mol per additional Cl=O bond, most likely reflecting the fact that the chlorine-oxygen DFTB3 repulsion profile was mostly parameterized on the basis of Cl−O single-bond data and, as a result, Cl=O double bonds are described less accurately by the model.

Harmonic vibrational frequencies, as they reflect the curvature of the potential energy surface (PES) around the equilibrium geometry, are typically more sensitive to the description of interatomic interactions than the molecular geometry or the energy itself. In general, when compared to DFT values, the frequencies of the Cl−Cl and Cl−H bond stretching modes are accurately predicted by DFTB3 whereas those of the Cl−O and Cl=O stretching modes tend to be moderately underestimated, especially for the larger

Table 2.1. Selected geometric and energetic properties of various chlorine compounds

Molecule		DFTB3	DFT[a]	Exp.
		Bond length (Å)		
Cl_2	Cl−Cl	2.025	2.024	1.988[b]
HCl	Cl−H	1.278	1.283	1.275[b]
HOCl	Cl−O	1.711	1.710	1.689[c]
$HClO_2$	Cl−O	1.723	1.730	
	Cl=O	1.504	1.524	
$HClO_3$	Cl−O	1.790	1.737	
	Cl=O	1.450, 1.463	1.459, 1.467	
$HClO_4$	Cl−O	1.730	1.684	1.64[d]
	Cl=O	1.437, 1.451 (2)	1.430, 1.440 (2)	1.404, 1.414 (2)[d]
Δ (DFT)[e]		0.9		
Δ (Exp.)		2.3	1.7	
		Bond angle (°)		
HOCl	Cl−O−H	109.8	102.8	103.1[c]
$HClO_2$	Cl−O−H	112.5	103.9	
$HClO_3$	Cl−O−H	112.3	103.0	
$HClO_4$	Cl−O−H	114.0	104.7	
Δ (DFT)		8.2		
Δ (Exp.)		6.5	0.3	
		AE (kcal/mol)		
Cl_2		53.1	53.1	57.2[f]
HCl		100.0	100.1	102.2[f]
HOCl		150.5	152.9	156.3[f]
$HClO_2$		202.2	181.9	
$HClO_3$		279.7	235.7	
$HClO_4$		346.4	277.0	
Δ (DFT)		9.4		
Δ (Exp.)		4.3	3.8	

a) B3LYP/cc-pVTZ. b) From Ref. 110. c) From Ref. 111. d) From Ref. 112. e) Δ is the absolute mean deviation of DFTB3 data from reference data in parentheses in %. f) From Ref. 113.

$HClO_{3-4}$ molecules (*cf.* Table S2). The calculated DFTB3 frequencies correlate well with the DFT values, as shown in Figure 2.2; with the exception of a very few outliers, DFTB3 underestimates frequencies by *ca.* 10 % on average.

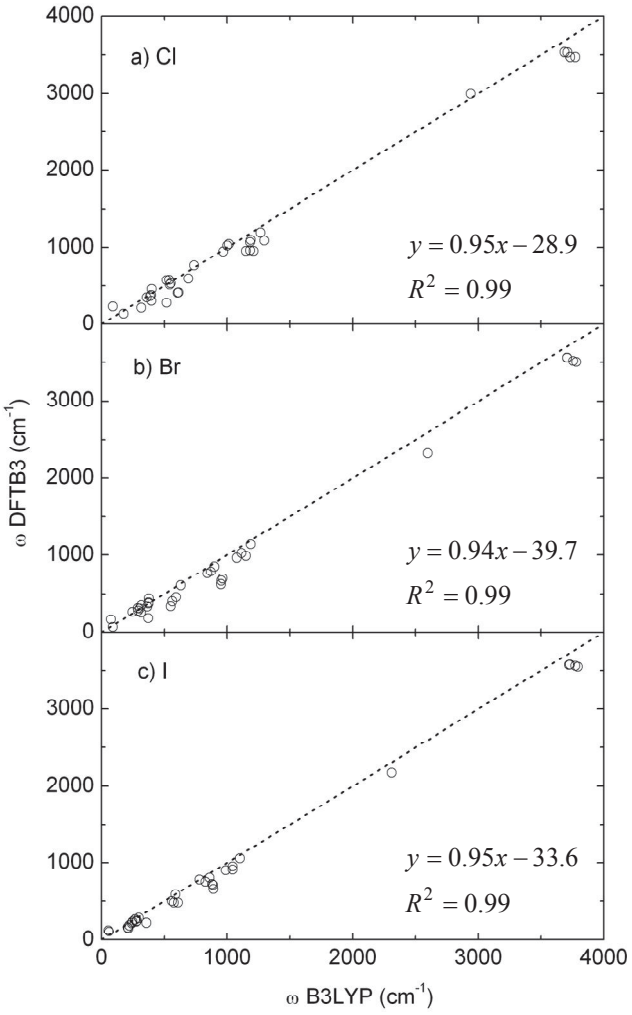

Figure 2.2. Calculated harmonic vibrational frequencies for halogen-containing compounds.

2.3.1.2. Bromine-containing molecules

Similar to chlorine-containing systems, molecular shapes of optimized DFTB3 structures of bromine-containing molecules agree well with those from DFT (*cf.* Figure 2.1), except for $HBrO_3$, for which the H atom rotates around the Br−O bond. DFTB3 predicts an asymmetric structure for $HBrO_3$ which differs from the DFT-optimized structure by 5.9 kcal/mol. Similar to the chlorine case, DFTB3 bond lengths are in good agreement with DFT and experimental values in most cases (*cf.* Table 2.2). DFTB3 maximum absolute

Table 2.2. Selected geometric and energetic properties of various bromine compounds

Molecule		DFTB3	DFT[a]	Exp.
		Bond length (Å)		
Br_2	Br−Br	2.335	2.316	2.281[b]
HBr	Br−H	1.423	1.425	1.414[b]
HOBr	Br−O	1.830	1.846	1.834[c]
$HBrO_2$	Br−O	1.860	1.859	
	Br=O	1.600	1.668	
$HBrO_3$	Br−O	1.890	1.847	
	Br=O	1.551, 1.569	1.616, 1.620	
$HBrO_4$	Br−O	1.873	1.807	
	Br=O	1.533, 1.551 (2)	1.597, 1.605 (2)	
Δ (DFT)[d]		2.4		
Δ (Exp.)		1.1	1.0	
		Bond angle (°)		
HOBr	Br−O−H	111.0	103.1	102.3[c]
$HBrO_2$	Br−O−H	113.8	104.8	
$HBrO_3$	Br−O−H	114.6	104.9	
$HBrO_4$	Br−O−H	115.4	105.6	
Δ (DFT)		8.7		
Δ (Exp.)		8.5	0.8	
		AE (kcal/mol)		
Br_2		48.5	47.9	45.5[e]
HBr		87.6	87.2	86.6[e]
HOBr		148.3	150.6	150.2[e]
$HBrO_2$		205.5	183.1	
$HBrO_3$		282.5	238.2	
$HBrO_4$		340.0	266.1	
Δ (DFT)		10.3		
Δ (Exp.)		3.0	2.1	

a) B3LYP/cc-pVTZ-PP. b) From Ref. 110. c) From Ref. 114. d) Δ is the absolute mean deviation of DFTB3 data from reference data in parentheses in %. e) From Ref. 113.

deviations for Br−O and Br=O bond lengths are 0.066 Å and 0.068 Å (observed for $HBrO_4$ and $HBrO_2$), respectively. DFTB3 bond angles are overestimated by about 9° relative to DFT and experimental values, which is comparable to the deviations observed for chlorine-containing compounds.

The DFTB3 AEs of Br_2, HBr and HOBr are in a good agreement with DFT and experimental values. As for the $HBrO_{2\text{-}4}$ molecules, DFTB3 predicts AEs that are

increasingly overestimated, presumably because of the growing number of Br=O bonds poorly described by the model, as was observed for chlorine.

The DFTB3 frequencies of the Br−Br and Br−H vibrations are underestimated relative to DFT values (Table S3), with deviations larger than those observed in the corresponding chlorine-containing molecules, but the magnitude of the deviations in the Br−O and Br=O stretching and bending frequencies are comparable to their counterparts for $HClO_{1-4}$ molecules in most cases. In general, DFTB3 frequencies correlate well with DFT values, as shown in Figure 2.2. Overall the average deviation of DFTB3 frequencies is about 10 % after exclusion of a few outliers.

2.3.1.3. Iodine-containing molecules

The DFTB3 optimized geometries of iodine-containing molecules follow the same trend in molecular shapes that has been observed in the case of bromine-containing molecules, including the differences in the optimized HIO_3 structure with the DFT one due to rotation of the O−H bond around the single iodine-oxygen bond (*cf.* Figure 2.1). DFTB3 predicts a HIO_3 structure which differs in energy by 3.8 kcal/mol from the DFT-optimized one. DFTB3 also predicts the HIO_4 DFT-optimized structure to be a transition state with an imaginary frequency of 167i cm^{-1}, lying only 0.2 kcal/mol above the minimum. This finding indicates that the DFTB3 PES is relatively flat along the direction towards the minimum-energy structure. The DFTB3 bond lengths and angles of iodine-containing molecules are also in good agreement with the reference data (*cf.* Table 2.3). The maximum absolute deviation relative to DFT is 0.084 Å for I−O, while the maximum deviation for I=O is only 0.029 Å, both in HIO_4. Deviations in bond angles

Table 2.3. Selected geometric and energetic properties of various iodine compounds

Molecule		DFTB3	DFT[a]	Exp.
		Bond length (Å)		
I_2	I−I	2.698	2.702	2.666[b]
HI	I−H	1.624	1.621	1.609[b]
HOI	I−O	2.020	2.015	1.987[c]
HIO_2	I−O	2.036	2.001	
	I=O	1.840	1.835	
HIO_3	I−O	2.042	1.974	
	I=O	1.808, 1.818	1.789, 1.790	
HIO_4	I−O	2.026	1.942	
	I=O	1.795, 1.808 (2)	1.779 (2), 1.785	
Δ (DFT)[d]		1.4		
Δ (Exp.)		1.3	1.2	
		Bond angle (°)		
HOI	I−O−H	111.0	104.4	103.9[c]
HIO_2	I−O−H	113.9	106.9	
HIO_3	I−O−H	114.5	108.3	
HIO_4	I−O−H	115.9	106.9	
Δ (DFT)		6.8		
Δ (Exp.)		6.8	0.5	
		AE (kcal/mol)		
I_2		42.8	42.7	35.6[e]
HI		74.8	74.6	70.4[e]
HOI		148.0	150.4	
HIO_2		200.5	191.0	
HIO_3		268.3	257.0	
HIO_4		316.2	290.5	
Δ (DFT)		3.4		
Δ (Exp.)		13.2	13.0	

a) B3LYP/cc-pVTZ-PP. b) From Ref. 110. c) From Ref. 115. d) Δ is the absolute mean deviation of DFTB3 data from reference data in parentheses in %. e) From Ref. 113.

within 7° are observed, relative to DFT and experimental data, which are smaller than those observed for chlorine- and bromine-contained molecules.

The DFTB3 AEs for I_2, HI and HOI are in good agreement with DFT values. For larger $HIO_{2\text{-}4}$ molecules, deviations in the AE of about 6–10 kcal/mol are observed upon addition of I=O bonds, which are less than those observed for chlorine- and bromine-containing molecules.

DFTB3 underestimates the frequency of the I−I and I−H stretching modes relative to DFT and experimental values (Table S4). The frequencies of the I−O and I=O stretching modes are mostly underestimated by DFTB3 relative to DFT values, with deviations increasing in larger molecules. However, the I−O stretching frequencies are better reproduced by DFTB3, compared to the Cl−O ones. As depicted in Figure 2.2, a fairly good correlation was found between the DFTB3 harmonic frequencies of the iodine systems under consideration and those from DFT. Overall, the average deviation of DFTB3 frequencies is about 10 % with respect to reference DFT values with the exception of a few points.

2.3.2. Halide–water clusters

Halide-water clusters containing each of the halides and up to four water molecules have been considered as a test set. All the minimum-energy cluster structures predicted by *ab initio* quantum-chemistry and shown in Figure 2.3 are correctly reproduced by DFTB3 (and all have the same geometrical arrangement of water molecules around the ion regardless of the halide). DFTB3 reference hydrogen-bond lengths and angles are presented in Tables 1.4 to 1.6, stepwise binding energies are plotted in Figure 2.4, ion-water potential energy curves are compared in Figure 2.5, selected harmonic vibrational frequencies are presented in Table 2.7 and all frequencies are compared to reference data in Figure 2.6, while atomic partial charges are presented in Table 2.8.

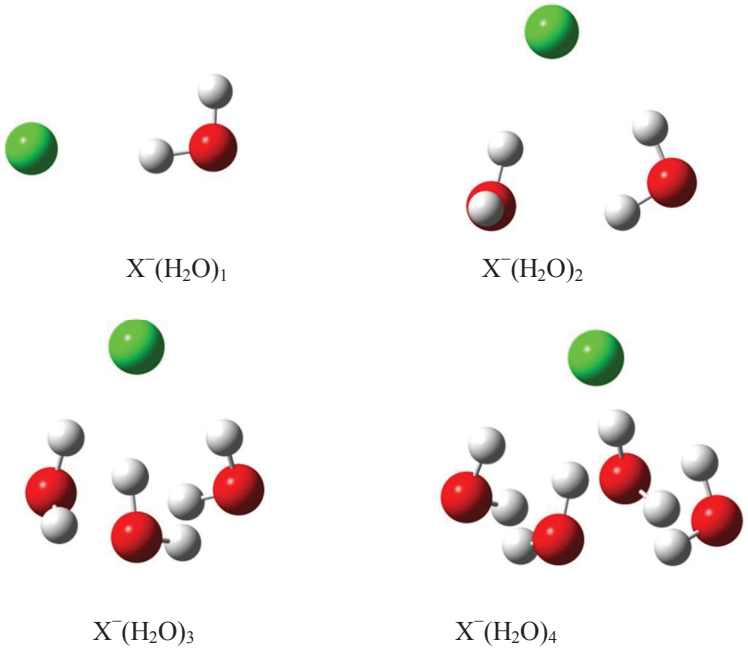

Figure 2.3. Optimized structures of $X^-(H_2O)_{1\text{-}4}$ clusters (X = Cl, Br, I).

2.3.2.1. Chloride–water clusters

The results of Table 2.4 indicate that DFTB3 underestimates bond lengths in all cases, with average deviations of 0.103 and 0.044 Å relative to DFT and *ab initio* values, respectively. Bond angles are in better agreement with DFT values, with deviations of about 7°, but are underestimated by about 11° compared to *ab initio* ones. These observations are in accord with the general tendency of DFTB models to predict short hydrogen bond lengths,[89] which has also been observed for other types of water clusters.[61]

DFTB3 stepwise cluster binding energies are in good agreement with reference data with average deviations of 1.1 and 0.3 kcal/mol relative to DFT and to *ab initio* values, respectively, and are consistent with similar data for singly-charged anion-water clusters. Interestingly, DFTB3 binding energies reproduce the trend of *ab initio* data

Table 2.4. Hydrogen-bonding geometrical characteristics of chloride–water clusters

Cluster	DFTB3	DFT[a]	*ab initio*[b]
	Bond length (Å)		
$Cl^-(H_2O)_1$	2.057	2.160	2.116
$Cl^-(H_2O)_2$	2.033	2.141	2.097
	2.303	2.365	2.294
$Cl^-(H_2O)_3$	2.218	2.332	2.266
$Cl^-(H_2O)_4$	2.296	2.423	2.335
Δ (DFT)[c]	4.5		
Δ (*ab initio*)	2.0	2.8	
	Bond angle (°)		
$Cl^-(H_2O)_1$	156.9	164.5	168.8
$Cl^-(H_2O)_2$	156.0	163.2	168.0
	145.6	153.6	156.1
$Cl^-(H_2O)_3$	145.0	152.0	154.4
$Cl^-(H_2O)_4$	141.0	148.6	151.7
Δ (DFT)	4.8		
Δ (*ab initio*)	6.8	2.1	

a) B3LYP/cc-pVTZ. b) MP2/aug-cc-pVTZ. c) Δ is the absolute mean deviation of DFTB3 data from reference data in parentheses in %.

better than that predicted by DFT (*cf.* Figure 2.4), presumably due to the good agreement between DFTB3 and *ab initio* Cl···H bond lengths, while DFT tends to overestimate Cl···H bond lengths relative to *ab initio* values. As for binding energies, the DFTB2 model underestimates the *ab initio* values by about 2 kcal/mol. The improvement in the energetics in DFTB3 model might be due to the better performance of this model in describing interatomic charge transfer, as shown from the data in Table 2.8, where charge distributions are seen to converge towards *ab initio* ones sequentially as one turns on the hydrogen bond and third order corrections. The chloride-water potential energy curve shown in Figure 2.5a further reflects the good agreement between DFTB3 and *ab initio* energetics.

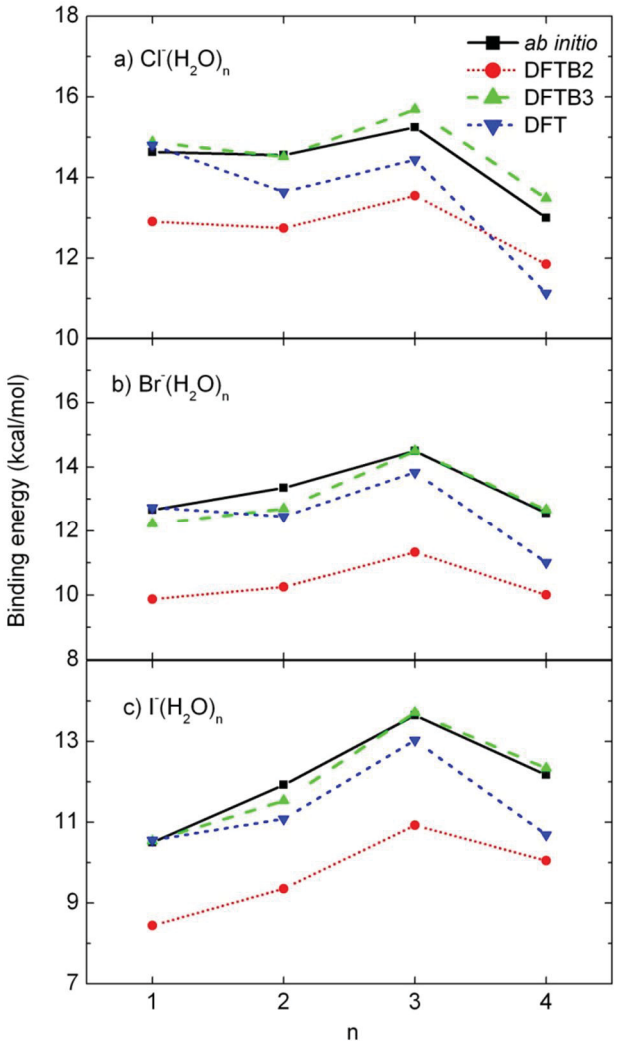

Figure 2.4. Stepwise binding energies of $X^-(H_2O)_n$ clusters (X = Cl, Br, I). *ab initio* = MP2/aug-cc-pVTZ for $Cl^-(H_2O)_{1\text{-}4}$ and MP2/aug-cc-pVTZ-PP for $Br^-(H_2O)_{1\text{-}4}$ and $I^-(H_2O)_{1\text{-}4}$.; DFT = B3LYP/cc-pVTZ for $Cl^-(H_2O)_{1\text{-}4}$ and B3LYP/cc-pVTZ-PP for $Br^-(H_2O)_{1\text{-}4}$ and $I^-(H_2O)_{1\text{-}4}$.

As shown in Figure 2.3, the global minimum structure in $Cl^-(H_2O)_1$ is asymmetric with only one semi-linear hydrogen bond. This asymmetric structure, which has been confirmed experimentally,[36] is correctly reproduced by DFTB3. Results in Table 2.7 indicate that the DFTB3 frequency of the free O−H stretch lies almost halfway between

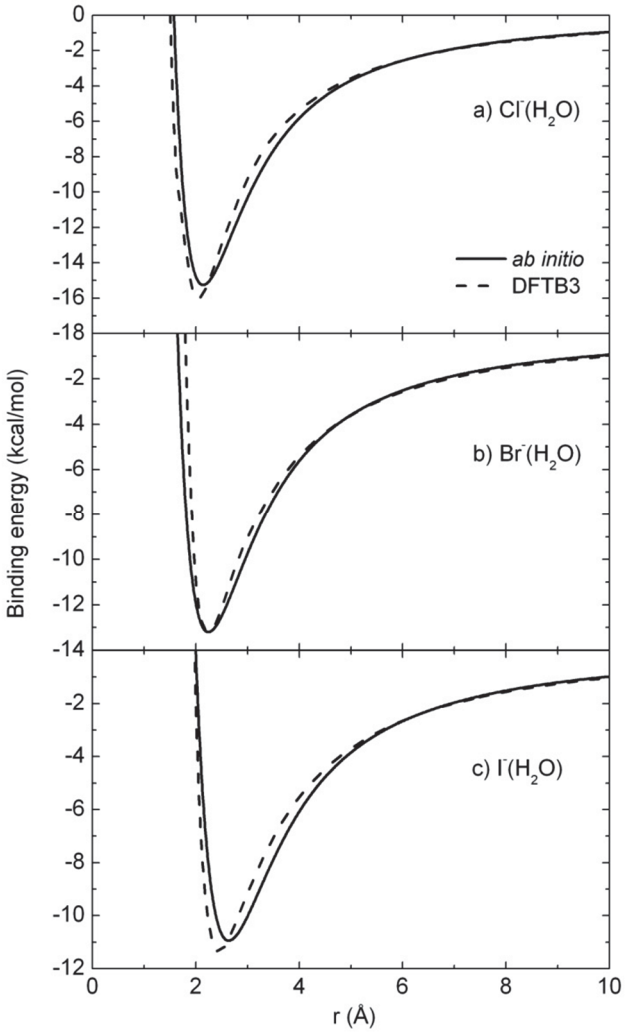

Figure 2.5. Potential energy curves for $X^-(H_2O)$ interactions (X = Cl, Br, I). *ab initio* = MP2/aug-cc-pVTZ for $Cl^-(H_2O)_1$ and MP2/aug-cc-pVTZ-PP for $Br^-(H_2O)_1$ and $I^-(H_2O)_1$. The horizontal axis coordinate is the hydrogen bond distance between each halide anion and water.

the reference data (DFT and *ab initio*) and the experimental one with DFT overestimating it by 151 cm^{-1} relative to the experimental value. DFTB3 predicts lower harmonic frequencies of the hydrogen-bonded O−H stretch − by 417 cm^{-1} and 224 cm^{-1} relative to DFT and experimental values, respectively. On the other hand, the red shift of the frequency of the water O−H stretch upon forming a hydrogen bond with chloride

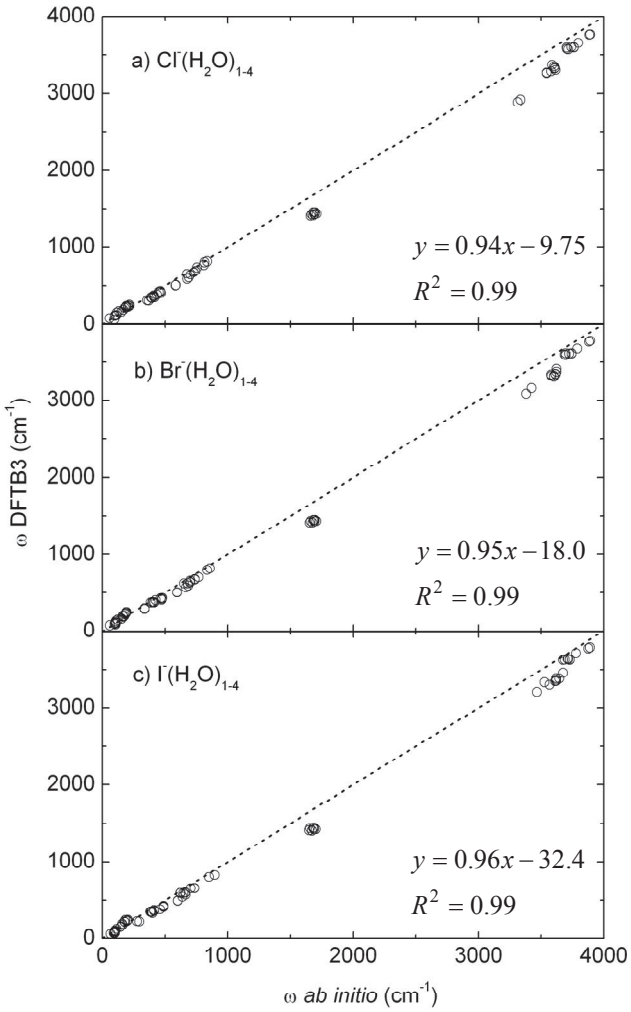

Figure 2.6. Calculated harmonic vibrational frequencies for $X^-(H_2O)_{1\text{-}4}$ clusters (X = Cl, Br, I). *ab initio* = MP2/aug-cc-pVTZ for $Cl^-(H_2O)_{1\text{-}4}$ and MP2/aug-cc-pVTZ-PP for $Br^-(H_2O)_{1\text{-}4}$ and $I^-(H_2O)_{1\text{-}4}$.

becomes too large with DFTB3 − by 336 cm^{-1} and 294 cm^{-1}, compared to DFT and experimental data, respectively. In addition, DFTB3 better reproduces lower frequencies relative to DFT, *ab initio* and experimental values. Overall, the average deviation of the DFTB3 frequencies from experimental data is comparable to that predicted by DFT and *ab initio* quantum-chemistry for this cluster size.

In $Cl^-(H_2O)_2$, the two water molecules form a single hydrogen bond with chloride and another hydrogen bond with each other. The DFTB3 frequencies for both hydrogen-bonded O−H stretching modes are smaller than for their DFT and experimental counterparts, but are in better agreement with experimental data than with DFT values. As observed in the case of $Cl^-(H_2O)$, DFTB3 also overestimates the magnitude of the frequency red shift for the O−H stretches upon hydrogen bonding by 337 cm^{-1} and 315 cm^{-1} with respect to DFT and experimental data, respectively. Interestingly, the average deviation of DFTB3 frequencies from available experimental data is smaller than that predicted by DFT and *ab initio* quantum-chemistry, presumably due to a fortunate cancellation of errors.

In $Cl^-(H_2O)_{3\text{-}4}$ all water molecules form a single hydrogen bond with chloride ion and hydrogen bonds with neighboring water molecules to form a ring below the ion. For these larger clusters, a few vibrational modes become strongly coupled and cannot be unequivocally identified. However, approximate assignment of the vibrational modes reveals similar deviations to those observed for the smaller clusters. In fact, DFTB3 vibrational frequencies correlate well with their *ab initio* counterparts, as shown in Figure 2.6. Overall, DFTB3 values for low and very high frequencies are in good agreement with *ab initio* ones, while intermediate frequencies are systematically underestimated.

2.3.2.2. Bromide–water clusters

Like in the case of chloride-water clusters, DFTB3 is found to underestimate bond lengths and angles in $Br^-(H_2O)_{1\text{-}4}$ relative to DFT and *ab initio* values (*cf.* Table 2.5). DFTB3 hydrogen-bond lengths are in better agreement with *ab initio* values, with

Table 2.5. Hydrogen-bonding geometrical characteristics of bromide–water clusters

Cluster	DFTB3	DFT [a]	*ab initio*[b]
	Bond length (Å)		
$Br^-(H_2O)_1$	2.280	2.374	2.293
$Br^-(H_2O)_2$	2.241	2.336	2.261
	2.485	2.612	2.463
$Br^-(H_2O)_3$	2.405	2.536	2.423
$Br^-(H_2O)_4$	2.471	2.625	2.479
Δ (DFT)[c]	4.8		
Δ (*ab initio*)	0.7	4.7	
	Bond angle (°)		
$Br^-(H_2O)_1$	154.2	160.9	167.5
$Br^-(H_2O)_2$	154.0	160.3	166.5
	146.7	150.9	155.1
$Br^-(H_2O)_3$	144.8	150.2	152.8
$Br^-(H_2O)_4$	140.8	146.5	150.6
Δ (DFT)	3.7		
Δ (*ab initio*)	6.5	3.0	

a) B3LYP/cc-pVTZ-PP. b) MP2/aug-cc-pVTZ-PP. c) Δ is the absolute mean deviation of DFTB3 data from reference data in parentheses in %.

average deviations of about 0.016 Å, whereas the average deviation reaches 0.12 Å for DFT data. On the other hand, the DFTB3 bond angles are closer to DFT values, within 6°, whereas the average deviation from *ab initio* data is 10°.

As was observed for chloride-water clusters, DFTB3 predicts accurate stepwise binding energies relative to DFT and *ab initio* values, and the average deviations are about 0.8 and 0.3 kcal/mol, respectively (*cf.* Figure 2.4). The DFTB3 results parallel their *ab initio* counterparts, presumably due to the better agreement of bond lengths as mentioned earlier for chloride-water clusters. Without addition of the modified γ^h function and third order correction to the DFTB2 model, the calculated binding energies deviate from *ab initio* data by about 3 kcal/mol. As shown from the data in Table 2.8, the accuracy of the predicted atomic partial charges is improved by including the hydrogen

bond and third order corrections in the DFTB3 model, although the uncorrected DFTB2 predicts partial charges in qualitative agreement with reference data. Moreover, as shown in Figure 2.5b, the DFTB3 potential energy curve for the bromide-water binary cluster is in perfect agreement with its *ab initio* counterpart.

DFTB3 underestimates the stretching frequency of the O−H bond implicated in hydrogen bonding to the ion in $Br^-(H_2O)_1$ relative to DFT and experimental values, but it overestimates the magnitude of its red shift upon hydrogen bonding by 215 cm^{-1} and 217 cm^{-1}, respectively (*cf*. Table 2.7). The average deviation of the DFTB3 frequencies from their experimental counterparts is similar to that predicted by *ab initio* quantum-chemistry, and comparable to that observed for chloride, but it is larger than that from DFT data. Similar trends as those discussed for chloride are observed for larger clusters. In general, DFTB3 frequencies correlate well with their *ab initio* counterparts, as shown in Figure 2.6.

2.3.2.3. Iodide–water clusters

Inspection of Table 2.6 reveals that the DFTB3 bond lengths in $I^-(H_2O)_{1\text{-}4}$ are smaller than their DFT and *ab initio* counterparts by about 0.196 and 0.046 Å, respectively, whereas bond angles are found in better agreement with DFT values (average deviation of less than 6°) than with *ab initio* values (average deviation of about 12°). These results are comparable to those observed previously for the other halides.

Like for the other halides, DFTB3 stepwise binding energies are in quantitative agreement with DFT and *ab initio* values, with deviations about 0.7 and 0.2 kcal/mol, respectively. Inclusion of hydrogen bond and third order corrections in DFTB3 improves

Table 2.6. Hydrogen-bonding geometrical characteristics of iodide–water clusters

Cluster	DFTB3	DFT[a]	*ab initio*[b]
	Bond length (Å)		
$I^-(H_2O)_1$	2.518	2.675	2.559
$I^-(H_2O)_2$	2.437	2.613	2.508
	2.761	2.950	2.745
$I^-(H_2O)_3$	2.612	2.827	2.673
$I^-(H_2O)_4$	2.690	2.931	2.733
Δ (DFT)[c]	7.0		
Δ (*ab initio*)	1.8	5.8	
	Bond angle (°)		
$I^-(H_2O)_1$	148.2	156.8	164.4
$I^-(H_2O)_2$	150.3	156.1	164.2
	143.5	147.7	152.9
$I^-(H_2O)_3$	142.7	147.2	151.6
$I^-(H_2O)_4$	137.8	145.2	147.9
Δ (DFT)	4.0		
Δ (*ab initio*)	7.4	3.5	

a) B3LYP/cc-pVTZ-PP. b) MP2/aug-cc-pVTZ-PP. c) Δ is the absolute mean deviation of DFTB3 data from reference data in parentheses in %.

the binding energies by about 2 kcal/mol compared to DFTB2 results. As shown from the data in Table 2.8, DFTB atomic partial charges are systematically improved upon inclusion of such corrections, similarly to what was observed in previous systems. It is important to note that, the minimal basis set approach of DFTB, which might cause the model to underestimate the polarizability of iodide, does not have a very significant effect on cluster binding energies in the first place, and inclusion of hydrogen bond and third order corrections partly compensate for this potential shortcoming as they predict accurate charge distributions. As for the other halides, the DFTB3 iodide–water potential energy curve, shown in Figure 2.5c, is in good agreement with its *ab initio* counterpart.

For $I^-(H_2O)_1$, the DFTB3 frequencies are underestimated relative to DFT and *ab initio* values in most cases and they are found in better agreement with experimental data (*cf.* Table 2.7). The magnitude of the red shift of the stretching frequency of the O−H

bond implicated in hydrogen bonding with the ion is smaller than for chloride and bromide, presumably due to the weaker iodide-water interaction. Moreover, the average deviation of the DFTB3 frequencies from experimental data is comparable to that predicted by DFT and *ab initio* quantum-chemistry and it is comparable to those of other halides. The deviations of DFTB3 frequencies from their experimental counterparts for larger clusters are comparable to that of the other halides, but DFTB3 seems to perform slightly better for iodide than for chloride and bromide. In general, DFTB3 frequencies correlate well with their *ab initio* counterparts, as shown in Figure 2.6.

2.4. Conclusions

New parameter sets have been developed to describe the interactions between halogen atoms and oxygen and hydrogen atoms by the approximate DFT-based DFTB3 model. The parameters have been used to investigate the main structural, energetic, and vibrational properties of various halogen-containing molecules as well as halide-water clusters. The newly parameterized DFTB3 model predicts structural properties, atomization energies and vibrational frequencies for small halogen-containing molecules, in good agreement with reference DFT data, but deviations increase for larger molecules containing multiple halide-oxygen double bonds. More importantly for the purpose at hand, the model accurately predicts the structures, energetics, and vibrational frequencies of halide-water clusters, when compared to the results of high-level MP2/aug-cc-pVTZ calculations and to available experimental data. Overall, hydrogen bond lengths and angles are slightly underestimated by DFTB3, but binding energies are in quantitative agreement with *ab initio* data (within less than 0.5 kcal/mol), an excellent

Table 2.7. Vibrational frequencies of $X^-(H_2O)_{1,2}$ (X = Cl, Br, I) clusters[a]

	$Cl^-(H_2O)$				$Br^-(H_2O)$				$I^-(H_2O)$			
	DFTB3	DFT[b]	MP2[c]	Exp.[d]	DFTB3	DFT[b]	MP2[c]	Exp.[d]	DFTB3	DFT[b]	MP2[c]	Exp.[d]
1 (ν_{OX})[e]	229	197	203	210/232	185	163	170	158/165	149	133	143	121/131
2 (ν_{ip})[e]	311	352	369	309	284	317	337	223/275	224	268	277	160/251
3 (ν_{oop})[e]	738	737	755	738	655	664	704	664	595	589	625	
4 (ν_{HOH})[e]	1427	1688	1670	1653	1433	1682	1663	1647	1441	1675	1655	1639
5 (ν_{OHi})[e]	2922	3339	3335	3146	3161	3446	3426	3296	3337	3552	3526	3393/3422
6 (ν_{OHf})[e]	3767	3848	3891	3697	3777	3847	3891	3695	3787	3845	3889	3692/3706
Δ_{abs} (Exp.)[f]	88	75	83		83	68	80		80	79	83	
Δ (Exp.)[g]	5	6	7		8	7	10		9	9	12	
	$Cl^-(H_2O)_2$				$Br^-(H_2O)_2$				$I^-(H_2O)_2$			
	DFTB3	DFT[b]	MP2[c]	Exp.[h]	DFTB3	DFT[b]	MP2[c]	Exp.[h]	DFTB3	DFT[b]	MP2[c]	Exp.[h]
1	110	104	101		97	90	97		69	78	90	
2	162	140	152		158	143	152		150	131	145	
3	217	190	178		197	186	177		178	167	162	
4	244	213	216		219	181	183		212	189	182	
5	314	351	356		294	320	334		221	269	294	
6	375	430	411		378	411	402		353	394	388	
7	410	511	469		405	484	473		380	439	460	
8	655	688	675		620	666	767		595	660	706	
9	772	822	810		700	766	651		654	694	622	
10	1407	1675	1661		1412	1669	1655		1413	1662	1648	
11	1452	1715	1695		1449	1709	1690		1443	1703	1685	
12 (ν_{OHi})[e]	2890	3307	3314	3130	3085	3388	3386	3207	3208	3478	3467	3331
13 (ν_{OHi})[e]	3370	3584	3588	3375	3409	3643	3625	3438	3459	3689	3674	3500
14 (ν_{OHw})[e]	3655	3750	3796	3633	3678	3735	3789	3625	3714	3731	3778	3616
15 (ν_{OHf})[e]	3761	3841	3885	3686	3768	3838	3881	3680	3773	3834	3876	3675
Δ_{abs} (Exp.)	86	165	190		73	164	183		90	153	168	
Δ (Exp.)	3	5	6		2	5	5		3	4	5	

a) All calculated values are harmonic vibrational frequencies. All frequencies in cm^{-1}. b) B3LYP/cc-pVTZ for $Cl^-(H_2O)_{1,2}$ and B3LYP/cc-pVTZ-PP for $Br^-(H_2O)_{1\text{-}2}$ and $I^-(H_2O)_{1,2}$. c) MP2/aug-cc-pVTZ for $Cl^-(H_2O)_{1,2}$ and MP2/aug-cc-pVTZ-PP for $Br^-(H_2O)_{1\text{-}2}$ and $I^-(H_2O)_{1,2}$. d) From Ref. 116. e) OX = halide-water stretch; ip = in-plane bend; oop = out-of-plane bend; HOH: water bend; OHi: ion-hydrogen-bonded OH stretch; OHw: water-hydrogen-bonded O−H stretch; OHf: free O−H stretch. f) Average absolute deviation from reference data in parentheses (in cm^{-1}). g) Average absolute deviation from reference data in parentheses in %. h) From Ref. 117.

Table 2.8. Atomic partial charge distributions in $X^-(H_2O)$ clusters (X = Cl, Br, I)

Cluster	Atom	DFTB2	DFTB3	ESP[a]
$Cl^-(H_2O)$	Cl	–0.9478	–0.9488	–0.9332
	H	0.3413	0.4238	0.4459
	O	–0.6692	–0.8301	–0.8539
	H	0.2757	0.3551	0.3412
Δ[b]		16.5	3.4	
$Br^-(H_2O)$	Br	–0.9597	–0.9660	–0.9443
	H	0.3370	0.4158	0.4277
	O	–0.6580	–0.8070	–0.8289
	H	0.2806	0.3572	0.3456
Δ		15.6	2.8	
$I^-(H_2O)$	I	–0.9803	–0.9785	–0.9394
	H	0.3330	0.4076	0.4142
	O	–0.6416	–0.7906	–0.8184
	H	0.2889	0.3615	0.3437
Δ		15.4	3.6	

a) Atomic partial charges obtained from the electrostatic surface potential (ESP)[118-120] with MP2/aug-cc-pVTZ for $Cl^-(H_2O)$ and MP2/aug-cc-pVTZ-PP for $Br^-(H_2O)$ and $I^-(H_2O)$. b) Δ is the absolute mean deviation from ESP data in %.

agreement due to inclusion of hydrogen-bond and third order corrections in this model. The model also predicts vibrational frequencies in good qualitative agreement with *ab initio* and experimental data. The relative accuracy of DFTB3 in predicting solvation properties of ions, together with its computational efficiency, make it a promising model for investigating much larger clusters and describing interatomic interactions in molecular dynamics simulations of such systems.

Supporting Information

Atomic spin constants for chlorine, bromine and iodine atoms. Vibrational frequencies of molecules investigated.

Table S1. Atomic spin constants for chlorine, bromine and iodine atoms

Atom		s	p	d
Cl	s	–0.022	–0.018	0.000
	p	–0.018	–0.016	0.000
	d	0.000	0.000	–0.290
Br	s	–0.018	–0.014	0.000
	p	–0.014	–0.014	0.000
	d	0.000	0.000	–0.799
I	s	–0.014	–0.012	0.000
	p	–0.012	–0.011	–0.001
	d	0.000	–0.001	–0.623

Table S2. Selected vibrational frequencies of various chlorine compounds[a]

Molecule		DFTB3	DFT[b]	exp.[c]
Cl_2		577	538	560
HCl		2995	2941	2991
HOCl	1 (ν_{Cl-O})	766	738	724
	2	1192	1266	1239
	3	3471	3773	
$HClO_2$	1	212	316	
	2	304	399	
	3 (ν_{Cl-O})	412	614	
	4 ($\nu_{Cl=O}$)	945	969	
	5	1099	1187	
	6	3472	3733	
$HClO_3$	1	230	90	
	2	347	361	
	3	460	399	
	4	572	519	
	5 (ν_{Cl-O})	409	607	
	6 ($\nu_{Cl=O}$)	1043	1015	
	7 ($\nu_{Cl=O}$)	953	1151	
	8	1069	1184	
	9	3531	3688	
$HClO_4$	1	135	176	
	2	367	387	
	3	379	396	
	4	279	519	
	5	518	544	
	6	534	551	
	7 (ν_{Cl-O})	595	692	
	8 ($\nu_{Cl=O}$)	1024	1003	
	9 ($\nu_{Cl=O}$)	965	1183	
	10 ($\nu_{Cl=O}$)	957	1211	
	11	1091	1296	
	12	3528	3710	

a) All calculated values are harmonic vibrational frequencies. All frequencies in cm^{-1}. b) B3LYP/cc-pVTZ.
c) From Ref. 113.

Table S3. Selected vibrational frequencies of various bromine compounds[a]

Molecule		DFTB3	DFT[b]	exp.[c]
Br_2		258	316	325
HBr		2327	2599	2649
HOBr	1 (ν_{Br-O})	610	632	620
	2	1140	1189	1163
	3	3504	3782	
$HBrO_2$	1	267	246	
	2	186	374	
	3 (ν_{Br-O})	407	563	
	4 ($\nu_{Br=O}$)	761	843	
	5	1025	1114	
	6	3519	3756	
$HBrO_3$	1	170	76	
	2	314	289	
	3	352	317	
	4	442	377	
	5 (ν_{Br-O})	340	552	
	6 ($\nu_{Br=O}$)	853	899	
	7 ($\nu_{Br=O}$)	624	951	
	8	960	1077	
	9	3559	3708	
$HBrO_4$	1	69	91	
	2	282	291	
	3	311	304	
	4	334	365	
	5	375	376	
	6	390	376	
	7 (ν_{Br-O})	457	595	
	8 ($\nu_{Br=O}$)	786	870	
	9 ($\nu_{Br=O}$)	668	954	
	10 ($\nu_{Br=O}$)	696	965	
	11	988	1151	
	12	3560	3709	

a) All calculated values are harmonic vibrational frequencies. All frequencies in cm^{-1}. b) B3LYP/cc-pVTZ-PP. c) From Ref. 113.

Table S4. Selected vibrational frequencies of various iodine compounds[a]

Molecule		DFTB3	DFT[b]	exp.[c]
I_2		153	214	215
HI		2178	2311	2309
HOI	1 (ν_{I-O})	586	589	
	2	1058	1103	
	3	3550	3793	
HIO_2	1	166	208	
	2	220	358	
	3 (ν_{I-O})	498	562	
	4 ($\nu_{I=O}$)	778	780	
	5	952	1045	
	6	3561	3774	
HIO_3	1	124	56	
	2	232	247	
	3	263	266	
	4	282	298	
	5 (ν_{I-O})	481	577	
	6 ($\nu_{I=O}$)	805	861	
	7 ($\nu_{I=O}$)	655	890	
	8	900	990	
	9	3575	3731	
HIO_4	1	105	62	
	2	189	222	
	3	218	242	
	4	263	269	
	5	239	277	
	6	247	283	
	7 (ν_{I-O})	481	610	
	8 ($\nu_{I=O}$)	751	829	
	9 ($\nu_{I=O}$)	720	881	
	10 ($\nu_{I=O}$)	710	889	
	11	910	1044	
	12	3574	3723	

a) All calculated values are harmonic vibrational frequencies. All frequencies in cm^{-1}. b) B3LYP/cc-pVTZ-PP. c) From Ref. 113.

Chapter 3

A Density-Functional Tight-Binding Investigation of Halide Cluster Hydration

To be submitted as:

S. Jahangiri, G. H. Peslherbe, *Chem. Phys. Lett.* 2013

3.1. Introduction

Recent experimental and computational investigations suggest that the larger halide anions are present at higher concentrations at aqueous interfaces than in the bulk.[28,57,65,68,121] This interfacial presence may have important consequences for the chemistry of these ions in biological systems and atmospheric droplets. For instance, the presence of halide anions at the surface of aqueous solutions has been suggested to increase the uptake of chlorine and bromine molecules in the gas phase[122] and affect the mechanisms of oxidation of anions by atmospheric oxidants.[29] Moreover, the affinity of ions for the water interface might provide new insights into the specific effect of ions in aqueous solution which is a well known, but not yet fully elucidated, phenomenon in chemistry and biology.[25]

Computational investigations of ions in water clusters have provided a new avenue for investigating the extent of ion hydration at the molecular level. Such investigations were triggered by the early simulations of Berkowitz[49-51,71] and Dang[52,53] and co-workers that showed that large and polarizable halide anions are asymmetrically hydrated in water clusters. Results of these simulations demonstrated that the polarizabilities of both the ions and the water molecules are key factors governing the interfacial presence of the larger halide anions.[28] However, recent simulations with non-polarizable force fields have also showed that the larger halide anions have a higher affinity for interfacial solvation (Ref. 123 and references therein), while *ab initio* molecular dynamics (AIMD) simulations of iodide in water clusters and bulk water led to the conclusion that polarizable force fields might in fact overestimate the interfacial affinity of larger halides.[13] It should be noted that empirical force fields have been widely

used in such investigations,[28,54,65] and only a limited number of AIMD simulations have been reported[13,124] as expensive computations associated with *ab initio* quantum-chemistry methods restrict their practical implementation in such simulations. This warrants further first-principles investigations of the hydration extent of halide anions. In particular, approximate quantum-chemistry methods that provide affordable first-principles-based calculations and accurately describe the ion–water and water–water interactions are promising models for this purpose, especially when effects such as polarization and charge transfer are deemed important.

In this article, the cluster hydration of halide anions is investigated by molecular dynamics (MD) simulations with the self-consistent-charge density-functional tight-binding (SCC-DFTB)[58] model with third-order extension (DFTB3)[61,83] to describe interatomic interactions. The DFTB3 model is an approximate quantum-chemistry approach that originates from density-functional theory (DFT) and has the transferability of first-principles methods, but it is much less computationally intensive such that it can be applied to a wide variety of physical, chemical and biological systems for which genuine first-principles calculations are computationally prohibitive.[74,75] This model has been shown to predict the properties of small halide–water clusters containing up to 4 water molecules with acceptable accuracy when compared to genuine first-principles predictions (see Chapter 2). The efficiency of conformational space sampling and possible first-principles refinements of the DFTB3-MD simulation results will also be explored to assess their validity and robustness. The article is organized as follows: the computational procedure is presented in Section 3.2, while results are reported and discussed in Section 3.3 and concluding remarks follow in Section 3.4.

3.2. Computational procedure

DFTB3-MD simulations were performed for ionic water clusters containing a halide and 12, 24 and 48 water molecules. The hydration extent of the ions was characterized based on the spatial probability distributions of halides in water clusters, obtained from accurate potential of mean force (PMF) calculations. The umbrella sampling[125] method was used to sample a coordinate defined as the distance between the ion and the cluster center of mass (r_{cm}) and the weighted histogram analysis method (WHAM)[126] was employed to remove the biasing potentials. Restraining harmonic potentials with a force constant of 5.0 kcal/mol/Å^2 were applied at 0.5 Å intervals of the r_{cm} coordinate with a total number of 11, 13 and 15 windows for clusters containing 12, 24 and 48 water molecules, respectively. All simulations were performed at 250 K for 120 ps, with 60 ps of equilibration and 60 ps of data collection. The equations of motion were integrated using the velocity Verlet algorithm with a time step of 1 fs. In order to prevent water evaporation, spherical boundary conditions[68,127-129] were imposed, with a radius of 10 Å, which is larger than typical cluster radii by at least 3 Å. The simulations were performed with our in-house MD engine while interatomic energies and forces were calculated with the DFTB+ code.[63] DFTB3 parameters were taken from the *DFTB**3** parameters for **o**rganic and **b**iological applications (3OB)*[83] and the *parameters for **m**aterials and **bio**logical systems (MIO)*[58] supplemented by the halogen parameters. The Hubbard derivative of fluorine was fitted to reproduce the *ab initio* stepwise binding energy of $F^-(H_2O)_{1-4}$ clusters; the value obtained is –0.31 au The WHAM program was used to remove biasing potentials and calculate the final probability distributions.[130]

Replica-exchange molecular dynamics (REMD) simulations were performed following the procedure developed by Sugita and Okamoto.[131] In this approach, independent MD simulations are performed at different temperatures and, after a limited number of simulation steps, resulting structures are swapped between adjacent replicas according to the following criterion:[132]

$$w_{ij} = \min\{1, e^{(\beta_i - \beta_j)(U_i - U_j)}\}, \qquad (3.1)$$

where w_{ij} represents the probability of exchange, U is the potential energy and $\beta = 1/k_B T$ where k_B is the Boltzmann constant and T is the temperature. This approach allows enhancement of the probability of sampling in regions of conformational space that are rarely sampled in standard single-temperature MD simulations. REMD simulations were performed at 8 different temperatures ranging from 150 to 325 K at 25 K intervals and resulting conformations were examined for possible exchange every 100 steps of simulation.

First-principles refinements of the potentials of mean force were performed by calculating the free energy change associated with replacing the DFTB3 ion–water interactions with their DFT counterparts for a limited number of uncorrelated structures selected from the DFTB3-MD trajectories. This procedure is further referred to as DFT//DFTB3-MD by analogy with the standard quantum-chemistry notation. For this purpose, 120 uncorrelated structures were selected for each window along the reaction coordinate (1320 structures in total for cluster size 12) for subsequent DFT calculations. The free energy change was then evaluated as:[133]

$$\Delta G = -k_B T \ln\left\langle e^{-\Delta U / k_B T} \right\rangle, \qquad (3.2)$$

where ΔU represents the difference between DFT and DFTB3 energies, and again k_B is the Boltzmann constant and T is the temperature. This procedure is analogous to that previously used for calculating ion hydration free energies.[133] All DFT calculations were performed with the hybrid exchange-correlation functional of Adamo[93] based on the pure functional of Perdew, Burke and Ernzerhof (PBE0)[92,93] and Dunning's augmented correlation consistent aug-cc-pVDZ basis set.[102,134] The PBE0 functional has been shown to accurately describe hydrogen-bonded systems.[135,136]

Ab initio quantum-chemistry calculations were also performed on small halide-water clusters for validation purposes of both DFT and DFTB3. For instance, stepwise cluster binding energies were evaluated with the coupled cluster with single, double and perturbative triple excitations CCSD(T) method[137] together with the aug-cc-pVQZ basis set, for geometries optimized with frozen-core second-order Møller-Plesset (MP2)[108] theory and the aug-cc-pVTZ basis set. In the case of iodine, core electrons were omitted from the electronic structure calculations with the use of pseudopotentials (PP).[104] Both the *ab initio* and DFT binding energies were corrected for basis set superposition error (BSSE) with the counterpoise approach of Boys and Bernardi.[109] All *ab initio* and DFT calculations were performed with the Gaussian09 suite of programs.

The accuracy of the DFT model in predicting halide–water binding energies is compared with high-level *ab initio* quantum-chemistry results in Table 3.1. Results of DFTB3 calculations are also shown for comparison. Inspection of the tabulated data

indicates that PBE0 values deviate by less than 0.5 kcal/mol from their corresponding *ab initio* values in most cases, except for the first hydration step of fluoride for which the deviation reaches 1 kcal/mol. However, this deviation is not significant enough to preclude the use of DFT for the refinement of PMFs, a quantum-chemistry method of choice in light of its reasonable computational cost compared to high-level *ab initio* quantum-chemistry. Results presented in Table 3.1 also demonstrate that the DFTB3 values deviate by ~0.5 kcal/mol, on average, from both DFT and *ab initio* data.

3.3. Results and discussion

The temperature of water clusters and their precise phase properties (i.e. liquid-like, glassy or solid-like) have been long-standing issues.[138] Accordingly, cluster phase properties are first investigated and discussed in Section 3.3.1. Ion hydration features and the results of structural analysis are then presented in Section 3.3.2. Finally, possible corrections due to enhanced conformational sampling and first-principles refinements are examined in Section 3.3.3.

3.3.1. Cluster phase properties

Water clusters are known to melt at lower temperatures than the bulk phase does.[138] Cluster phase transitions have been typically determined from the temperature dependence of the cluster internal energy or the oxygen-oxygen Lindemann index[139]

Table 3.1. Stepwise binding energies of halide–water clusters[a]

Method[b]	$F^-(H_2O)_{1-2}$		$Cl^-(H_2O)_{1-2}$		$Br^-(H_2O)_{1-2}$		$I^-(H_2O)_{1-2}$		Δ^c
	$D_e^{0,1}$	$D_e^{1,2}$	$D_e^{0,1}$	$D_e^{1,2}$	$D_e^{0,1}$	$D_e^{1,2}$	$D_e^{0,1}$	$D_e^{1,2}$	
DFTB3	26.4	21.1	14.9	14.5	12.2	12.7	10.5	11.5	0.4
DFT	28.5	21.5	15.2	14.9	13.1	13.7	11.0	12.2	0.6
	(28.2)	(21.3)	(15.1)	(14.6)	(12.9)	(13.3)	(10.9)	(11.9)	(0.4)
ab initio	27.6	21.5	15.0	15.2	13.8	14.5	11.9	13.4	
	(27.0)	(21.0)	(14.7)	(14.8)	(12.6)	(13.6)	(10.5)	(12.2)	

a) All binding energies (D_e) are in kcal/mol. Results in parentheses are corrected for BSSE.
b) DFT = PBE0/aug-cc-pVDZ, ab initio = CCSD(T)/aug-cc-pVQZ//MP2/aug-cc-pVTZ.
c) Δ is the absolute mean deviation of data from the *ab initio* data in kcal/mol.

calculated over a wide range of temperatures by MD simulations.[138] More specifically, melting temperatures are characterized by the change of slope in the cluster internal energy curve[138] or an increase of up to 0.1 of the Lindemann index.[140] The Lindemann index is calculated from the number of molecules in the cluster (n) and their intermolecular distances (r_{ij}), represented by the oxygen-oxygen distances in the case of water clusters, as:[140]

$$\delta_{OO} = \frac{2}{n(n-1)} \sum_{i<j} \frac{\left(\left\langle r_{ij}^2 \right\rangle - \left\langle r_{ij} \right\rangle^2 \right)^{1/2}}{\left\langle r_{ij} \right\rangle} . \qquad (3.3)$$

The internal energy and δ_{OO} curves for the $(H_2O)_{12}$ cluster are shown in Figure 3.1 over the temperature range 20 to 300 K. Inspection of Figure 3.1 reveals a clear change in the slope of the internal energy curve at about 190 K, accompanied by a significant increase in the magnitude of δ_{OO} from 0.05 to more than 0.1. Accordingly, both criteria indicate that the phase-transition temperature of the $(H_2O)_{12}$ cluster predicted by our DFTB3-MD simulations is about 190 K, which is close to the value previously obtained (~200 K) by

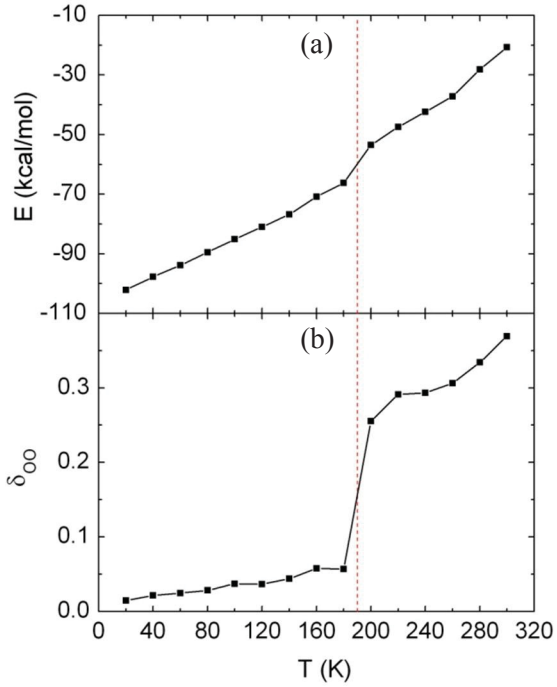

Figure 3.1. Temperature dependence of (a) the internal energy and (b) the oxygen–oxygen Lindemann index of the $(H_2O)_{12}$ cluster obtained from DFTB3-MD simulations. The vertical dashed line identifies the phase-transition temperature.

MD simulations with the TIP5P force field.[127] The melting temperatures of the $(H_2O)_{24}$ and $(H_2O)_{48}$ clusters were found to lie around 170 K, which is also consistent with the range predicted by simulations with force fields.[127] According to these observations, a temperature of 250 K was adopted in all subsequent simulations to ensure the liquid-like state of the water clusters.

3.3.2. Hydration extent and structural analysis

The probability distributions of the distance between halides and the water cluster center of mass, which characterize the hydration extent of the ions, are shown in Figure 3.2. The curve for $F^-(H_2O)_{12}$ exhibits a peak around 1 Å which is clearly indicative of the

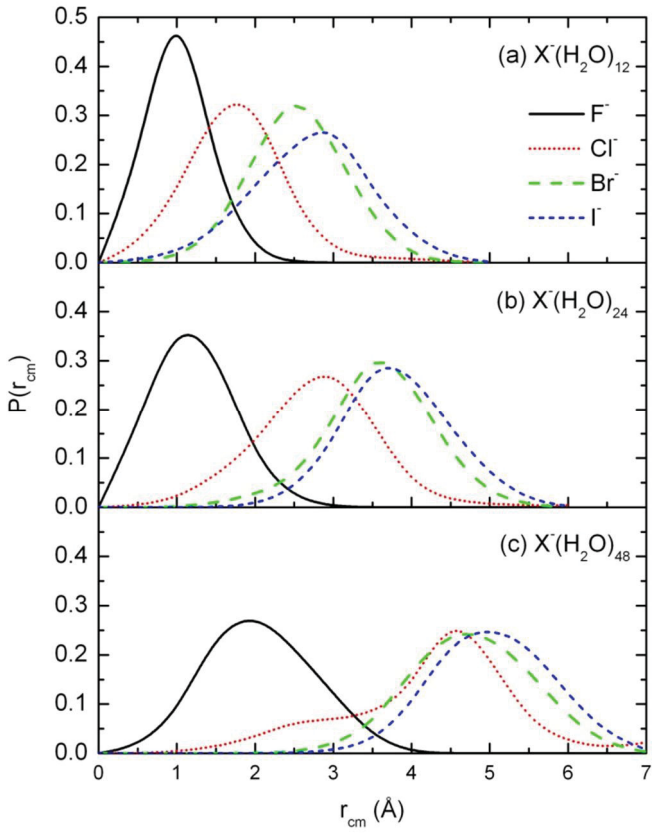

Figure 3.2. Probability distributions of the distance between the halide and the water cluster center of mass, $P(r_{cm})$, for clusters containing a given halide and (a) 12, (b) 24 and (c) 48 water molecules. Obtained from DFTB3-MD simulations at 250 K.

affinity of fluoride for full hydration inside the cluster. In the case of $Cl^-(H_2O)_{12}$, the peak appears around 1.75 Å, a larger value relative to that for fluoride, indicating a reduced affinity of chloride for the interior regions of the water cluster. As for $Br^-(H_2O)_{12}$ and $I^-(H_2O)_{12}$, the spatial probability distributions are characterized by a peak at much larger distances (2.5–3 Å), clearly reflecting that both bromide and iodide are asymmetrically solvated at the cluster surface. Further inspection of Figure 3.2 demonstrates that for cluster size 24, fluoride remains fully hydrated inside the cluster at around 1 Å from the cluster center of mass, while chloride continues to shift towards the

cluster surface, with r_{cm} values centered around 3 Å, and both bromide and iodide remain partially solvated at the cluster surface, with r_{cm} values around 3.75 Å. Similarly, for cluster size 48, fluoride remains fully hydrated at around 2 Å from the cluster center, while chloride (to a slightly lesser extent), bromide and iodide preferentially locate at the cluster surface, with r_{cm} values centered around 4–5 Å. These results unambiguously show that fluoride prefers full hydration inside water clusters, while chloride prefers to locate in interfacial regions, especially in larger clusters, and bromide and iodide prefer partial hydration at the cluster surface. These findings confirm the results of previous investigations.[28,68]

The hydration extent of ions depends on the relative strengths of the ion–water and water–water interactions, as well as entropic effects, which tend to favor of interior hydration.[68] According to the results presented in Table 3.1, strong hydrogen bonds between fluoride and water molecules, which are due to the relatively high charge density of fluoride, prevail over water–water interactions and force water molecules to tightly enclose the anion. However, in the case of the larger halides, weaker ion–water interactions and entropic effects are dominated by the water–water interactions which results in the preferential location of the larger halides towards the surface of a strongly hydrogen-bonded water network. In order to provide molecular details about this, the spatial probability distributions and the number of hydrogen atoms around halides in a cluster of 12 water molecules were calculated and are shown in Figure 3.3. The halide-hydrogen distance probability distributions (Figure 3.3a) exhibit two peaks for all halides. However, these peaks are very pronounced and clearly separated by a very low minimum for fluoride, while both peaks broaden, shift towards larger distances and are separated by

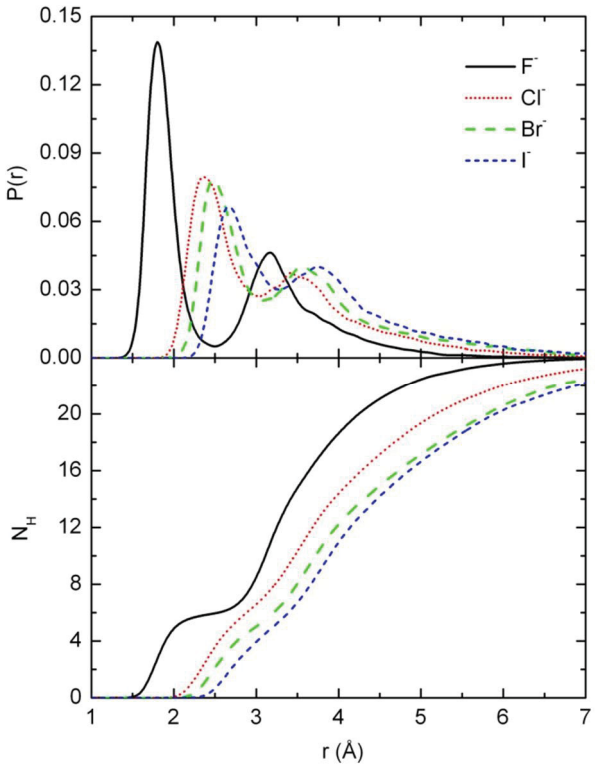

Figure 3.3. Selected structural features of $X^-(H_2O)_{12}$ (X = F, Cl, Br, I) clusters. (a) Spatial probability distributions and (b) number of hydrogen atoms (N_H) around halide anions. Obtained from DFTB3-MD simulations at 250 K.

a less pronounced minimum for the larger halides. The existence of the two peaks might be attributed to the formation of asymmetric halide–water structures with single linear hydrogen bonds.[41,105] Figure 3.4 displays the potential energy profile for the interconversion of a hydrogen-bonded halide–water binary complex to its mirror-image conformer. For $F^-(H_2O)$, the symmetric transition state for interconversion lies ~8 kcal/mol higher in energy than the asymmetric linear hydrogen-bonded structures. However, for larger halides, the barrier for interconversion is much reduced, down to 1 kcal/mol for $I^-(H_2O)$ (*cf.* Figure 3.4).These observations indicate that water molecules

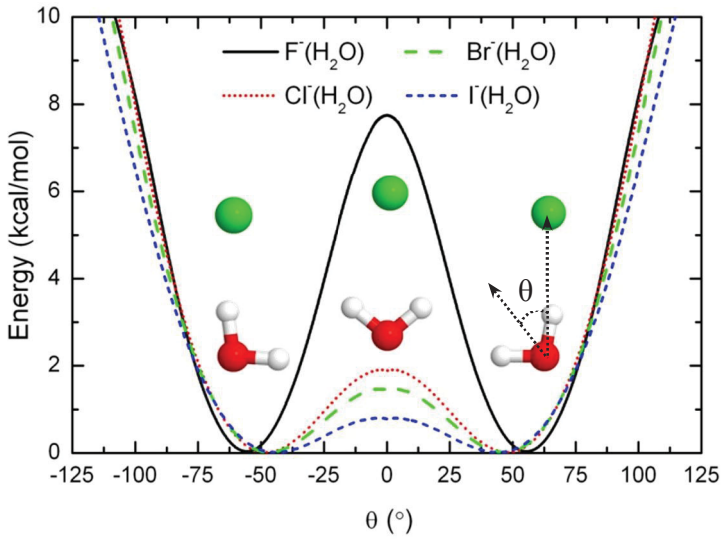

Figure 3.4. Potential energy profiles for halide–water binary cluster interconversion plotted as a function of the angle (θ) between the line that connects the water oxygen to the halide and the HOH bisector. Obtained from MP2/aug-cc-pVTZ calculations.

form a rigid shell around fluoride, due to the strong fluoride–water interactions, while they are loosely bound to the larger halides.

Based on the relative strengths of the ion–water interactions listed in Table 3.1, one would expect chloride to behave like more bromide and iodide, since their cluster binding energies are much closer, and half of the fluoride–water interaction strength or less. The fact that chloride does not seem to exhibit a pronounced affinity for interfacial hydration like bromide and iodide might be surprising at first. In fact, the ion–water interactions are stronger for chloride than for bromide and iodide (even if not dramatically more so) and the chloride–water interactions compete more effectively with the water–water interactions in small clusters, resulting in a behavior closer to that of fluoride in small clusters, i.e. some affinity for the interior regions of the cluster, even if much reduced relative to fluoride. However, as cluster size increases, the cooperative

interactions of a strongly hydrogen-bonded water network may start prevailing over the chloride–water interactions, resulting in the higher affinity for interfacial regions of the clusters.

Interestingly, according to the calculated number of hydrogen atoms around the ions, plotted as a function of distance from the halides in Figure 3.3b, the first hydration shell of *all* halides contains about six water molecules. Hence, the only partially hydrated larger halides have the same number of adjacent water molecules as the fully hydrated fluoride. This is not too surprising, since the first hydration shell of larger halides would presumably accommodate a larger number of water molecules due to their larger ionic radius, a feature compensated by partial hydration resulting in the same number of adjacent water molecules for all halides.

3.3.3. REMD simulations and first-principles refinement

Water clusters have long been known to possess a convoluted potential energy surface with a large number of local minima[141,142] that may render thorough conformational space sampling difficult with finite-time MD simulations. To investigate the significance of this issue, REMD simulations were performed on a cluster containing chloride and 12 water molecules as a test case. The probability distributions of the distance between chloride and the $(H_2O)_{12}$ cluster center of mass obtained from REMD simulations is shown and compared with the result of single-temperature MD simulations in Figure 3.5. Inspection of this figure indicates that the hydration extent of chloride obtained from both procedures is analogous, which demonstrates that single-temperature

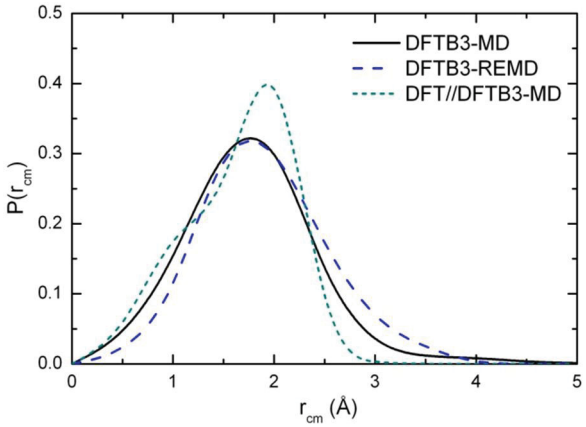

Figure 3.5. Probability distributions of the distance between chloride and the water cluster center of mass for $Cl^-(H_2O)_{12}$ at 250 K.

simulations have sufficiently sampled the different regions of the cluster conformational space. Chloride spatial probability distributions obtained at different temperatures are shown in Figure 3.6. Inspection of the figure reveals that, as temperature increases, the probability distribution curves broaden and shift towards slightly smaller values, reflecting a higher affinity for the interior regions of the cluster, presumably due to the entropic effect mentioned earlier.

In order to further validate the accuracy of the simulation results, DFT refinements were performed on the DFTB3-MD PMFs obtained for a cluster containing chloride and 12 water molecules, again as a test case. The refined DFT//DFTB3-MD spatial probability distribution of chloride in $Cl^-(H_2O)_{12}$ shown in Figure 3.5 indicates that the DFT refinement provides a distribution of chloride inside the cluster analogous to that of the DFTB3-MD simulations. This further demonstrates the validity and robustness of the DFTB3-MD simulation results.

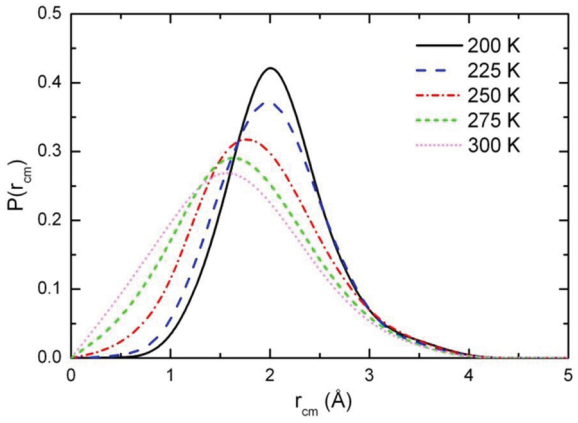

Figure 3.6. Probability distributions of the distance between chloride and the water cluster center of mass for $Cl^-(H_2O)_{12}$ at different temperatures. Obtained from DFTB3-REMD simulations.

3.4. Conclusions

The hydration of halide anions in water clusters containing 12, 24 and 48 water molecules has been investigated by MD simulations in which interatomic interactions were described by the DFTB3 model. In order to find a proper simulation temperature at which the clusters are ensured to be liquid, cluster melting temperatures were first determined from DFTB3-MD simulations for all cluster sizes. The latter were found in the range 170–190 K, in agreement with the predictions of previous models, and a temperature of 250 K was adopted in subsequent simulations. Our first-principles-based simulation results demonstrate unambiguously that fluoride prefers full hydration in the interior regions of the water clusters, but bromide and iodide prefer to reside at the cluster surface, while chloride exhibits an intermediate behavior with a higher surface affinity in larger clusters. These observations are in agreement with the results of previous investigations employing MD simulations and surface sensitive experimental techniques.

REMD simulations were performed to ensure the adequacy of conformational space sampling in single-temperature MD simulations and selected results were further validated with first-principles refinements performed with DFT. This makes the DFTB3-MD a method of choice based on first-principles to investigate the cluster hydration of not only halide anions but also other types of ions.

Chapter 4

Benchmarking of Density-Functional Tight-Binding Models for Describing Hydrogen-Bonded Anionic-Water Clusters

To be submitted as:

S. Jahangiri, L. Cai, G. H. Peslherbe, *J. Comput. Chem.* 2013

4.1. Introduction

Ions have crucial effects on the physical properties of aqueous solutions. Such effects are quite specific and depend on the nature of the solvated ions.[25,143,144] Among the many solution properties affected by the introduction of ions, one of particular interest is protein solubility, which was initially investigated by Franz Hofmeister.[20,145] This early work led to a categorization of ions, based on their ability to salt in or out proteins, in what is nowadays referred to as the Hofmeister series. Interestingly, the effect of ions on other solution properties follows a trend similar to that observed by Hofmeister.[21,22,143,146] However, despite the large impact of specific ion effects in chemistry, biology and biochemistry, many questions about the microscopic details underlying this phenomenon remain unclear and the molecular mechanisms by which solvated ions alter water properties are not well understood. For instance, the traditional theories of electrolytes fail to describe such effects,[143] and the effects of solvated ions on water structure, which is believed to be a key point in understanding specific ion effects, remains controversial.[18] Comprehensive studies are first needed to clarify fundamental aspects of ion solvation and their underlying molecular mechanism. In this respect, theoretical investigations prove to be essential companions to experimental studies in clarifying the molecular details of specific ion effects.[13,28]

Semiempirical and/or approximate quantum-chemistry methods have been used to study a variety of systems with an accuracy comparable to that of high-level quantum-chemistry methods,[147,148] but at a fraction of the computational cost. Due to their efficiency, and because they tend to be more robust than empirical force fields, semiempirical and/or approximate methods can be applied routinely to very large systems

or can be used in computationally-intensive molecular dynamics simulations.[80,82,149] However the theoretical approximations and the parameterization, empirical or not, employed in such methods may limit the extent of their application to particular systems, and therefore, very much like for force fields, a careful benchmarking of the method must be performed against experimental data or high-level quantum-chemistry results before using them for a particular system. Approximate density-functional theory (DFT) methods, such as density-functional tight-binding (DFTB) models,[58,59] have shown great promise in predicting energetic and structural properties of various systems.[73,78,149-157] In this work, the accuracy and performance of DFTB models in describing the structural properties, energetics, and vibrational frequencies of small anionic water clusters are evaluated. The anions investigated are the polyatomic ions of the Hofmeister series, namely carbonate, sulfate, hydrogen phosphate, acetate, nitrate, perchlorate and thiocyanate. The outline of this article is as follows: computational details are provided in Section 4.2, results of DFTB calculations are presented and discussed in Section 4.3, where they are compared to the predictions of high-level *ab initio* quantum-chemistry, while concluding remarks follow in Section 4.4.

4.2. Computational procedure

4.2.1. DFTB models

The DFTB model is an approximate quantum-chemistry method based on DFT and the tight-binding model.[58,61,91] The DFTB energy is obtained by expanding the DFT total energy in terms of charge density fluctuations around a reference electron density which

is usually considered to be the electron density of neutral atoms. The original DFTB model, denoted DFTB0 herein, is obtained on the basis of a zero[th]-order expansion as:[74]

$$E^{DFTB\,0} = \sum_{i}^{occ} \langle \Psi_i | \hat{H}_0 | \Psi_i \rangle + E^{rep} \qquad (4.1)$$

where the first term represents orbital energies and E^{rep} is a sum over short-range repulsion potentials. The Hamiltonian operator is constructed on the basis of a given reference density and the single-electron wave functions are represented as linear combinations of Slater-type orbitals. Second-order expansion of the DFT energy results in a self-consistent-charge term which augments the DFTB0 energy to form the self-consistent-charge DFTB energy, which will be referred to as DFTB2 herein:[58]

$$E^{DFTB2} = E^{DFTB0} + \frac{1}{2}\sum_{ab} \Delta q_a \Delta q_b \gamma_{ab} \qquad (4.2)$$

In this equation, Δq_a and Δq_b are atomic charge fluctuations that are obtained from the Mulliken scheme in a self-consistent manner and γ_{ab} is a function that describes the extent of charge interactions. It has been shown that adding an additional term with an adjustable parameter (ξ) to the γ_{ab} function, denoted γ^h herein, provides better results for systems containing hydrogen atoms.[61,91] Finally, extending the expansion up to third order leads to the DFTB3 model for which the energy is represented as:[61]

$$E^{DFTB3} = E^{DFTB2} + \frac{1}{3}\sum_{ab} \Delta q_a^2 \Delta q_b \Gamma_{ab} \qquad (4.3)$$

The last term in equation 4.3, accounts for the third-order contribution, where Γ_{ab} represents the change of γ_{ab} with respect to charge variation.[61]

4.2.2. Computational details

The Gaussian03/09[158] and DFTB+[63] packages were used to perform *ab initio* quantum-chemistry and DFTB calculations, respectively, while the Modes[63] program was used to calculate DFTB vibrational frequencies. The Slater-Koster parameters used in DFTB2 calculations are those of the MIO-1-1[58,61,153] set while DFTB3 calculations were performed with both the MIO-1-1 and 3OB-1-1[83] sets. The ξ parameter in the hydrogen-corrected γ^h function was set to 4.5[91] for the DFTB2-γ^h model and to 4.2[61] and 4.0[83] for the DFTB3 model used in conjunction with the MIO and 3OB parameter sets, respectively. The third-order parameters for DFTB3/MIO calculations were taken from the "fit" set of Ref. 61, except for sulfur-containing systems where parameters from the "calc" set of Ref. 61 were used. The conjugate-gradient method was used in all DFTB geometry optimizations, with a force threshold of 1×10^{-5} au The *ab initio* quantum-chemistry calculations were performed with frozen-core second-order Møller-Plesset (MP2) theory[108] using Dunning's correlation-consistent basis set augmented with diffuse functions, aug-cc-pVTZ.[134] Binary cluster binding energies were also calculated at the coupled cluster with single, double and perturbative triple excitations [CCSD(T)] level[137] with the aug-cc-pVQZ basis set for MP2/aug-cc-pVTZ geometries. *Ab initio* binding energies were corrected for basis set superposition error (BSSE) using the counterpoise method of Boys and Bernardi.[109] Zero-point vibrational energy corrections and binding enthalpies were calculated under the rigid rotor-harmonic oscillator approximation. The reported *ab initio* harmonic vibrational frequencies were scaled with factors of 0.9557 and 1.0634 for high (> 1000 cm^{-1}) and low (< 1000 cm^{-1}) frequencies, respectively.[159]

4.3. Results and discussion

Properties of pure and anionic water clusters with up to four water molecules are presented in this section. Optimized binary cluster structures are shown in Figure 4.1 while hydrogen-bond lengths and angles are collected in Table 4.1. Binary cluster binding energies and enthalpies are listed in Tables 4.2 and 4.3, respectively, while stepwise binding energies for larger clusters are plotted in Figure 4.2. Selected vibrational frequencies are collected in Table 4.4 while all DFTB vibrational frequencies are plotted against their *ab initio* counterparts for comparison in Figure 4.3.

$H_2O(H_2O)_n$. The *ab initio* structure of the $H_2O(H_2O)$ complex, shown in Figure 4.1, is reproduced by all DFTB models. Deviations in hydrogen-bond lengths and angles are less than 0.10 Å and 3° for DFTB2 and 0.12 Å and 7° for DFTB3. Relative to CCSD(T) data, the water dimer binding energy (Table 4.2) is underestimated by DFTB2 by about 1.6 kcal/mol, even though inclusion of the γ^h function improves its accuracy by 1.0 kcal/mol, while DFTB3 reproduces the CCSD(T) value within 0.3 kcal/mol. The decreasing trend of *ab initio* binding energies for larger clusters is reproduced by all models, with DFTB3 yielding the best quantitative agreement. The *ab initio* zero-point-energy corrected binding energy and binding enthalpy are better reproduced by DFTB2-γ^h and DFTB3, and the DFTB3 binding enthalpy is in better agreement with the experimental value. DFTB overestimates vibrational frequencies of the water dimer relative to experimental and *ab initio* data in most cases (*cf*. Table 4.4). The DFTB2 calculated O−H stretching vibrational frequencies exhibit a mean deviation of 80 cm^{-1}

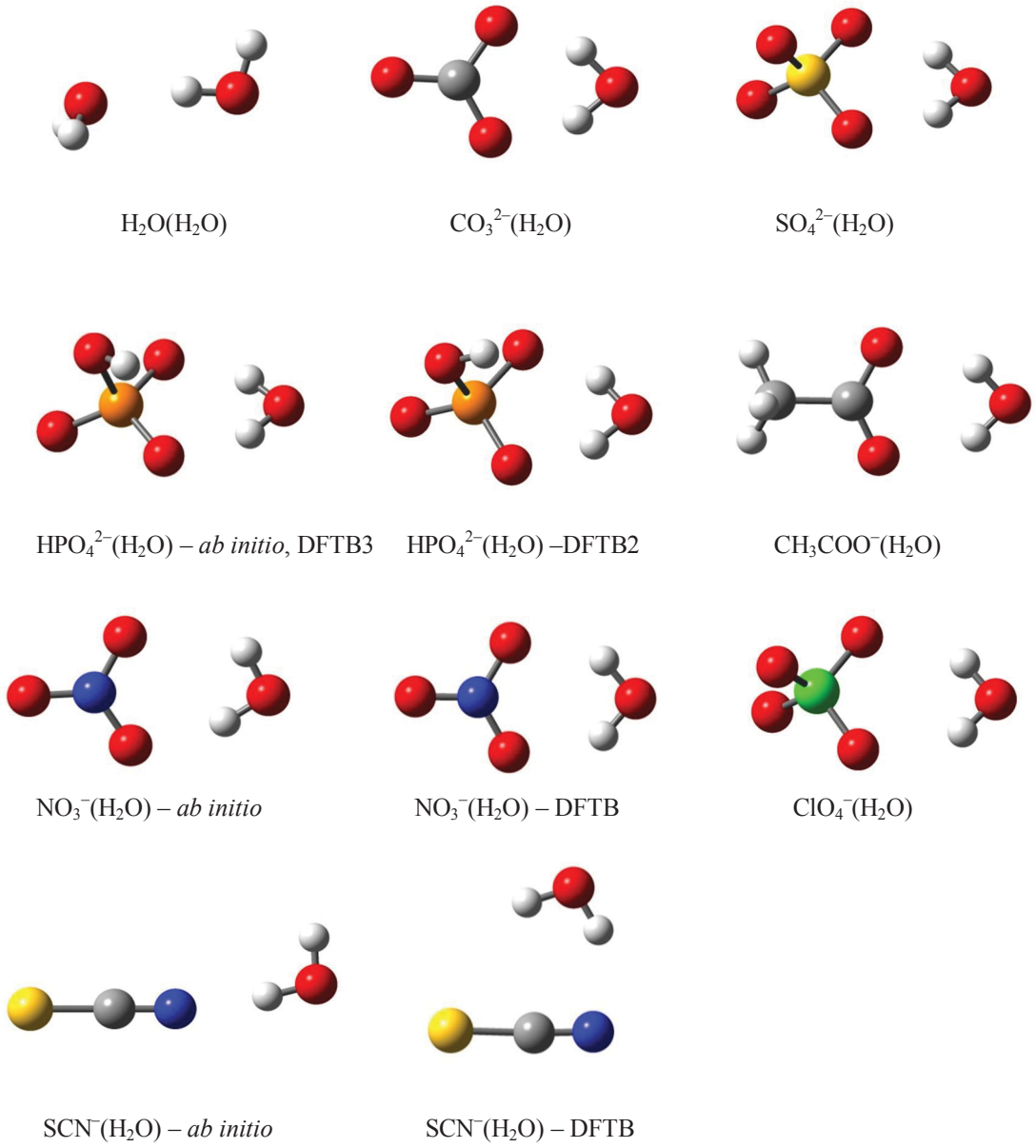

Figure 4.1. Optimized structures of binary clusters. *ab initio* = MP2/aug-cc-pVTZ.

with respect to harmonic frequencies estimated through an empirical scaling of experimental data,[160] as reported previously.[149]

Table 4.1. Selected structural properties of binary clusters

system	*ab initio*[a]	DFTB2	DFTB2-γ^h	DFTB3/MIO	DFTB3/3OB
		Bond Length (Å)			
$H_2O(H_2O)$	1.95	1.89	1.85	1.83	1.91
$CO_3^{2-}(H_2O)$	1.73	1.65	1.62	1.70	1.62
$SO_4^{2-}(H_2O)$	1.84	1.77	1.74	1.71	
$HPO_4^{2-}(H_2O)$	1.83	1.73	1.70	1.75	
$CH_3COO^-(H_2O)$	1.96	1.84	1.81	1.80	1.83
$NO_3^-(H_2O)$	1.85, 2.33	1.92	1.88	1.88	1.92
$ClO_4^-(H_2O)$	2.11	1.99	1.96	1.91	1.99
$SCN^-(H_2O)$	1.82	2.03	2.03	2.03	
Δ[b]		0.10	0.12	0.12	0.09
		Bond Angles (°)			
$H_2O(H_2O)$	171.7	174.5	174.4	176.5	178.4
$CO_3^{2-}(H_2O)$	150.7	152.0	153.1	148.1	151.0
$SO_4^{2-}(H_2O)$	150.2	151.3	151.9	151.4	
$HPO_4^{2-}(H_2O)$	151.8	153.4	154.1	149.7	
$CH_3COO^-(H_2O)$	144.7	143.7	144.1	142.8	142.9
$NO_3^-(H_2O)$	161.7, 123.5	140.5	140.8	139.4	140.1
$ClO_4^-(H_2O)$	143.7	143.0	143.2	142.7	141.3
$SCN^-(H_2O)$	173.4	146.9	146.1	144.8	
Δ		7.0	7.3	8.0	6.5

a) Results from MP2/aug-cc-pVTZ calculations.
b) Δ is the absolute mean deviation of the DFTB data from *ab initio* reference data in Å and ° for bond lengths and angles, respectively.

$CO_3^{2-}(H_2O)_n$. The *ab initio* optimized structure of $CO_3^{2-}(H_2O)$ which is a symmetric complex with two approximately equal hydrogen-bond lengths (*cf.* Figure 4.1) is reproduced by DFTB models. However, all models underestimate the *ab initio* hydrogen-bond lengths by about 0.04–0.11 Å while deviations in the bond angles are about 0.03–2.6° (Table 4.1). Inclusion of the γ^h function in DFTB2 decreases bond lengths and angles as the function contains a damping term to account for the smaller size of the hydrogen atom. The shorter bond lengths predicted by DFTB result in overestimated binding energies compared to *ab initio* values. DFTB2 overestimates the CCSD(T) value by 0.3 kcal/mol but inclusion of the γ^h function increases the binding energy such that DFTB2-γ^h overestimates the CCSD(T) value by 5.5 kcal/mol (*cf.* Table 4.2).

Table 4.2. Binding energies of binary clusters

clusters	binding energy[a]	*ab initio*[b]	DFTB2	DFTB2-γ[h]	DFTB3/MIO	DFTB3/3OB
$H_2O(H_2O)$	D_e	5.2 (5.1)				
	$D_{e/BSSE}$	4.7 (4.9)	3.3	4.2	4.9	4.6
	$D_{0/BSSE}$	2.6	1.7	2.5	3.1	2.9
$CO_3^{2-}(H_2O)$	D_e	37.6 (37.4)				
	$D_{e/BSSE}$	36.3 (36.7)	39.0	42.2	37.5	40.5
	$D_{0/BSSE}$	34.2	39.0	42.2	35.0	38.9
$SO_4^{2-}(H_2O)$	D_e	29.9 (29.9)				
	$D_{e/BSSE}$	28.6 (29.2)	25.4	29.0	32.1	
	$D_{0/BSSE}$	26.3	23.5	27.8	30.0	
$HPO_4^{2-}(H_2O)$	D_e	31.9 (31.9)				
	$D_{e/BSSE}$	30.6 (31.4)	30.0	34.2	31.8	
	$D_{0/BSSE}$	28.1	28.2	32.1	29.6	
$CH_3COO^-(H_2O)$	D_e	19.8 (19.9)				
	$D_{e/BSSE}$	18.9 (19.5)	16.4	19.2	21.4	21.0
	$D_{0/BSSE}$	16.5	14.9	17.0	18.7	18.5
$NO_3^-(H_2O)$	D_e	16.0 (16.0)				
	$D_{e/BSSE}$	15.3 (15.7)	12.9	15.1	16.2	15.9
	$D_{0/BSSE}$	13.2	11.6	13.6	14.1	14.4
$ClO_4^-(H_2O)$	D_e	12.9 (12.8)				
	$D_{e/BSSE}$	12.0 (12.4)	9.9	11.5	13.1	12.7
	$D_{0/BSSE}$	10.2	8.4	9.8	11.7	11.0
$SCN^-(H_2O)$	D_e	13.8 (13.2)				
	$D_{e/BSSE}$	13.0 (12.8)	10.0	11.3	12.5	
	$D_{0/BSSE}$	11.3	7.7	9.1	10.0	
Δ[c]			2.3	1.6	0.9	1.2

a) D_e is the uncorrected binding energy, $D_{e/BSSE}$ is the binding energy corrected for basis set superposition error, $D_{0/BSSE}$ is the binding energy corrected for zero-point energy and basis set superposition error. All values are in kcal/mol. b) Results from MP2/aug-cc-pVTZ calculations, with CCSD(T)/aug-cc-pVQZ//MP2/aug-cc-pVTZ results in parenthesis. c) Δ is the absolute mean deviation of the DFTB data from CCSD(T) data in kcal/mol.

The DFTB3/MIO value deviates from the reference data by only 0.8 kcal/mol while for DFTB3/3OB the deviation increases to 3.8 kcal/mol. As shown in Figure 4.2, all DFTB binding energies parallel the *ab initio* ones for larger clusters and deviations significantly decrease by increasing cluster size such that DFTB3 values lie within 0.5 kcal/mol of their *ab initio* counterparts. The *ab initio* zero-point-energy corrected binding energy and binding enthalpy (*cf.* Tables 4.2 and 4.3) are best reproduced by the DFTB3/MIO model, with an overestimation of about 1 kcal/mol. It should be noted that the $CO_3^{2-}(H_2O)$

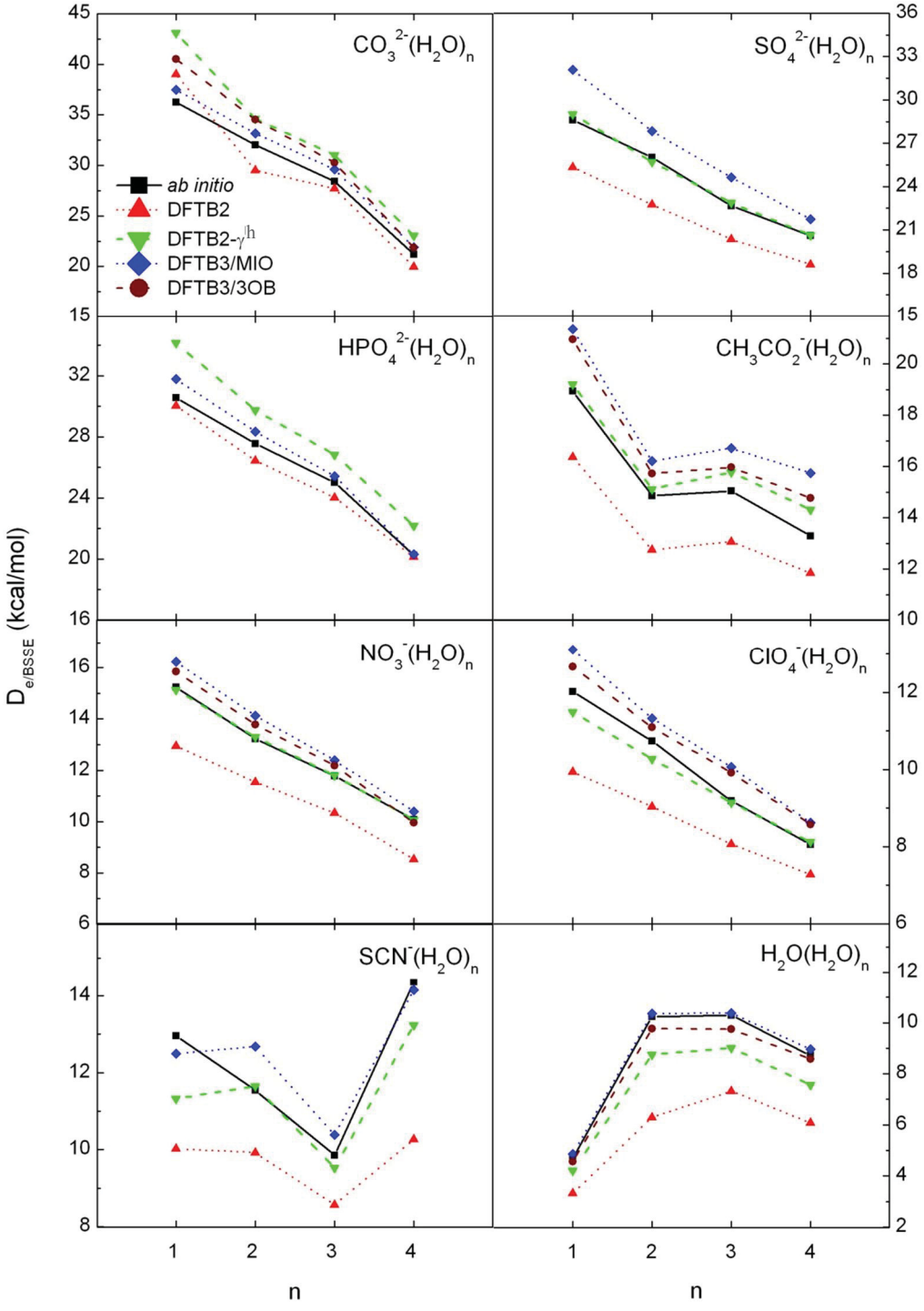

Figure 4.2. Stepwise binding energies of ion–water clusters. *ab initio* = MP2/aug-cc-pVTZ.

Table 4.3. Binding enthalpies of binary clusters[a]

system	*ab initio*[b]	DFTB2	DFTB2-γ^h	DFTB3/MIO	DFTB3/3OB	experiment
$H_2O(H_2O)$	3.1	2.0	2.9	3.5	3.2	3.6[c]
$CO_3^{2-}(H_2O)$	35.1	37.9	43.2	36.1	39.9	
$SO_4^{2-}(H_2O)$	27.1	24.5	28.5	31.1		
$HPO_4^{2-}(H_2O)$	29.0	29.5	33.5	30.6		
$CH_3COO^-(H_2O)$	17.2	15.5	17.9	19.6	19.3	16.4[d], 15.8[e]
$NO_3^-(H_2O)$	13.7	12.1	14.2	14.9	14.8	14.1[d], 14.6[f]
$ClO_4^-(H_2O)$	10.5	8.7	10.3	12.1	11.5	11.8[d]
$SCN^-(H_2O)$	11.7	8.4	9.8	10.8		
Δ[g]		1.9	2.2	1.6	1.8	

a) All values are in kcal/mol. b) Results from MP2/aug-cc-pVTZ calculations. c) From Ref. 161 (measured in the temperature range 358–386 K). d) From Ref. 32. e) From Ref. 162. f) From Ref. 163. g) Δ is the absolute mean deviation of the DFTB data from *ab initio* reference data in kcal/mol.

cluster has the highest binding energy of the anion series due to the higher charge density on the oxygen atoms of carbonate. Formation of strong hydrogen bonds in $CO_3^{2-}(H_2O)$ result in a red-shift of the water O−H stretching vibrational frequency relative to that of free water, but this shift is overestimated by about 600 cm^{-1} for DFTB2 and 110 cm^{-1} for DFTB3, in average, compared to *ab initio* data (Table 4.4). Thus, DFTB3 performs better in predicting vibrational frequencies (*cf*. Figure 4.3), while inclusion of γ^h has a marginal effect.

$SO_4^{2-}(H_2O)_n$. The *ab initio* optimized structure of $SO_4^{2-}(H_2O)$ cluster is also symmetric with two equal hydrogen bonds (*cf*. Figure 4.1). This structure is reproduced by both DFTB2 and DFTB3 models, and bond lengths are underestimated by about 0.07 and 0.13 Å, respectively (Table 4.1). However inclusion of the γ^h function in DFTB2 increases the deviation to 0.1 Å. Bond angles are only overestimated by 1° with both models. DFTB2

Table 4.4. Selected vibrational frequencies of binary clusters[a]

clusters	modes[b]	*ab initio*[c]	DFTB2	DFTB2-γ^h	DFTB3/MIO	DFTB3/3OB	experiment
$H_2O(H_2O)$	ν_{OHs}	3761, 3742	3965, 3887	3998, 3922	4001, 3942	3640, 3551	3714, 3698
	ν_{OHa}	3645, 3554	3716, 3555	3746, 3581	3747, 3596	3895, 3848	3626, 3548[d]
	ν_{HOH}	1577, 1557	1524, 1513	1486, 1472	1413, 1411	1389, 1378	
$CO_3^{2-}(H_2O)$	ν_{OHs}	3075	2458	2509	3058	2834	
	ν_{OHa}	2912	2593	2621	3208	2929	
	ν_{HOH}	1614	1376	1385	1530	1496	
$SO_4^{2-}(H_2O)$	ν_{OHs}	3325	3008	3002	3085		
	ν_{OHa}	3267	3241	3213	3085		
	ν_{HOH}	1636	1559	1503	1521		
$HPO_4^{2-}(H_2O)$	ν_{OHs}	3262	2768	2801	3183		
	ν_{OHa}	3199	3002	3013	3378		
	ν_{HOH}	1642	1528	1510	1515		
$CH_3COO^-(H_2O)$	ν_{OHs}	3462	3261	3293	3369	3319	3188–3506[e]
	ν_{OHa}	3456	3500	3522	3576	3520	
	ν_{HOH}	1629	1556	1553	1522	1482	
$NO_3^-(H_2O)$	ν_{OHs}		3414	3431	3482	3435	
	ν_{OHa}	3382, 3663	3658	3670	3706	3656	
	ν_{HOH}	1624	1570	1549	1520	1475	1324, 1353[f]
$ClO_4^-(H_2O)$	ν_{OHs}	3635	3786	3801	3772	3731	
	ν_{OHa}	3587	3538	3556	3539	3499	
	ν_{HOH}	1609	1570	1542	1483	1477	
$SCN^-(H_2O)$	ν_{OHs}	3729	3859	3872	3873		
	ν_{OHa}	3253	3634	3649	3655		
	ν_{HOH}	1613	1647	1614	1575		
Δ^g			148	170	120	143	

a) All values are in cm^{-1}. b) OHs = symmetric O−H stretch; OHa = asymmetric O−H stretch; HOH = water bend. c) Results from MP2/aug-cc-pVTZ calculations. d) From Ref. 160. e) From Ref. 164. f) From Ref. 165. g) Δ is the absolute mean deviation of the DFTB data from *ab initio* reference data in cm^{-1}.

underestimates the CCSD(T) binding energy by 3.8 kcal/mol while inclusion of the γ^h function produces a very accurate value only 0.2 kcal/mol smaller than the CCSD(T) one. The deviation for DFTB3 is about 3 kcal/mol for the binary cluster but the model performs better for larger cluster sizes (*cf*. Figure 4.2). DFTB2-γ^h predicts very good

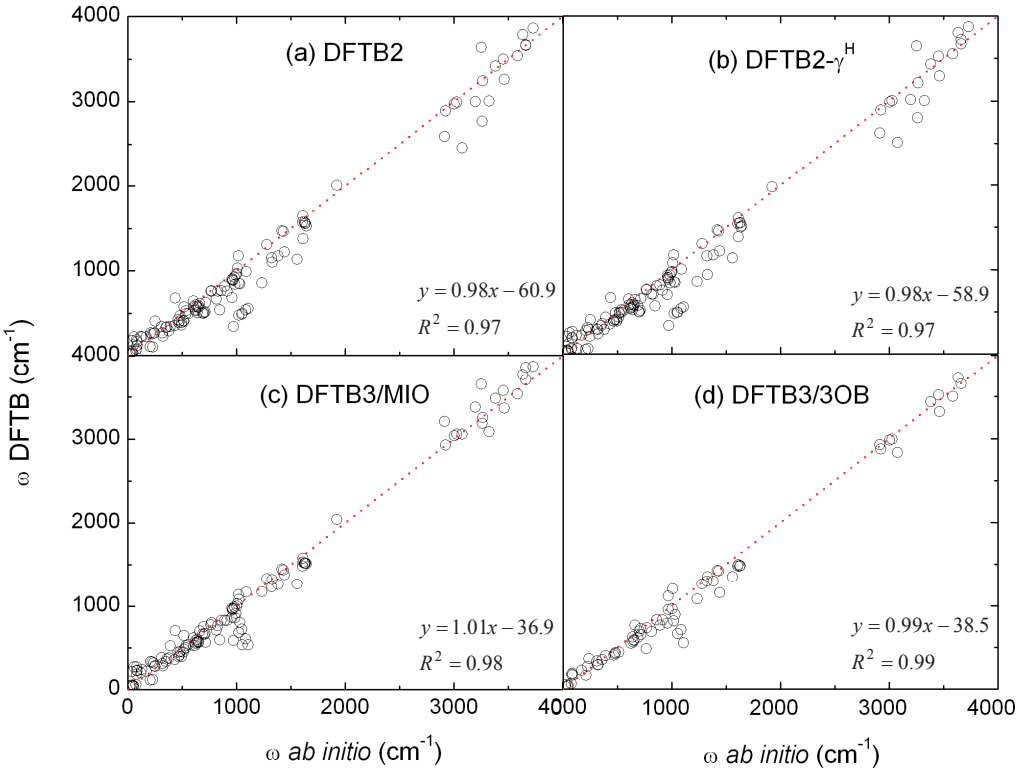

Figure 4.3. Calculated harmonic vibrational frequencies of binary clusters. a) DFTB2, b) DFTB2-γ^h, c) DFTB3/MIO, d) DFTB3/3OB. Dotted lines represent a perfect correlation.

stepwise binding energies for the larger clusters, and a better zero-point-energy corrected binding energy and binding enthalpy for the binary complex. The water O−H stretching mode in $SO_4^{2-}(H_2O)$ is also considerably red-shifted due to the formation of strong hydrogen bonds, and the magnitude of the *ab initio* red-shift is overestimated by about 330 and 305 cm^{-1} by DFTB2 and DFTB3, respectively (Table 4.4).

$HPO_4^{2-}(H_2O)_n$. The optimized *ab initio* structure of $HPO_4^{2-}(H_2O)$ is also symmetric with two equal hydrogen bonds in which the O−H bond of HPO_4^{2-} is eclipsed with respect to the P−O bond, as shown in Figure 4.1. However the DFTB2 minimum-energy structure is a staggered stricture, also shown in Figure 1. The energy difference between the

staggered and eclipsed structure is ~ 0.5 kcal/mol for DFTB2, which is hardly significant compared to the magnitude of the cluster binding energy. Both DFTB3 models reproduce the eclipsed *ab initio* structure. Deviations in the DFTB2 bond lengths and angles are about 0.10 Å and 1.6°, respectively, while inclusion of the γ^h function increases the deviation of bond lengths to 0.13 Å and 2.3° (Table 4.1). The corresponding deviations are only about 0.08 Å and 2° with DFTB3. DFTB models reproduce the CCSD(T) binding energy of $HPO_4^{2-}(H_2O)$ with smaller deviations compared to previous systems (*cf*. Table 4.2), while inclusion of the γ^h function in DFTB2 causes overestimations. DFTB3 gives the best value for the binary cluster binding energy, with a deviation from the CCSD(T) value of only 0.4 kcal/mol. The decreasing trend of the *ab initio* stepwise binding energies in larger clusters (Figure 4.2) is reproduced by all models, with DFTB3 yielding the best agreement. DFTB3 model better reproduces the *ab initio* zero-point-energy corrected binding energy and binding enthalpy of the binary complex. The significant red-shift in the *ab initio* water O−H stretching vibrational frequencies is reproduced but again overestimated by about 485 and 130 cm^{-1} with DFTB2 and DFTB3, respectively. Overall, DFTB3 more faithfully reproduces *ab initio* data (*cf*. Figure 4.3).

$CH_3COO^-(H_2O)_n$. Both DFTB models reproduce the *ab initio* $CH_3COO^-(H_2O)$ symmetric structure with two equal hydrogen bond lengths (*cf*. Figure 4.1), but the calculated hydrogen-bond lengths are shorter by about 0.12–0.16 Å. The magnitude of this underestimation is slightly larger than those for previously discussed anions, but the deviations of the bond angles are similar, with values about 0.6–1.9°. DFTB2 underestimates the CCSD(T) binding energy by about 3.1 kcal/mol but inclusion of the γ^h

function improves its accuracy to within 0.3 kcal/mol (Table 4.2). Both DFTB3 models overestimates the CCSD(T) value by less than 1 kcal/mol, while DFTB2-γ^h and DFTB3/3OB yield better stepwise binding energies for larger clusters (*cf*. Figure 4.2). DFTB2-γ^h better reproduces the binary cluster *ab initio* zero-point-energy corrected binding energy and binding enthalpy, though the model overestimates the experimental binding enthalpy by about 2 kcal/mol. The experimental infrared spectrum of $CH_3COO^-(H_2O)$ exhibits complex features with five peaks in the water O−H stretching region,[164] while *ab initio* calculations yield only two approximately equal values for the symmetric and asymmetric O−H stretching frequencies, a discrepancy that may stem from anharmonic effects. DFTB models also predict two distinct frequencies for the symmetric and asymmetric O−H stretching modes, in agreement with *ab initio* data, and the accuracy of the predicted red-shifts is much better than that for doubly-charged anions, with overestimates of only 215 cm^{-1} for DFTB2 and 135 cm^{-1} for DFTB3, presumably due to the weaker hydrogen bonds in $CH_3COO^-(H_2O)$. Overall, DFTB3 again appears to perform the best of all DFTB models (*cf*. Figure 4.3).

$NO_3^-(H_2O)_n$. In contrast to the binary clusters discussed so far, the *ab initio* optimized structure of $NO_3^-(H_2O)$ is asymmetric with two hydrogen bonds that differ in length by 0.48 Å (*cf*. Figure 4.1), a feature also reported for $NO_2^-(H_2O)$, possibly because of the short distance between the terminal oxygen atoms of nitrate, compared to other anions, which may prevent a symmetric structure due to the higher strain involved with the formation of two nonlinear hydrogen bonds.[164] Interestingly, Hartree-Fock calculations predict a symmetric structure, indicating that accurate treatment of electron correlation is

necessary to obtain the asymmetric structure.[166] Both DFTB models predict a symmetric structure with two equal hydrogen-bond lengths close to the shorter *ab initio* bond length (1.85 Å), within 0.03–0.07 Å. DFTB2 underestimate the CCSD(T) binding energy by about 3 kcal/mol, but inclusion of the γ^h function reduces the deviation to 0.6 kcal/mol, while DFTB3 reproduce the CCSD(T) binding energy within 0.5 kcal/mol. All models reproduce the trend of *ab initio* stepwise binding energies, with smaller deviations observed for the larger clusters, and DFTB2-γ^h and DFTB3 performing the best (*cf.* Figure 4.2). The latter models also better reproduce the *ab initio* zero-point-energy corrected binding energy and experimental binding enthalpy of the binary complex (Tables 4.2 and 4.3, respectively). The discrepancy between the DFTB and *ab initio* structures mentioned above appears to have a negligible effect on the accuracy of the predicted binding energies, particularly in larger clusters. The asymmetric structure of $NO_3^-(H_2O)$ results in two differently red-shifted *ab initio* O−H stretching frequencies, by only 10 cm^{-1} for the longer hydrogen bond and by 271 cm^{-1} for the shorter hydrogen bond, relative to that of the free water molecule (*cf.* Table 4.4). This feature is obviously not reproduced by DFTB due to the symmetric structure such that DFTB models predict redshifts of about 300 cm^{-1}. DFTB3 again performs slightly better, predicting a water bending frequency in good agreement with the experimental value.

$ClO_4^-(H_2O)_n$. The *ab initio* optimized symmetric structure of $ClO_4^-(H_2O)$ is reproduced by all DFTB models with deviations in hydrogen-bond lengths and angles of about 0.12 Å and 0.6° for DFTB2 and 0.12 Å and 2.3° for DFTB3, respectively. However, inclusion of the γ^h function in DFTB2 slightly increases these deviations. DFTB2 underestimates –

again – the CCSD(T) binding energy by 2.5 kcal/mol and inclusion of the γ^h function improves the results by about 1.5 kcal/mol. The DFTB3 results are in a quantitative agreement with the CCSD(T) binding energy, with deviations of about 0.3–0.7 kcal/mol. The decreasing trend of the *ab initio* stepwise binding energies for larger clusters is reproduced by all models, with DFTB2-γ^h and DFTB3 performing the best (*cf*. Figure 4.2). These models also reproduce the *ab initio* zero-point-energy corrected binding energy and binding enthalpy of the binary complex and the experimental binding enthalpy with better accuracy. The O−H stretching vibrational frequencies of $ClO_4^-(H_2O)$ are also red-shifted compared to free water and DFTB predicts red-shifts within 90–100 cm^{-1} of their *ab initio* counterpart (*cf*. Table 4.4). This good agreement is presumably due to the weaker hydrogen bonds between water and perchlorate.

$SCN^-(H_2O)_n$. The *ab initio* optimized structure of $SCN^-(H_2O)$ has an almost linear hydrogen bond between the water hydrogen and the thiocyanate nitrogen atom, while all DFTB models predict a structure with two hydrogen bonds between the water hydrogen atoms and the terminal atoms of SCN^- (Figure 4.1). As a result, all DFTB models overestimate the *ab initio* H···N hydrogen-bond length in the binary complex by about 0.21 Å. However, the $SCN^-(H_2O)_4$ *ab initio* structure is reproduced by DFTB (not shown), presumably due to the good performance of DFTB in describing water–water interactions. The discrepancy between the structural features of the binary complex does not appear to have significant effects on the cluster binding energies, as pointed out earlier for nitrate. DFTB2 underestimates the CCSD(T) binding energies by 2.8 kcal/mol while inclusion of the γ^h function improves its accuracy by about 1.3 kcal/mol (Table

4.2). The DFTB3 value is within 0.3 kcal/mol of the CCSD(T) one. Moreover, the trend of *ab initio* stepwise binding energies for larger clusters is qualitatively reproduced by all DFTB models (Figure 4.2), with DFTB2-γ^h and DFTB3 performing the best. The latter also reproduce the *ab initio* zero-point-energy corrected binding energy and the binding enthalpy of the binary complex with the best accuracy (*cf*. Tables 4.2 and 4.3). Formation of a single hydrogen bond structure in $SCN^-(H_2O)$ results in two distinct *ab initio* O−H stretching vibrational frequencies, with the free O−H stretching frequency red-shifted by only 76 cm^{-1} and the other hydrogen-bonded O−H stretching frequency considerably red-shifted by 400 cm^{-1} relative to that of free water. The magnitude of the red-shift in this case is comparable to those observed for doubly charged anions, reflecting the strength of the single hydrogen bond in $SCN^-(H_2O)$. The DFTB O−H stretching frequencies are also red-shifted, but by about 100–150 cm^{-1}.

4.4. Conclusions

The accuracy of various DFTB models in predicting hydration properties of anionic-water clusters has been benchmarked for the polyatomic anions of the Hofmeister series. All DFTB models reproduce the structural features predicted by *ab initio* quantum-chemistry in most cases. The DFTB model systematically underestimates *ab initio* hydrogen-bond lengths by about 0.10 Å. The average deviations in the binary cluster binding energies with respect to CCSD(T) values are about 2 and 1 kcal/mol for the DFTB2 and DFTB3 models, respectively. Inclusion of the γ^h function generally improves DFTB2 binding energies by about 0.7 kcal/mol, although the accuracy of the predicted bond lengths and angles is not improved by this correction. Overall, the stepwise binding

energies calculated by the DFTB2-γ^h and DFTB3 models are in a good agreement with *ab initio* values, with deviations within the limit of chemical accuracy (about 1 kcal/mol), in particular for larger clusters. Harmonic vibrational frequencies are moderately underestimated by DFTB models, though developing appropriate scaling factors might slightly improve their accuracy. Overall, the DFTB2 and DFTB3 models tend to underestimate *ab initio* frequencies, but to a lesser extent for the latter model. Average deviations of the calculated vibrational frequencies are less than 130 and 100 cm^{-1} for DFTB2 and DFTB3, respectively, compared to *ab initio* values. Results presented here demonstrate that the self-consistent-charge DFTB model accurately describes various properties of the anionic water clusters and therefore might be used as a reliable model for investigating larger clusters.

Chapter 5

A Computational Investigation of the Hydration of the Polyatomic Anions of the Hofmeister Series in Water Clusters

To be submitted as:

S. Jahangiri, G. H. Peslherbe, *Phys. Chem. Chem. Phys.* 2013

5.1. Introduction

The preferential interactions between water and charged species regulate a broad variety of natural phenomena ranging from protein solubility and stability in biological systems[4-6] to heterogeneous nucleation in atmospheric droplets.[1,2] Despite the strong interactions between water molecules and these ions, it has been proven by means of recent experimental and theoretical techniques that large and polarizable (soft) anions are highly concentrated at aqueous interfaces.[121] This is in contradiction to the traditional picture of electrolyte solutions which assumes an ion-free layer of water molecules at the surface of such solutions.[27] Moreover, the literature contains numerous reports of the higher propensity of soft anions for water/organic[72] and water/macromolecule[167] interfaces, as well as interfaces between water and organic molecules with polar[168] and charged[169] head groups.

The seemingly inconsistent hydrophobic behavior of soft ions, which was first observed in the asymmetric hydration of larger halides in water clusters,[49,53,71] may provide hints to explain the specific effects of ions in aqueous solutions.[22,25] Such effects, which are usually referred to as the Hofmeister effect,[19] represent the specific ability of various ions, e.g. halides and polyatomic anions such as carbonate, sulfate, hydrogen phosphate, acetate, nitrate, perchlorate, and thiocyanate, to change the physical properties of solutions according to a general trend that is common to many solution properties.[143] The increased interfacial adsorption or depletion of these ions may also have important consequences on their chemistry in various contexts. For instance, the ability of carbonate, a carbon dioxide carrier in the liquid phase, to separate carbon dioxide from flue gas emissions[170] might depend significantly on its interfacial presence or absence in

separating membranes. Similarly, the uptake of carbon dioxide by the ocean and atmospheric droplets may depend on the availability of carbonate at the aqueous interface. The hydration extent of sulfate and nitrate, which are abundant in atmospheric aerosols,[171] may also influence their behavior in such systems.[172-174] It has been shown that the increased propensity of perchlorate for the surface affects the evaporation rate and stability of water clusters.[175] The diffusion of biologically relevant ions, such as phosphates[176] and thiocyanate,[177] to the cell membrane requires their dehydration at the membrane surface as a first step; a process that might be further facilitated for anions with a higher affinity for the interface.[45] Moreover, the differential propensity of anions for partial hydration at interfaces could be used to design effective anion-recognition agents which are of particular interest in separation technology.[178] Therefore, the much needed progress towards elucidating the mechanism of reaction and interaction of hydrated ions at the molecular level requires a fundamental understanding of their hydration behavior, and particularly their hydration extent. This highlights the need for a comprehensive investigation of a broad range of ions with varying charge, size, geometry and polarizability.

The extent of hydration of polyatomic ions has been previously investigated by means of experimental and computational techniques.[28,65,179] In particular, a number of molecular dynamics (MD) simulations with polarizable force fields have been reported,[180-188] although such simulations suffer from some limitations.[47,180,181] On the other hand, simulations employing quantum-chemistry models to describe interatomic interactions are scarce due to the prohibitive computational cost associated with first-principles calculations. Jungwirth *et al*. investigated the hydration of sulfate in a cluster

containing 13 water molecules by *ab initio* MD (AIMD) simulations and reported complete hydration of the ion with all water molecules accommodated in the first hydration shell.[48] Analogous simulations were carried out for nitrate in a cluster containing 10 water molecules, in which case surface solvation was observed to be more favorable.[47] The hydration of perchlorate was also investigated by AIMD simulations, confirming the tendency of the anion to undergo partial hydration at the air–water interface observed experimentally.[189]

In this article, we have implemented the self-consistent-charge density-functional tight-binding model with third-order extension (DFTB3), an approximate quantum-chemistry method based on density-functional theory, in MD simulations to systematically investigate the hydration behavior of the polyatomic anions of the Hofmeister series in water clusters. The DFTB3 model has been found to predict the structural and energetic properties of anionic clusters with good accuracy compared to high-level *ab initio* quantum-chemistry methods, but at a significantly reduced computational cost (see Chapter 4). The ability of the method to describe the hydration of halide anions in water clusters has also been benchmarked; the model was found to accurately predict the extent of hydration of halides, including the increased propensity of the larger halides for the cluster interfacial regions, in agreement with recent computational and experimental results (see Chapter 3). Moreover, the model was also successfully implemented in MD simulations to describe the behavior of alkyl-chlorides at aqueous interfaces.[190] This brings confidence in this approach to systematically investigate the hydration of the Hofmeister ions in water clusters. The article is organized as follows: the computational procedure is described in Section 5.2; results are presented

and discussed in Sections 5.3 and 5.4, respectively, and concluding remarks follow in Section 5.5.

5.2. Computational procedure

Simulations were performed on water clusters containing 12, 24 and 48 water molecules and each of the polyatomic anions mentioned earlier. The spatial probability distributions of the ions inside clusters were obtained from potential of mean force (PMF) calculations. Interatomic interactions were described by the DFTB3 model with parameters taken from the MIO-1-1[58,61,153] and 3OB-1-1[83] sets. All systems were equilibrated for 60 ps prior to data collection in the subsequent 60 ps. The temperature was held constant at 250 K, which is the optimal temperature to minimize water evaporation without simulating the solid phase. The velocity Verlet algorithm with a time step of 1 fs was used for integrating the equations of motions. The umbrella sampling method[125] was used to guarantee sufficient sampling and the weighted histogram analysis method (WHAM)[126] was used to remove the biasing potentials. *Ab initio* quantum-chemistry calculations were performed to calculate the polarizability of the ions with second-order Møller-Plesset perturbation theory (MP2)[108] and Dunning's augmented correlation consistent aug-cc-pVTZ[102,134] basis set using the Gaussian09 suite of programs. All simulations were performed with our in-house MD engine and DFTB3 calculations were carried out with the DFTB+ code.[63] The WHAM program was used to calculate the final probability distributions.[130]

5.3. Simulation results

Results of MD simulations are presented in this Section. More specifically, the hydration extent of the ions obtained from PMF calculations are presented in Section 5.3.1, while spatial probability distributions of the water molecules around the ions are presented to provide additional insight into the hydration process in Section 5.3.2.

5.3.1. Hydration extent of the polyatomic anions

The spatial probability distributions of the ions with respect to the water cluster interior are presented in Figure 5.1. Inspection of Figure 5.1a indicates that carbonate, sulfate and hydrogen phosphate are mostly localized in regions close to the center of a cluster containing 12 water molecules. However, the affinity of hydrogen phosphate for the cluster core is less pronounced than for carbonate and sulfate, presumably due to the presence of the OH group in HPO_4^{2-}, which carries a less negative charge compared to the terminal oxygen atoms of the other ions, resulting in weaker interactions with water molecules. Snapshots of typical conformations sampled during the simulations are presented in Figure 5.2; for hydrogen phosphate, the PO_3 pyramidal moiety of the ion is clearly fully hydrated inside the cluster while the OH group points towards the cluster surface. However, the strong hydration of PO_3 moiety prevails and the ion tends to be fully hydrated in larger clusters as shown below.

The singly-charged anions have a much higher affinity for the cluster surfaces in a cluster containing 12 molecules, as evident from Figure 5.1a. For acetate, the carboxylate group is fully hydrated by the cluster due to the high charge density of the terminal oxygen atoms, but the hydrophobic methyl group drives the anion

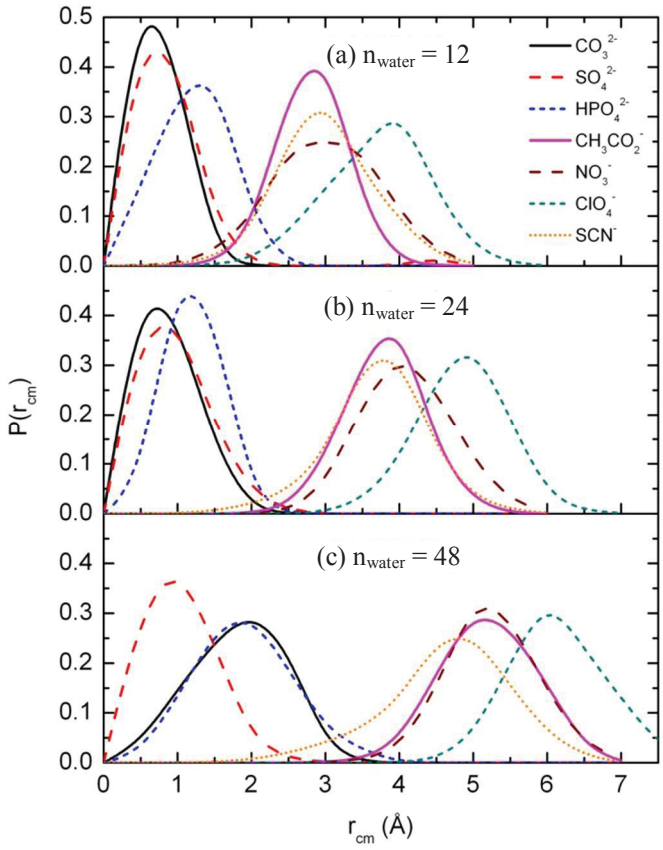

Figure 5.1. Probability distributions of the distance between polyatomic anions and the water cluster centers of mass in clusters containing (a) 12, (b) 24, (c) 48 water molecules. Calculated from PMF results obtained from DFTB3-MD simulations at 250 K.

towards the cluster surface (*cf*. Figure 5.2). The planar nitrate anion adopts a position tangential to the cluster surface to maximize the number of hydrogen bonds formed between the nitrate oxygen atoms and the water hydrogen atoms (*cf*. Figure 5.2). Perchlorate has the highest affinity for the cluster surface, as evident from Figure 5.1. In fact, both cluster structures with all the oxygen atoms of perchlorate hydrogen-bonded to water molecules (Figure 5.2f) and structures with free perchlorate oxygen atoms at the cluster surface (Figure 5.2g) were frequently observed during the simulations. Similarly to the case of nitrate, both the terminal nitrogen and sulfur atoms of thiocyanate are

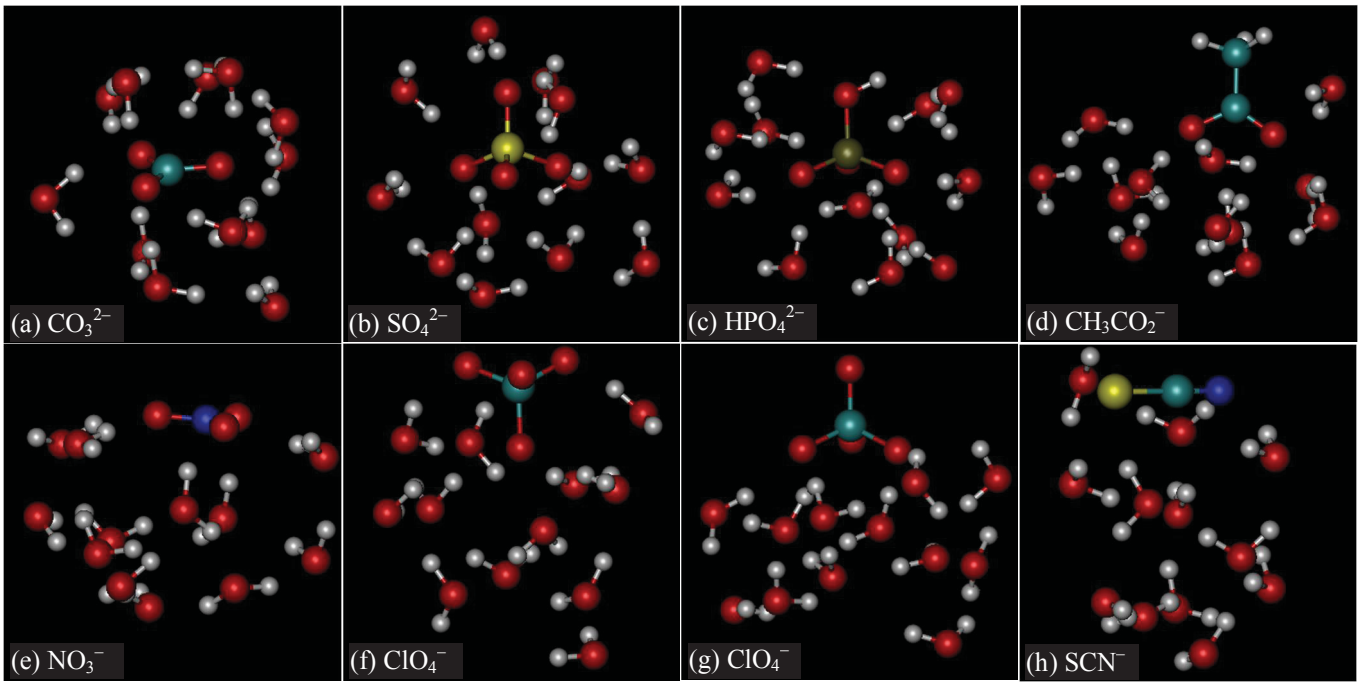

Figure 5.2. Snapshots of typical cluster conformations sampled during MD simulations of ionic clusters containing 12 water molecules and (a) CO_3^{2-}, (b) SO_4^{2-}, (c) HPO_4^{2-}, (d) $CH_3CO_2^-$, (e) NO_3^-, (f) and (g) ClO_4^-, and (h) SCN^-. Obtained from DFTB3-MD simulations at 250 K.

involved in hydrogen bonds with water molecules, and therefore thiocyanate tends to align horizontally with the cluster surface (*cf*. Figure 5.2).

For $(H_2O)_{24}$ and $(H_2O)_{48}$ clusters containing 24 and 48 molecules (*cf*. Figures 5.1b and 5.1c, respectively), the situation is analogous: the doubly-charged carbonate, sulfate and hydrogen phosphate are fully hydrated inside the cluster, with distributions of ion-to-water-cluster-center distances peaking at 0–3 Å, while the singly-charged acetate, nitrate, perchlorate, and thiocyanate tend to be located towards the cluster surface with distributions of ion-to-water-cluster-center distances peaking at 3–7 Å. Perchlorate migrates even further out towards the cluster surface for both cluster sizes. These findings are further confirmed by inspection of the calculated distances between the ions and the

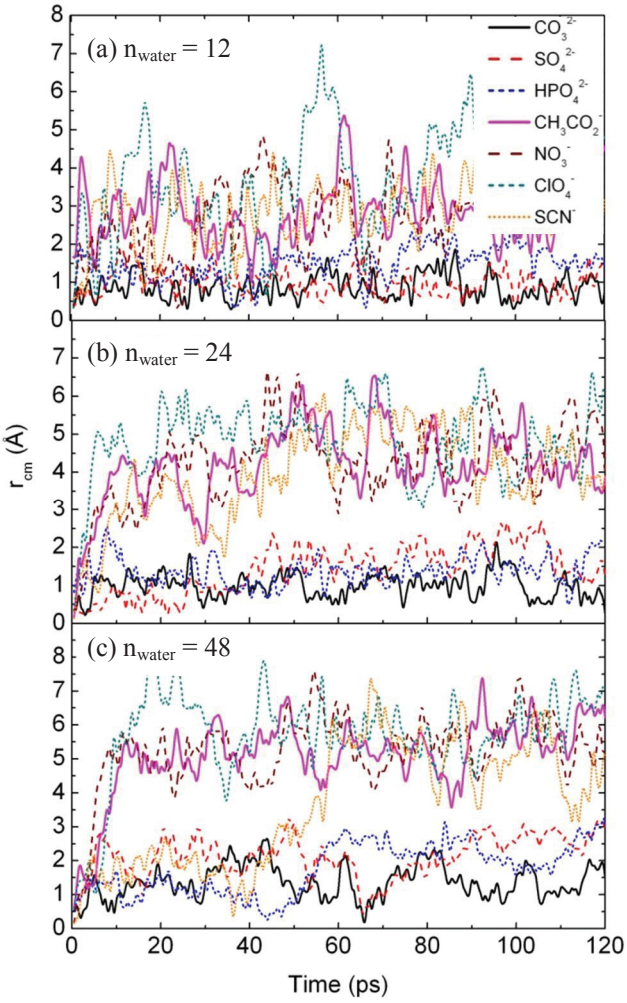

Figure 5.3. The distances between polyatomic anion and water cluster centers of mass as a function of simulation time for clusters containing (a) 12, (b) 24, (c) 48 water molecules. Obtained from DFTB3-MD simulations at 250 K.

water cluster centers of mass (r_{cm}) along non-constrained MD simulation trajectories, which are shown in Figure 5.3.

Inspection of Figure 5.3a reveals that the calculated distances between the doubly-charged ions and the centers of water clusters containing 12 water molecules exhibit small fluctuations around 1 Å over the whole simulation period, which clearly indicates that carbonate, sulfate and hydrogen phosphate prefer full hydration inside the cluster.

Table 5.1. Anion–water stepwise binding energies (D_e) of clusters containing 1–4 water molecules[a]

ion	$D_e^{0,1}$	$D_e^{1,2}$	$D_e^{2,3}$	$D_e^{3,4}$
CO_3^{2-}	40.5	34.5	30.3	21.9
SO_4^{2-}	31.7	27.5	24.4	21.5
HPO_3^{2-}	31.8	28.3	25.4	20.3
$CH_3CO_2^-$	21.0	15.7	16.0	14.8
NO_3^-	15.9	13.8	12.2	10.0
ClO_4^-	12.7	11.1	9.9	8.6
SCN^-	12.4	12.7	10.3	14.3
H_2O	4.6	9.8	9.8	8.6

a) The average water–water interaction energy of $(H_2O)_{1-4}$ clusters is shown for comparison. Obtained from DFTB3 calculations. All values are in kcal/mol.

However, the corresponding distances for singly-charged anions quickly rise after only a few ps of simulation, demonstrating the preferential migration of acetate, nitrate, perchlorate and thiocyanate to the cluster surface. The smaller fluctuations in the ion-to-water-cluster-center distances observed for the doubly-charged ions is a reflection of the strong ion-water interactions, as presented in Table 5.1, resulting in water molecules uniformly enclosing these ions to form a tight hydration shell while the relatively large fluctuations observed for singly-charged anions reflect weaker ion-water interactions (*cf*. Table 5.1) that make the anions more mobile. In larger clusters containing 24 and 48 water molecules (*cf*. Figures 5.3b and 5.3c, respectively), analogous features are observed, but as all ions were initially placed at the cluster center, the retention time for the singly-charged anions increases with cluster size increase.

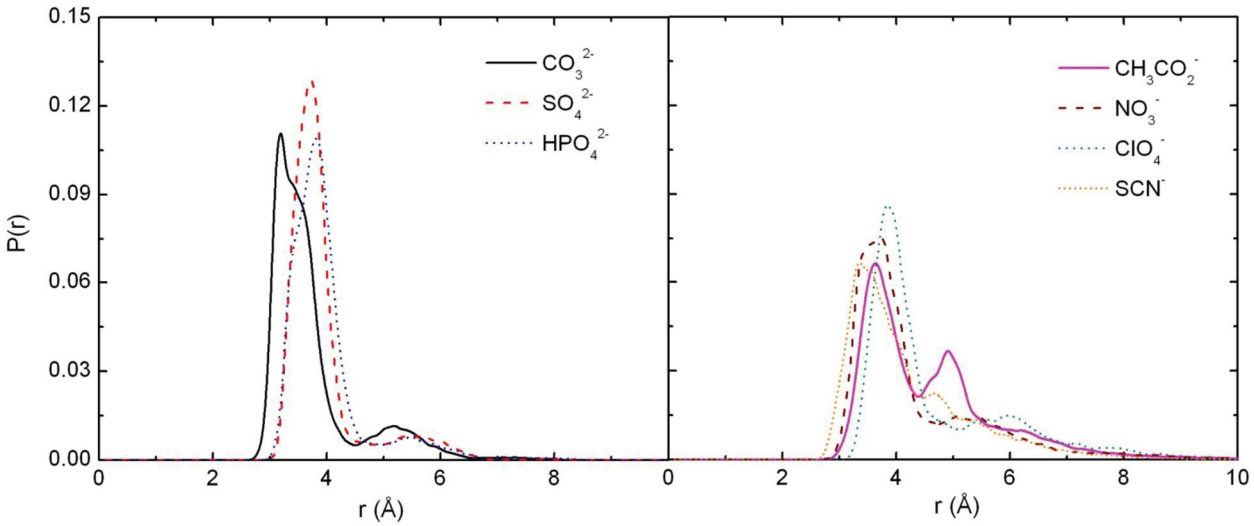

Figure 5.4. Spatial probability distributions of water molecules around polyatomic anions in clusters containing 12 water molecules. Obtained from DFTB3-MD simulations at 250 K.

5.3.2. Structural features of the anion–water clusters

The spatial probability distributions of water molecules around the ions are shown in Figure 5.4. For doubly-charged anions in clusters containing 12 water molecules, the spatial probability distributions exhibit a sharp peak around 3–3.5 Å, indicative of a well defined hydration shell. Integration of the spatial probability distribution over the range of this peak indicates that the first hydration shell contains 9, 10 and 10 water molecules for carbonate, sulfate and hydrogen phosphate, respectively, and thus the majority of water molecules are in close contact with the ions and only a few of them are relegated to a nascent second hydration shell. The spatial probability distribution of water molecules around the ions in larger clusters (not shown) also exhibit a sharp peak at analogous distances as for cluster size 12, but the number of water molecules in the first hydrations shell increase to 14, 14, and 15.5 for carbonate, sulfate and hydrogen phosphate,

respectively, which are close to the experimental values of 12 and 15 measured for sulfate[191] and hydrogen phosphate,[192] respectively, in the bulk phase.

The spatial probability distributions of water molecules around singly-charged anions for cluster size 12 also exhibit peaks, at a slightly larger distance of 3.5–4 Å, but they are much less pronounced than for doubly-charged anions (*cf*. Figure 5.4), but still indicative of a well-defined hydration shell. The number of water molecules in the first hydration shell of these ions was calculated to be 4, 6, 5.5, and 6 for acetate, nitrate, perchlorate, and thiocyanate, respectively, which is significantly less than for the doubly-charged anions. Also, except for acetate, for which a second peak is clearly observed, the spatial probability distributions past the first peak are characterized by a broad, long tail. These features can be attributed to the weaker binding energies of water molecules to singly-charged anions, which compete less effectively with water–water interactions, and as a result, the first hydration shell contains fewer water molecules that are more loosely bound to the anions. This is further reflected by the height of the minimum separating the first peak from the rest, which is much larger for the singly-charged anions than for the doubly-charged anions, demonstrating a high probability of water exchange between these two regions. Acetate deserves special attention, as it is the only anion for which a second peak is clearly observed in the spatial probability distribution. This feature is due to the strong interactions between the acetate carboxylate group and water molecules (*cf*. Table 5.1), which result in strong hydration with two well-defined shells, while the hydrophobic methyl group sticks out of the cluster (*cf*. Figure 5.2d). It should be noted that analogous features are observed for larger cluster sizes (results not shown).

The structural features of the anion–water clusters presented here are consistent with the extent of hydration of the anions presented in the Section 5.3.1. While water molecules tightly wrap around doubly-charged anions, resulting in a fully hydrated ion inside the water cluster, singly-charged anions are loosely hydrated and free to migrate to the cluster surface.

5.4. Discussion

The hydration extent of ions depends on the outcome of energetic and entropic forces that favor full hydration of the ions and those that favor partial hydration.[68,193] On one hand, strong ion–dipole interactions between hydrated ions and water molecules and entropic effects due to the disruption of the water hydrogen-bonded network by the ions force the ions to adopt a fully hydrated structure without approaching the interfaces. On the other hand, ionic polarizability was shown to favor surface solvation,[194] as partial hydration leads to significant localization of ionic charge density in the hydrated part,[67] resulting in favorable conditions in which the ion sits at the surface of a stable, non-disrupted, water hydrogen-bonded network. The interactions between the induced dipole of the partially hydrated ions and the permanent water dipoles may further stabilize polarizable anions in the anisotropic interfacial area. The ionic radius is another factor that affects the hydration extent of ions such that larger ions might be forced towards the interface to minimize the energetic penalty associated with breaking the water hydrogen-bonded network.[195] The polarizability of the ions investigated here are presented in Table 5.2 for comparison.

Table 5.2. Polarizability of polyatomic anions[a]

ion	α (Å^3)
CO_3^{2-}	8.2
SO_4^{2-}	8.2
HPO_3^{2-}	9.3
$CH_3CO_2^-$	6.8
NO_3^-	5.0
ClO_4^-	6.0
SCN^-	8.1

a) Obtained from MP2/aug-cc-pVTZ calculations.

Turning our attention to the relative strengths of the ion–water and water–water binding energies, as presented in Table 5.1, the average binding energies of all anions are larger than the water–water interaction energy, but those of the doubly-charged anions are about three times larger while those of the singly-charged anions are only about twice (or less for perchlorate) the water–water interaction energy. Accordingly, strong interactions between water molecules and doubly-charged anions such as carbonate, sulfate, and hydrogen phosphate overcome competing surface-driving forces, while singly-charged anions can not form hydrogen bonds strong enough to prevail over such forces. As a result, the former anions are fully hydrated in the interior parts of water clusters despite their large size and polarizability (*cf*. Table 5.2), while the latter ones reside at interfaces. Perchlorate, which has the highest propensity of all anions for interfacial hydration and the lowest average stepwise binding energy (only 1.5 kcal/mol larger than the water–water interaction energy), deserves special attention. Water molecules experience a lower electrostatic potential in the vicinity of singly-charged anions compared to that of doubly-charged anions. The ion–water interactions become even weaker upon addition of water molecules to the ions (*cf*. Table 5.1). In fact, the second, third and fourth stepwise binding energies of $ClO_4^-(H_2O)_{2\text{-}4}$ clusters are found to

have magnitudes comparable to those of $(H_2O)_{2-4}$ clusters, as presented in Table 5.1. This indicates that, after addition of the first few water molecules, strong ion–dipole interactions level off and formation of inter-water hydrogen bonds becomes as favorable or more than direct ion–water interactions. These observations are in agreement with the results of the previous investigations of Lambrecht *et al.*[42] revealing that ion–water electrostatic interactions are dominant in smaller clusters, while polarization and charge transfer effects which are characteristics of water–water interactions become more significant in larger clusters.

5.5. Conclusions

The hydration of the polyatomic anions of the Hofmeister series in water clusters was investigated by MD simulations in which the interatomic interactions were described by a first-principles-based approximate density-functional theory (DFTB3-MD). The results of the simulations show unambiguously that the carbonate, sulfate and hydrogen phosphate doubly-charged anions are fully hydrated in the interior regions of water clusters, while the acetate, nitrate, perchlorate and thiocyanate singly-charged anions tend to prefer partial hydration towards the surface of the clusters. For acetate, despite the tendency of the carboxylate group towards bulk hydration, the hydrophobic methyl group drives the ion towards the cluster surface. The interaction energy between the anions and water molecules might play a dominant role in determining the ultimate preferential partitioning of the ions between the bulk phase and the interface, such that doubly-charged anions which are tightly surrounded by a shell of water molecules naturally possess a high affinity for the cluster interior, while singly-charged anions – with average

binding energies comparable to the water–water interaction energy – only loosely bind water molecules, and consequently, easily migrate towards the surface where they only undergo partial hydration. The average ion–water binding energies are found to decrease over the series of the polyatomic anions investigated according to the Hofmeister ranking. An analogous trend – although not exactly the same – is also observed for the partitioning of ions between the interior and surface of the clusters. Overall, large and polarizable ions that only weakly bind water molecules prefer surface hydration while strongly water-binding ions will tend to avoid interfacial regions. The present results highlight that the hydration extent of ions should be considered, along with their effect on water structure (structure-making or structure-breaking effect), to explain their behavior in solutions. Further investigations of the hydration behavior of other polyatomic ions, both negatively and positively charged, with the presented methodology is under way.

Chapter 6

Computational Investigation of the Hydration of Alkyl Diammonium Cations in Water Clusters

To be submitted as:

S. Jahangiri, V. Legris-Falardeau, G. H. Peslherbe, *Chem. Phys. Lett.* 2013

6.1. Introduction

The hydration of ions has been extensively investigated due to their ubiquitous in nature.[2,17] Such investigations have provided useful information about the structural and thermodynamic aspects of ion hydration which could be used to obtain insight into the nature of important chemical phenomena.[10,25] In particular, the hydration extent of ions, which reflects their propensity for interior vs. surface solvation, and their effect on the orientation of surrounding water molecules, usually referred to as the structure-making or structure-breaking effect, have been used to explain the behavior of ions in electrolyte solutions.[18,23]

Ionic groups such as ammonium play an essential role in the hydration of peptides, proteins and other biomolecules as they are one of the primary binding targets of water molecules.[15,16] Sequential hydration analysis of peptides and other biomolecules reveals that the hydration extent of ammonium groups is affected by their surrounding organic domain which regulates their level of exposure to the aqueous phase.[16] The extent of the interactions between water and such ionic groups is key in explaining the structural and thermodynamic aspects of the hydration of large and complex biomolecules.[15,196]

The hydration of the ammonium cation and ammonium groups attached to different hydrophobic domains has been previously investigated using both experimental[33,34,197,198] and computational[199-204] methods. In particular, α,ω-alkyl diammonium dications lend themselves as paradigms for investigating the effect of the aliphatic domain – and its size – on the hydration of the ammonium group in a systematic manner.[33,34] The hydration extent and the water-induced conformational change of these ions upon sequential addition of water molecules may provide insight into the hydration of more complex

biological molecules such as peptides and proteins[205,206] and also help to understand the hydration behavior of neighboring charged groups in multiply charged molecules.[15,16] More importantly, such information is also useful to explain the "specific effect" of ions on the properties of electrolyte solutions.[196] In this respect, the specific hydration behavior of alkyl diammonium salts has been used to design environmental-friendly switchable water solvents.[8,207]

The stepwise ion–water binding energies of α,ω-alkyl diammonium dications in clusters with up to six water molecules have been measured by Kebarle and co-workers, revealing that the α and ω terminal sites are hydrated sequentially.[33,34] However, infrared photodissociation experiments show that, upon increasing the number of water molecules, the $NH_3(CH_2)_7NH_3^{2+}$ dication folds and the water molecules around the ammonium groups form a single water cluster which hydrates both terminal groups at the same time.[208] Analogous hydration behavior and conformational change upon addition of water molecules has been reported for a dicarboxylate dianion.[209,210]

In this article, we report an investigation of the cluster hydration of α,ω-alkyl diammonium cations with an alkyl chain of 5 to 10 carbon atoms from molecular dynamics (MD) simulations. The objective is to address the hydration behavior of the dications in water clusters to shed light onto their surface vs. interior propensity as a function of the alkyl chain length. Moreover, conformational stability of the dications upon sequential addition of water molecules has been comprehensively investigated. For this purpose, accurate two-dimensional potential of mean force calculations have been carried out.

This article is organized as follows: computational details of the simulations are

described in Section 6.2, results are presented, discussed and compared with available experimental and high-level computational data in Section 6.3 while concluding remarks follow in Section 6.4.

6.2. Computational procedure

In order to investigate the hydration behavior of the dications as a function of cluster size, potential of mean force (PMF) calculations were performed on water clusters containing 10 to 40 water molecules and each of $NH_3(CH_2)_{5\text{-}10}NH_3^{2+}$ dications. In particular, free energy of folding of each dication upon addition of water molecules was calculated as a function of the distance between the dication terminal nitrogen atoms (r_{NN}). To characterize the relation between hydration extent of the dications and their conformational change, analogous PMF were obtained as a function of the distance between the ions and the cluster centers of mass (r_{cm}) for a cluster containing 200 water molecules.

The optimized potentials for liquid simulations (OPLS)[64] force field was used to describe interatomic interactions in the MD simulations together with a modified transferable interaction potential with three points (TIP3P)[211] that was used for water molecules. The self-consistent-charge density-functional tight-binding model[58] with its third-order extension (DFTB3)[61] was used in sample MD simulations to provide a reference benchmark for the OPLS-MD results. In this respect, OPLS-MD simulations were performed for a cluster containing $NH_3(CH_2)_5NH_3^{2+}$ dication and 40 water molecules, as a sample system, and results were compared with those of DFTB3-MD simulations. In particular, the hydration extent and the conformational stability of the

dication were evaluated and compared.

In order to validate the accuracy of the models, various geometric and energetic properties of small ion–water clusters were evaluated and compared with *ab initio* results and available experimental data. *Ab initio* quantum-chemistry calculations were performed with second-order Møller-Plesset perturbation theory (MP2)[108] and Dunning's augmented correlation consistent aug-cc-pVTZ[134] basis set. Thermal corrections were calculated under the rigid rotor-harmonic oscillator approximations. It should be noted that both DFTB3 and OPLS models have been successfully used to investigate the hydration of ammonium-based cations in several previous studies.[208,212,213]

PMF calculations were performed with the umbrella sampling[125] method to increase the efficiency of sampling and the unbiased free energies and distributions were obtained with the weighted histogram analysis method (WHAM).[126] Restraining harmonic potentials with a force constant of 10.0 and 5.0 kcal/mol/Å^2 were applied at 0.25 Å and 0.5 Å intervals along the r_{NN} (represents folding) and r_{cm} (represents hydration extent) distances, respectively. All PMFs were corrected for the effects of increased conformational space with increase of the intermolecular distance.[214] The OPLS-MD simulations were performed for water clusters of varying size with spherical boundary conditions[129] containing each of the ions investigated at a constant temperature of 250 K. The simulations were performed with a timestep of 1 fs for 2 ns, with the first half of the simulation for equilibration and the second half for data collection. The DFTB3-MD simulations were performed for clusters with spherical boundary conditions to prevent cluster evaporation[129] at a constant temperature of 250 K. Simulations were performed for 120 ps with a timestep of 1 fs; the simulations were equilibrated for 60 ps and data

was collected for the last 60 ps. Overall, more than 3.5 ns of MD simulations were performed with DFTB3 and more than 13 μs with OPLS.

The Gaussian09[158] suite of programs was used for all *ab initio* quantum-chemistry calculations. The DFTB+ code was used for DFTB3 calculations and the Modes program was used to calculate the DFTB3 vibrational frequencies.[63] The *DFTB**3** parameters for **o**rganic and **b**iological applications* (3OB)[83] were used for all DFTB3 calculations. The DFTB3-MD simulations were performed with our in-house MD engine coupled with the DFTB+ program and the NAMD[215] software package was used for OPLS-MD simulations. The WHAM[130] code was used to obtain the final PMFs.

6.3. Results and discussion

6.3.1. Method validation

Selected geometrical parameters predicted by various models are listed in Table 6.1 for $NH_3(CH_2)_{5\text{-}10}NH_3^{2+}(H_2O)$ clusters. The DFTB3 and OPLS hydrogen bond lengths for $NH_3(CH_2)_5NH_3^{2+}(H_2O)$ cluster are deviated from the *ab initio* value by 0.027 and 0.037 Å, respectively, and both models overestimate the *ab initio* hydrogen bond angle by 1.9 and 4.7°, respectively. In the case of longer dications, OPLS underestimates the DFTB3 hydrogen bond lengths data by ~0.09, on average, while it overestimates the hydrogen bond angles by an average of ~2.6°. Overall, the geometrical parameters predicted by OPLS are deviated by only ~3 % from the *ab initio* and DFTB3 data.

Table 6.1. Hydrogen-bonding geometrical characteristics of $NH_3(CH_2)_mNH_3^{2+}(H_2O)_1$ clusters

	Bond length (Å)			Bond angle (°)		
	OPLS	DFTB3	*ab initio* [a]	OPLS	DFTB3	*ab initio* [a]
m=5	1.626	1.690	1.663	179.6	176.8	174.9
m=6	1.626	1.704		180.0	176.3	
m=7	1.633	1.714		178.4	176.3	
m=8	1.633	1.721		178.4	176.0	
m=9	1.633	1.726		178.5	176.1	
m=10	1.633	1.730		178.5	176.0	
Δ (*ab initio*) [b]	2.2	1.6		2.7	1.1	
Δ (DFTB3)	4.9			1.5		

a) *ab initio* = MP2/aug-cc-pVTZ
b) Δ is the absolute mean deviation of OPLS and DFTB3 data from reference data in parenthesis in %.

Thermodynamic properties of $NH_3(CH_2)_{5\text{-}10}NH_3^{2+}(H_2O)_{1,2}$ clusters are listed in Table 6.2. The DFTB3 binding enthalpy of $NH_3(CH_2)_5NH_3^{2+}(H_2O)$ cluster is in a very good agreement with the experimental value with a deviation of 0.2 kcal/mol (*cf*. Table 6.2), while OPLS overestimates it by about 2.6 kcal/mol. Both models reproduce the experimental binding enthalpy obtained upon addition of a second water molecule with a deviation of less than 1 kcal/mol (*cf*. Table 6.2). Inspection of Table 6.2 also reveals that in the case of longer dications, DFTB3 reproduces the experimental hydration enthalpies with an average deviation of only 0.3 kcal/mol. The OPLS model overestimates the experimental values by about 3.3 kcal/mol for the first hydration step while the average deviation decreases to 2.2 kcal/mol for addition of the second water molecules.

Comparing the structural and thermodynamic properties of small cluster minimum-energy structures by no means provide a thorough validation of the interaction

Table 6.2. Stepwise enthalpies of hydration of $NH_3(CH_2)_mNH_3^{2+}(H_2O)_{1,2}$ clusters

	$\Delta H_{0,1}$ (kcal/mol)			$\Delta H_{1,2}$ (kcal/mol)		
	OPLS	DFTB3	exp.[a]	OPLS	DFTB3	exp.[a]
m=5	21.2	18.8	18.6	17.5	18.3	18.4
m=6	21.1	17.9	17.8	20.9	17.6	17.3
m=7	20.4	17.3	17.8	16.6	17.1	17.2
m=8	20.5	16.8	16.9	18.7	16.7	16.8
m=9	20.5	16.5	16.5	18.9	16.4	16.3
m=10	20.5	16.2	16.8	20.5	16.2	16.8
Δ[b]	3.3	0.3		2.2	0.2	

a) Data from Ref. 33.
b) Δ is the absolute mean deviation of OPLS and DFTB3 data from experimental data in kcal/mol.

models, and we now turn our attention to the validation of OPLS-MD results against those of first-principles-based DFTB3-MD for selected test cases. The probability distribution of the distance between $NH_3(CH_2)_5NH_3^{2+}$ and the water cluster center of mass, which provides a measure of the hydration extent of the ion, obtained from PMFs calculated by DFTB3-MD and OPLS-MD simulations are plotted in Figure 6.1. Both DFTB3 and OPLS curves exhibit a band around 5–6 Å that reveals the higher propensity of the ion for interfacial regions of the water cluster. The long hydrophobic alkyl chain of the $NH_3(CH_2)_5NH_3^{2+}$ dication – not surprisingly – drives the ion towards the water cluster surface, where the dication adopts a handle-like shape such that both ammonium groups are hydrated in the cluster while the alkyl chain is folds outward, as shown in Figure 6.2.

Given the demonstrated validity of OPLS as an interaction model and OPLS-MD as an approach to describe cluster hydration for dication–water clusters, all results presented and discussed thereafter were obtained from OPLS-MD simulations.

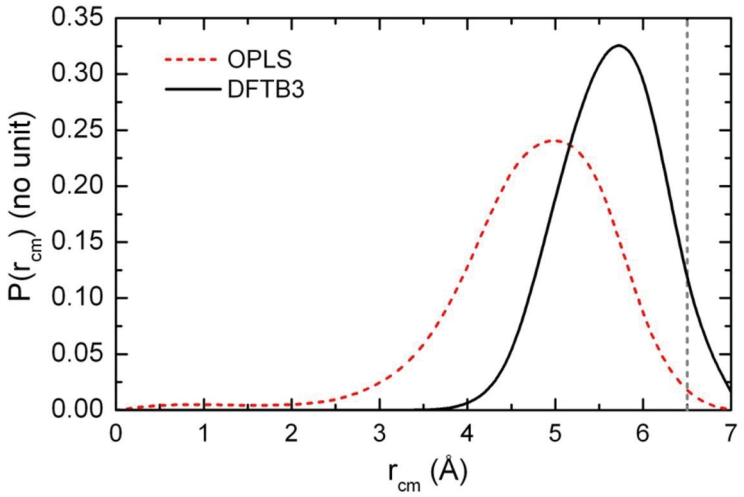

Figure 6.1. Spatial probability distributions of the ion in $NH_3(CH_2)_5NH_3^{2+}(H_2O)_{40}$ cluster. Obtained from DFTB3-MD and OPLS-MD simulations at 250 K. The coordinate is the distance between the ion and the cluster center of mass (r_{cm}). The vertical dashed line identifies the radius of a perfectly spherical cluster calculated from the experimental density of bulk water.

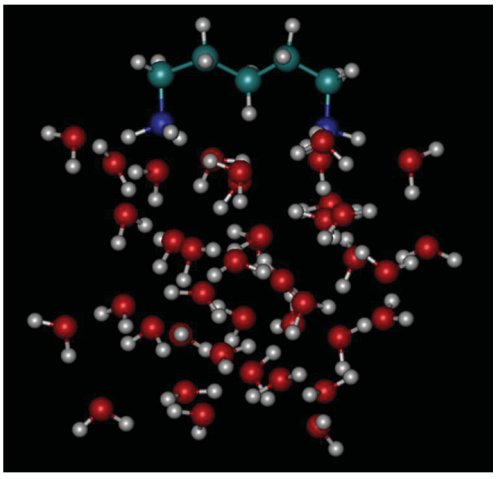

Figure 6.2. Snapshot of a surface hydrated dication in $NH_3(CH_2)_5NH_3^{2+}(H_2O)_{40}$ cluster. Conformation obtained from OPLS-MD simulation at 250 K.

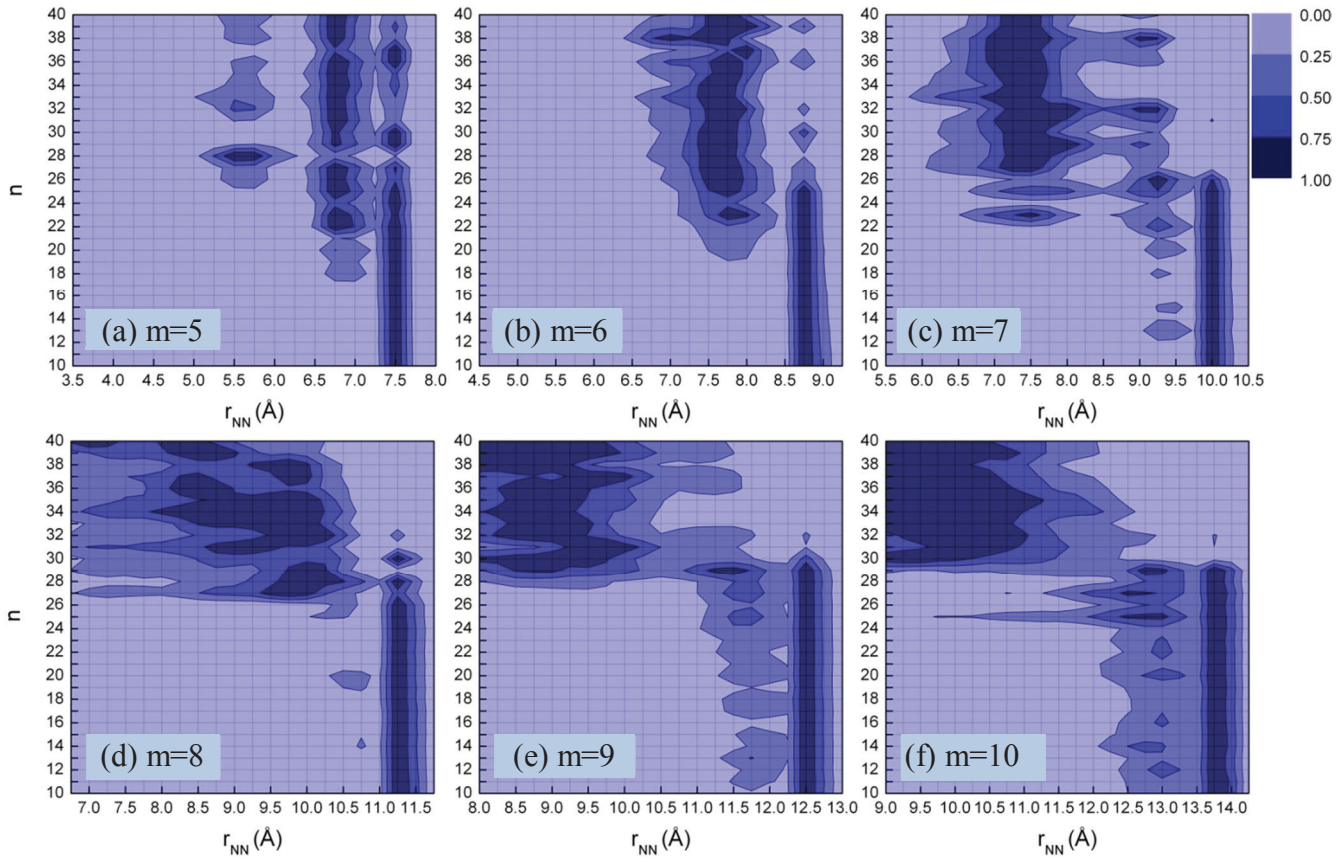

Figure 6.3. Probability distributions (no unit) of the distance between the nitrogen atoms (r_{NN}) of dications of varying alkyl chain length as a function of the number of water molecules in $NH_3(CH_2)_mNH_3^{2+}(H_2O)_n$ (m=5–10, n=10–40) clusters. Obtained from PMFs calculated by OPLS-MD simulations at 250 K.

6.3.2. Hydration of $NH_3(CH_2)_{5\text{-}10}NH_3^{2+}$ *dications: effects of cluster size*

The probability distributions of the distance between the dication nitrogen atoms, obtained from PMF calculations, which represent the ion folding in $NH_3(CH_2)_{5\text{-}10}NH_3^{2+}(H_2O)_n$ (n=10–40) clusters are displayed in Figure 6.3. For $NH_3(CH_2)_5NH_3^{2+}$, the surface exhibits three regions of high probability depending on cluster size (Figure 6.3a). In clusters containing up to 17 water molecules, the linear conformer of the dication, with an r_{NN} value of ~7.5 Å, is the only stable form. Detailed examination of the cluster structures along MD trajectories reveals that the terminal ammonium groups of the

dication are distinctly hydrated by two small water clusters in a dumbbell-like structure. With cluster size increase, these two small clusters merge and the dication slightly folds, with an r_{NN} value of ~6.75 Å, such that both terminal ammonium groups remain hydrated while the alkyl chain sticks out of the cluster. Finally, for the cluster containing more than 25 water molecules, a fully folded dication, with an r_{NN} value of about 5.5 Å clearly located at the cluster surface (obvious from a detailed examination of cluster structures – data not shown, but see next section) becomes stable as well.

The situation is analogous for $NH_3(CH_2)_6NH_3^{2+}$ (Figure 6.3b) and $NH_3(CH_2)_7NH_3^{2+}$ (Figure 6.3c), but the cluster sizes at which the ion starts folding increase to 19 and 22, respectively, and the fully folded conformer becomes the dominant form of the ion at 26 in both cases. It is interesting to point out that the number of water molecules required to fold the dication is increased compared to the previous system because more water molecules are needed to form a bridge between the terminal ammonium groups of the longer dications.

Similar features are observed for $NH_3(CH_2)_{8\text{-}10}NH_3^{2+}$ dications (*cf.* Figures 6.3d–6.3f). Generally, in clusters containing less than 27–29 water molecules, the linear dication conformers with two water clusters around the terminal ammonium groups are dominant and further addition of water molecules results in a folded dication which preferentially locates towards the surface of the cluster. The increased number of water molecules required to fold these dications is again due to the longer distance between the terminal ammonium groups of their folded conformers.

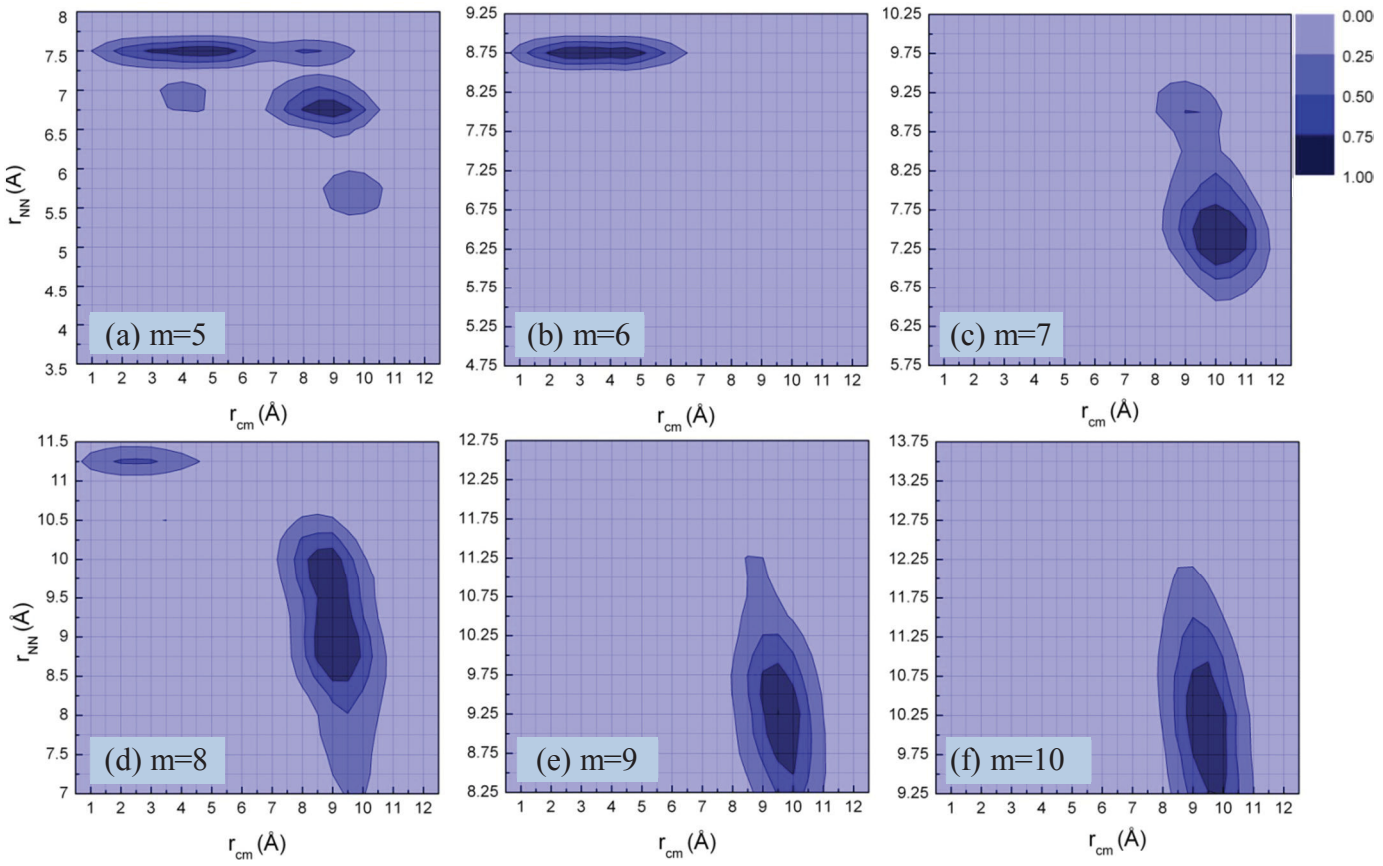

Figure 6.4. Probability distributions (no unit) of the distance between the nitrogen atoms (r_{NN}) of dications of varying alkyl chain length as a function of the distance between the ion and the water cluster center of mass (r_{cm}) in $NH_3(CH_2)_mNH_3^{2+}(H_2O)_{200}$ clusters (m=5–10). Obtained from PMFs calculated by OPLS-MD simulations at 250 K.

6.3.3. Hydration of $NH_3(CH_2)_{5\text{-}10}NH_3^{2+}$ *dications: effects of conformational change*

The probability distributions of the distance between the dication nitrogen atoms (monitors the folding of the dication) as a function of the distance between the ion and the water cluster centers of mass (monitors the hydration extent of the dication) is shown in Figure 6.4 for $NH_3(CH_2)_{5\text{-}10}NH_3^{2+}(H_2O)_{200}$ clusters. The probability distribution surface obtained for $NH_3(CH_2)_5NH_3^{2+}(H_2O)_{200}$ (Figure 6.4a) exhibits three regions of high probability. The first region corresponds to the linear form of the dication, with an r_{NN} value of ~7.5 Å, which is mainly hydrated inside the cluster, with r_{cm} distances of

about 2–6 Å. The second region represents a slightly folded conformer, with an r_{NN} value of ~6.75 Å, located towards the cluster surface, with r_{cm} distances around 9 Å. Finally the third region represents a fully folded structure, with an r_{NN} value of 5.75 Å, located at the surface of the water cluster, with an r_{cm} distance around 9.5 Å which is almost equal to the radius of the water cluster. These observations demonstrate a relationship between the dication conformation and its hydration extent: linear conformers are mainly stabilized when the dication is fully hydrated inside the cluster, due to Coulomb repulsions between the terminal ammonium groups, while folded conformers become predominant as the ion migrate towards the cluster surface.

In the case of $NH_3(CH_2)_6NH_3^{2+}$ dication, surprisingly at first, the fully hydrated linear ion conformation (r_{NN} = 8.75 Å, r_{cm} = 2–5 Å) is more stable despite the longer hydrophobic alkyl chain of the ion. Upon increase of the alkyl chain length, the folded conformation located towards or at the cluster surface becomes the predominant or sole stable form of the $NH_3(CH_2)_7NH_3^{2+}$ and $NH_3(CH_2)_8NH_3^{2+}$ (r_{NN} = 7.25 Å, r_{cm} = 10 Å and r_{NN} = 8.5–10 Å, r_{cm} = 9 Å, respectively), even though $NH_3(CH_2)_8NH_3^{2+}$ surprisingly again to a greater extent, may also adopt a less favorable fully hydrated linear conformation (r_{NN} = 11.25 Å, r_{cm} = 2 Å). The surprising results observed for $NH_3(CH_2)_6NH_3^{2+}$ and $NH_3(CH_2)_8NH_3^{2+}$ are possibly due to the specific orientation of the ammonium groups in the folded dications which may prohibit appropriate hydration of the dication at the cluster surface. This decreased surface affinity despite increase in the alkyl chain length might be considered as the result of the odd–even effect observed in the physical properties of linear organic compounds.[216,217] This issue is under further investigation. The probability distribution surface obtained for $NH_3(CH_2)_9NH_3^{2+}(H_2O)_{200}$ and

$NH_3(CH_2)_{10}NH_3^{2+}(H_2O)_{200}$ (Figures 6.4e and 6.4f) also demonstrate the stability of folded conformers of the dications at the cluster surface.

6.4. Conclusions

Water clusters containing alkyl diammonium cations of varying alkyl chain lengths have been investigated by MD simulations to characterize their hydration behavior. The OPLS force field and an approximate density-functional theory (DFTB3) were first validated on the basis of high-level quantum-chemistry calculations and experimental data. The OPLS force field, when implemented in MD simulations, was found to reproduce the main features of the hydration behavior of $NH_3(CH_2)_5NH_3^{2+}$ ion in a medium-sized water cluster, compared to those obtained with the more rigorous first-principles-based DFTB3-MD simulations, but at a much lower computational cost. Accordingly, the OPLS force field was adopted to describe interatomic interactions in all subsequent simulations.

A number of OPLS-MD simulations were then performed to provide a comprehensive picture of the hydration extent and conformational change of alkyl diammonium dications in water clusters. For clusters containing up to ~20 water molecules, the terminal ammonium groups of the dications are separately hydrated by two small water clusters, but upon further cluster size increase these two clusters tend to merge and form a larger one which tends to expel the dication towards its surface to form a handle-like folded shape. The number of water molecules required to initiate the folding of the dications increases with alkyl chain length, and fully hydrated linear dication conformations become unstable in clusters containing more than ~27 water molecules, indicating that cluster size – and the extent of hydration – governs conformational

changes of the dications. In larger clusters containing 200 water molecules, linear dication conformations are more stable when the dications are fully hydrated inside the cluster, while partial hydration at the interface mediates significant conformational changes. Surface hydration becomes more favorable upon increasing the alkyl chain length, although an odd-even effect in the relative hydration extent of shorter dications was observed. The present results indicate that, according to the different interfacial affinity of the dications investigated, they might demonstrate significantly different behavior in aqueous solutions.

Chapter 7

Computational Investigation of the Hydration of Alkyl Diammonium Chlorides and Their Effect on THF/Water Phase Separation

Published as:

S. Jahangiri, S. M. Mercer, P. G. Jessop, G. H. Peslherbe, *J. Phys. Chem. B*

DOI: 10.1021/jp403984q

7.1. Introduction

The effects of ions on the physical properties of aqueous systems have been extensively investigated since the introduction of the so-called specific ion effect.[17,20-22,145] Among the large number of properties for which ions show specific effects,[143] their relative influence on the solvation of other solutes or on the structure of macromolecules is particularly important.[4,218] Even though the molecular details of such effects are not well understood, two distinct mechanisms have been proposed in the literature.[18] Traditionally, the change in water structure induced by ions in solution is believed to be the key factor in characterizing their specific effects. This led to the categorization of ions into structure-makers (kosmotropes) and structure-breakers (chaotropes); for instance, small ions with large charge densities tend to organize the structure of water beyond their first solvation shell, while large ions with small charge densities tend to disorganize the structure of water and disrupt its hydrogen-bond network.[21,23]

Direct interaction between the ions and macromolecules has also been recently proposed to rationalize specific ion effects;[18,22,25,26,219,220] the hydration extent of the ions, which characterizes their propensity towards interior or interface solvation, would play an important role in determining ion-specific properties. Recent studies employing surface-sensitive experimental techniques and molecular dynamics (MD) simulations have clearly demonstrated the enhanced concentration of various anions at interfaces.[28,179] A clear example is the distribution of halide anions at the air/water interface, which increases systematically from fluoride to iodide.[54-57,121] Surface solvation has also been reported for other anions such as thiocyanate,[181] nitrate[187] and azide.[221] For instance, the interfacial concentration of thiocyanate anions increases at the dodecanol/water

interface.[168] Such investigations bring to light the importance of the direct influence of ions, along with their indirect effects through disruption of the water structure, in specific ion effects on macromolecules.

Recently, a class of alkyl diamines with reversible salting-out effects has been used to design "switchable-water" solvents.[8,207] Introduction of CO_2 to such solvents alters the pH of the solution and leads to the formation of diammonium dications and bicarbonate anions that can salt out small organic species such as THF and acetonitrile:

$$Me_2N(CH_2)_nNMe_2 + 2CO_2 + 2H_2O \rightleftharpoons [Me_2HN(CH_2)_nNHMe_2][HCO_3]_2. \quad (7.1)$$

Removing CO_2 from the solution reverses the process and makes the solvent mixture miscible again. To gain insight into how dications exert their salting-out effect and to further characterize the effect of dication alkyl chain length on the extent of phase separation, we performed a systematic investigation of salting-out effects of α,ω-alkyl diammonium chlorides with alkyl chains containing from 2 to 10 carbons on THF/water and acetonitrile/water mixtures.[207] The ions with shorter alkyl chains (up to 6 carbon atoms) were found to salt out organic molecules while those with longer alkyl chains were not. Interestingly, adding hydrophilic substituents to the alkyl chain (*e.g.*, replacing two central methylene groups with oxygen atoms) increases the salting-out properties of the longer dications.[207]

Based on these observations and in light of the proposed mechanisms underlying specific ion effects, the hydration extent of dications with varying alkyl chain length, and the resulting differences in their interaction with other (organic) molecules, could be responsible for the differences in their salting-out characteristics. This warrants a detailed investigation of the solvation behavior of this class of ions as a function of alkyl chain

length. In addition to its practical importance, a systematic theoretical investigation of these systems could help further understand the molecular mechanism(s) behind the specific effects of ions that have a significant role in a broad range of biological and chemical phenomena. To that end, MD simulations, and when necessary potential of mean force (PMF) calculations are performed to investigate the solvation behavior of α,ω-alkyl diammonium chlorides, $[H_3N(CH_2)_nNH_3]Cl_2$, in bulk water, a water slab and THF/water mixtures. The outline of this article is as follows: the computational procedure is described in Section 7.2, simulation results are presented and discussed in Section 7.3, and concluding remarks follow in Section 7.4.

7.2. Computational procedure

All MD simulations were performed at constant pressure (1 atm) and temperature (298.15 K) in the NPT ensemble, with periodic boundary conditions, and a timestep of 1 fs. Simulations of water and THF solutions employed a cubic cell containing 800 and 200 molecules, respectively, while these numbers were adjusted to evaluate THF-water mixing properties for mixtures of different mole fraction keeping the cell length at *ca*. 30 Å. Aqueous ~1.0 M salt solutions were prepared by adding 14 diammonium and 28 chloride ions to the 800 water molecules, while THF/water ~0.5 M salt solutions were prepared by adding 12 diammonium and 24 chloride ions to 900 water and 100 THF molecules (simulations were also performed for other mole fractions and similar results – not reported here – were obtained). The water slab was generated with 500 water molecules in a rigid cell of dimension 25 Å x 25 Å x 100 Å, with the slab placed at the

center of the cell and harmonic potentials applied to both slab surfaces to prevent water evaporation.

All systems were first minimized for 1000 steps with the conjugate-gradient method, then equilibrated for 2 ns, and data was collected for 8 ns. Molecules were distributed randomly in a cubic box (of length 40 Å) with a smaller initial density than its experimental value to allow better mixing. A modified transferable interaction potential with three points (TIP3P)[211] was used to describe water and the optimized potentials for liquid simulations (OPLS)[64] was used for α,ω-alkyl diammonium chlorides. In order to properly describe THF-water interactions, a modified OPLS force field in which non-bonded parameters were replaced by those of Girard *et al.*[222] was used. Interatomic Lennard-Jones parameters were evaluated as the geometric mean of atomic parameters and all non-bonded interactions were turned off at a cut-off distance of 12 Å. The NAMD[215] simulation package was used for all simulations and the Packmol[223] program was used to prepare the simulation cell data. The temperature was kept constant with Langevin dynamics and a damping coefficient of 5 ps^{-1}, while the pressure was controlled with a modified Nose-Hoover method implemented in the NAMD program with barostat oscillation and damping time constants set to 200 fs and 100 fs, respectively,[215] except for PMF calculations where the Berendsen pressure bath coupling[224] was used because of technical difficulties with the latter approach.

The calculated volumes of the simulation cells and the non-bonded potentials were averaged over trajectories to obtain the density and enthalpy of vaporization of THF, respectively, with the latter calculated as:[225]

$$\Delta H_{vap} = -\left(\langle U(l)\rangle / n_m - \langle U(g)\rangle\right) + RT\,, \qquad (7.2)$$

where *U(l)* represents the sum of the non-bonded (Coulombic and van der Waals) interactions for the liquid, n_m represents the number of molecules in the simulation cell and *U(g)* is the analogous sum for a single molecule in the gas phase. Enthalpies and volumes of mixing of the THF/water mixture were calculated as:[226]

$$\Delta H_{mix} = \langle U_{mixture} \rangle - \left(x_{water} \langle U_{water} \rangle + x_{THF} \langle U_{THF} \rangle \right), \quad (7.3)$$

$$\Delta V_{mix} = \langle V_{mixture} \rangle - \left(x_{water} \langle V_{water} \rangle + x_{THF} \langle V_{THF} \rangle \right), \quad (7.4)$$

where ΔH_{mix} and ΔV_{mix} represent the enthalpy and volume of mixing, respectively, U is again the sum of the non-bonded interactions of a given system, V is the volume of the cell, and x represents mole fractions. Because of the negligible effect of volume change on the calculated enthalpy of mixing, it is assumed that $\Delta H_{mix} = \Delta U_{mix}$.[227]

Selected PMF calculations were performed with the umbrella sampling method[125] in which restraining harmonic potentials with force constant 5.0 kcal/mol/Å^2 were applied at 0.5 Å intervals of the reaction coordinate, and the weighted histogram analysis method (WHAM)[228] was used to compute unbiased free energy profiles. In PMF calculations, the minimization step was skipped, and the simulations of the water slab were performed for only 2 ns, since it was found sufficient to obtain converged results. All PMF calculations were carried out in infinite dilution, *i.e.* for a single solute molecule/salt. A correction term $2RT\ln(r)$ was added to the calculated dication-THF PMFs in order to incorporate the effects of increased conformational space with increase of intermolecular distance.[214] The WHAM[130] program was used to compute PMFs from simulation data.

Table 7.1. Properties of liquid THF and THF/water mixtures

	ρ (gr/mL)	ΔH_{vap} (kJ/mol)	ΔH_{mix} (kJ/mol)	ΔV_{mix} (mL/mol)
MD/OPLS	0.843	30.08	0.25	–0.02
MD/OG1[a]	0.885	31.84	–2.43	–1.25
MD/OG4	0.882	32.05	–2.43	–1.08
MD/OG5	0.878	30.92	–1.21	–0.47
MD/OG7	0.882	29.83	–0.25	–0.50
MD/OG8	0.894	33.85	–14.69	–3.22
Experiment	0.884[b]	31.80[b]	–0.71[c]	–0.74[d]

a) OGn refers to the combination of the OPLS force field with the different sets of non-bonded parameters of Ref. 222. Mixing properties are evaluated for the mole fraction x_{water} = 0.8 from MD simulations performed at 298.15 K and 1 atm. b) From Ref. 229. c) From Ref. 230. d) From Ref. 231. Experimental data have been interpolated to the mole fraction x_{water} = 0.8.

7.3. Results and discussion

7.3.1. Force field validation

The force field employed in the simulations of ionic mixtures was first validated by comparing the simulated properties of liquid THF and THF/water mixtures to experimental data (Table 7.1). The OPLS force field yields a positive enthalpy of mixing, in contrast to experimental data, and it seriously underestimates the magnitude of the experimental volume of mixing, indicating the tendency of the force field to predict unfavorable mixing of THF and water. In fact, two separate layers were observed to form after a few nanoseconds of simulation time, resulting in unphysical organic-water phase separation even in the absence of ions.

To remediate this problem, we turned our attention to a set of force fields developed by Girard *et al.*[222] to reproduce the experimental density and heat of vaporization of liquid THF, all with different parameter sets[232-236] for non-bonded interactions, the latter having been shown to play a predominant role in reproducing the

Table 7.2. THF non-bonded parameters of the different models of Girard *et al.* [a]

Model	ε (kJ/mol)			σ (Å)			q (e)				
	C	O	H	C	O	H	$C_{1,4}$ [b]	$C_{2,3}$ [c]	O	$H_{1,4}$ [d]	$H_{2,3}$ [e]
1	0.290	0.628	0.170	2.95	3.00	2.40	0.231	0.061	–0.584	0.000	0.000
4	0.200	0.500	0.150	3.43	3.00	2.36	0.231	0.061	–0.584	0.000	0.000
5	0.276	0.550	0.126	3.50	2.90	2.45	0.208	0.000	–0.528	0.028	0.000
7	0.190	0.360	0.150	3.85	3.50	1.90	0.231	0.061	–0.584	0.000	0.000
8	0.340	0.490	0.390	2.30	2.20	2.40	0.231	0.061	–0.584	0.000	0.000

a) From Ref. 222. b) Carbon atoms bonded to oxygen, labeled C_1 and C_4. c) Carbon atoms not bonded to oxygen, labeled C_2 and C_3. d) Hydrogen atoms bonded to C_1 and C_4. e) Hydrogen atoms bonded to C_2 and C_3.

physical properties of the solutions. We thus implemented in our MD simulations the non-bonded parameters of Girard *et al.* (Table 7.2) within the OPLS force field, models hereafter referred to as OG1-OG8 following the original numbering scheme of Girard *et al.*,[222] and we were able to reproduce the liquid THF density and heat of vaporization within 2% of the values reported in the original work, and sometimes in better agreement with experimental data.

As for water–THF mixing, the OG7 force field appears to yield the best prediction for the enthalpy and volume of mixing (Table 7.1), and since it simultaneously provides an accurate description of the heat of vaporization and density of liquid, this model is adopted hereafter for all simulations. In fact, proper mixing of THF and water is observed in simulations initiated with two separate layers of solvent after only a few nanoseconds, demonstrating the judicious choice of non-bonded parameters/force field. The calculated enthalpy and volume of mixing for THF/water mixtures of varying composition are plotted in Figure 7.1 along with experimental data. In THF-rich mixtures, *i.e.* x_{water} = 0.1−0.3, calculated values are in very good, quantitative, agreement with experimental

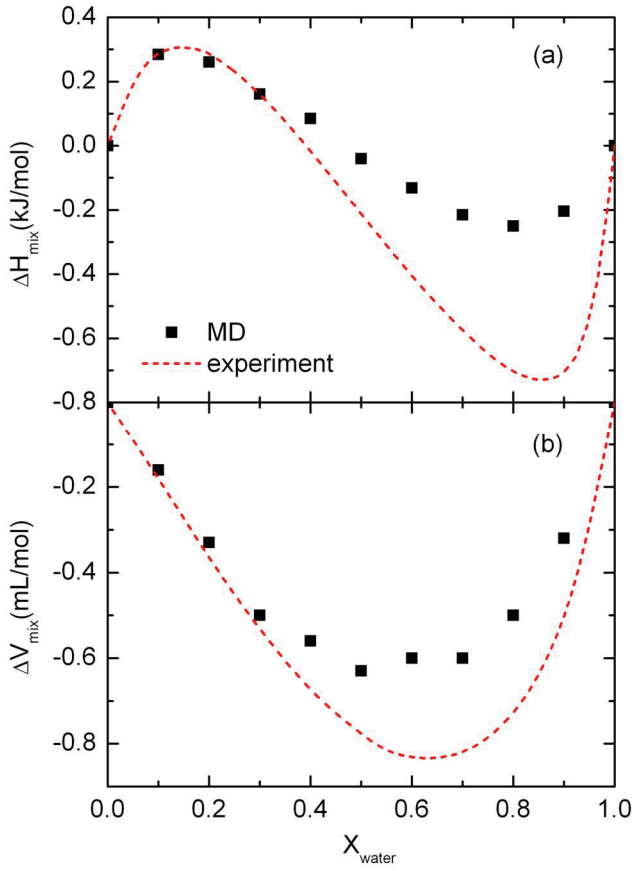

Figure 7.1. Properties of THF/water mixtures of varying composition. a) enthalpy of mixing, and b) volume of mixing. Obtained from MD simulations performed with the OG7 force field at 298.15 K and 1 atm. Experimental enthalpies and volumes of mixing are taken from Refs. 230 and 231, respectively.

ones, while the agreement is only qualitative for mixtures with higher mole fractions of water, *i.e.* x_{water} = 0.4−0.9, where both mixing properties are underestimated by calculations, presumably due to some deficiencies in the description of water by the TIP3P force field. We note that organic/water mixing properties usually have rather small magnitudes, *e.g.* the maximum value of ΔH_{mix} is less than –0.8 kJ/mol for THF/water, and therefore a truly quantitative reproduction of experimental values is not an easy task.[226,237]

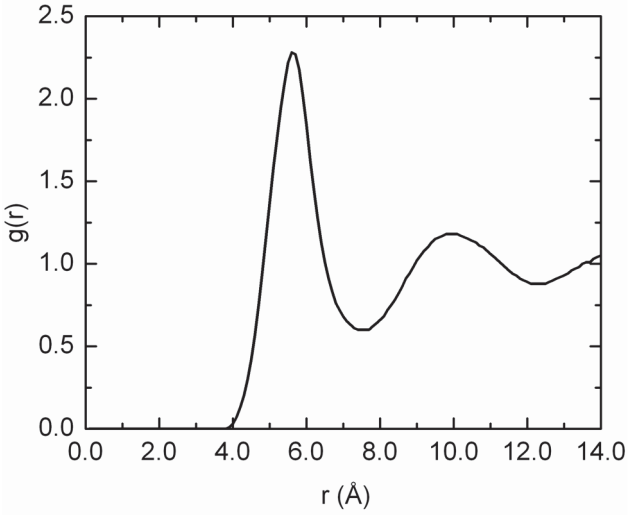

Figure 7.2. Structural properties of liquid THF: intermolecular RDF as a function of the distance between the geometric centers of THF molecules. Obtained from MD simulations performed with the OG7 force field at 298.15 K and 1 atm.

Finally, the validity of the OG7 force field was further examined by comparing features of the calculated THF intermolecular radial distribution function (RDF) with experimental data. As shown in Figure 7.2, the calculated RDF exhibits two peaks around 5.5 and 10 Å and a minimum at 7.7 Å, in good agreement with corresponding experimental values.[238]

7.3.2. Hydration behavior of α,ω-alkyl diammonium chlorides

The hydration of α,ω-alkyl diammonium chlorides of varying alkyl chain length was first investigated from a structural and thermodynamic point of view. Structural properties obtained from MD simulations are shown in Figure 7.3. The sharp peak in the intermolecular N–O RDF around 3 Å (Figure 7.3a) reflects the highly organized hydration shell around the positively charged terminal groups of the dications via strong ammonium–water interactions. Furthermore, the very similar shape of the RDFs with

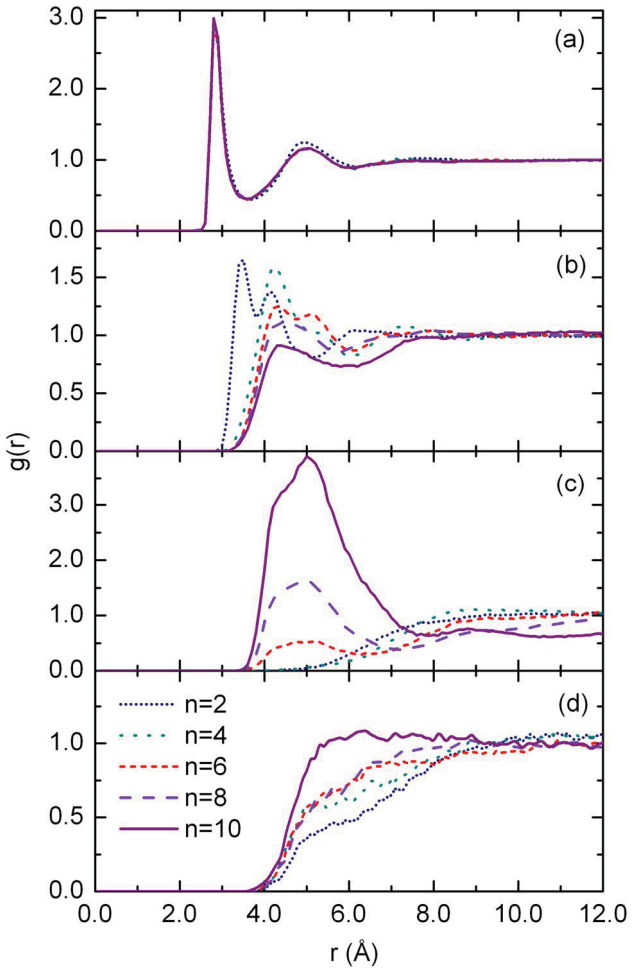

Figure 7.3. Structural properties of aqueous solutions containing alkyl-diammonium chlorides of varying alkyl chain length, $[H_3N(CH_2)_nNH_3]Cl_2$. a) dication-water RDF, with the dication N to water O distance as the intermolecular coordinate; b) dication-water RDF, with the central C to water O distance as the intermolecular coordinate (averaged over both central carbons); c) dication-dication RDF, with the distance between the central carbons as the intermolecular coordinate (again averaged over both central carbons); d) dication-dication RDF, with the distance between the N atoms as the intermolecular coordinate. Obtained from MD simulations of ~1.0 M salt solution performed at 298.15 K and 1 atm.

varying alkyl chain length indicate that the latter has a negligible effect on the hydration structure of the ammonium groups.

The intermolecular central C–O RDFs (Figure 7.3b) exhibit two pronounced peaks only for the dications with short alkyl chains, with the first peak corresponding to water molecules of the ammonium hydration shell on the side of the alkyl chain, and the second peak corresponding to those on the nitrogen side away from the alkyl chain. With

increasing alkyl chain length, the first peak gradually disappears and the RDFs broaden, reflecting the increased hydrophobicity of the dication and the lack of water ordering around the middle of the alkyl chain. The lack of particular structure in the intermolecular C–C RDFs (Figure 7.3c) for the shorter dications reflects the fact that they are well separated and hydrated, while the emergence of a pronounced peak around 5 Å for dications with an alkyl chain containing 6, 8 and 10 carbon atoms is indicative of increased aggregation of the dications, again because of their increased hydrophobicity. The intermolecular N–N RDFs (Figure 7.3d) exhibit no particular structure for all dication alkyl chain lengths, reflecting the lack of interaction between the ammonium groups and their uniform distribution in the solution. This is consistent with the full hydration of the shorter dications and the fact that longer dications aggregate "perpendicularly" to one another to maximize the distance between the positively charged ammonium groups.

To further characterize the relative hydrophobicity, *i.e.* the hydration extent, of dications with varying alkyl chain length, the PMFs corresponding to the transfer of a dication from a water slab to vacuum were evaluated. These PMFs (Figure 7.4) clearly show that the interior of the water slab is thermodynamically favorable for shorter dications, while dications with alkyl chains containing more than 8 atoms clearly prefer to migrate towards the air/water interface (with a clear minimum in the PMF close to this position). The changes in free energy between surface and bulk solvation amount to about 40, 20, 10, –5 and –10 kJ/mol for dications with alkyl chains containing 2, 4, 6, 8 and 10 carbon atoms, respectively. This reflects the propensity of shorter ions for complete hydration inside bulk water, while longer ions with an hydrophobic part only adopt

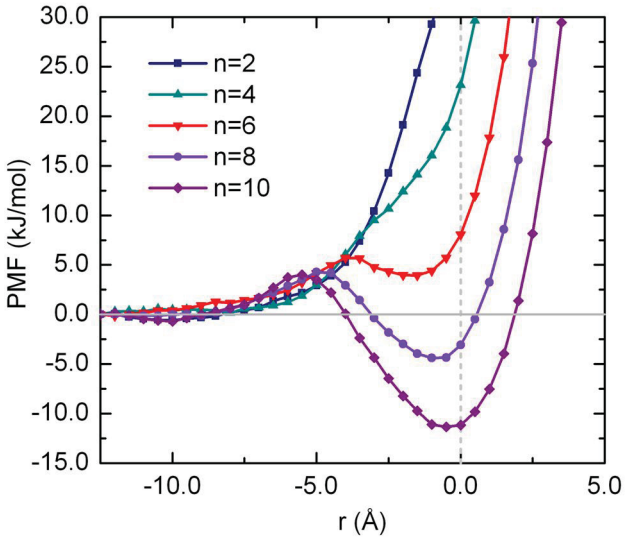

Figure 7.4. PMF for transfer of dications with varying alkyl chain length from a water slab to vacuum. The coordinate is the distance between the air-water interface (at the origin) and the center of mass of the dication. Obtained from MD simulations performed at 298.15 K and 1 atm at infinite dilution.

partial hydration, in this case hydration of the ammonium groups with the alkyl chain sticking out of the water slab. We note that the longer dication alkyl chains at the interface are observed to fold, forming a bent handle-like conformation in vacuum similar to that observed in clusters. The surface hydration of the longer dications and their folding at the interface is also analogous to the behavior of dicarboxylate dianions observed in molecular dynamics simulations and confirmed by photoelectron spectroscopy.[209,210]

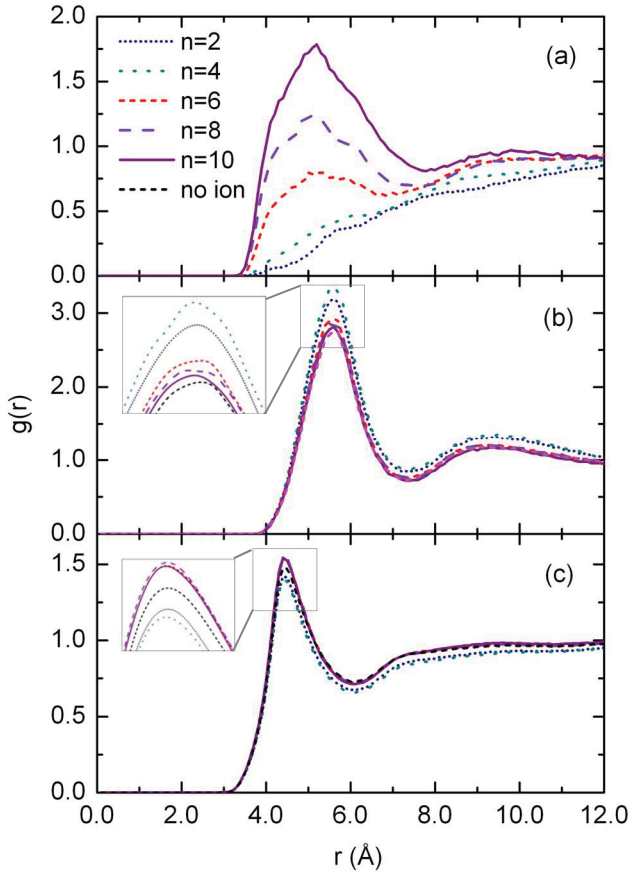

Figure 7.5. Structural properties of THF/water mixtures containing alkyl diammonium chlorides of varying alkyl chain length, $[H_3N(CH_2)_nNH_3]Cl_2$. a) dication-THF RDF, with the distance between the dication and THF central carbons (averaged over both central carbons of the dication alkyl chain and THF carbons not bonded to oxygen) as the intermolecular coordinate; b) intermolecular THF-THF RDF, with the distance between the geometric centers of THF molecules as the intermolecular coordinate; c) THF-water RDF, with the distance between the THF geometric center and the water O as the intermolecular coordinate. Obtained from MD simulations of ~0.5 M salt solution with $x_{THF} = 0.1$ performed with the OG7 force field at 298.15 K and 1 atm.

7.3.3. Effects of α,ω-alkyl diammonium chlorides on THF/water mixture

Structural results of MD simulations of THF/water mixtures containing α,ω-alkyl diammonium chlorides of varying alkyl chain length are shown in Figures 7.5 and 7.6. The dication–THF RDF in Figure 7.5a exhibits a clear peak around 5 Å for the longer dications. Increasing the dication alkyl chain length also results in a significant increase in the number of THF nearest-neighbor molecules from 0.8 for n = 2 to 2.5 for n = 10 because of increased hydrophobic interactions between the THF molecules and dications.

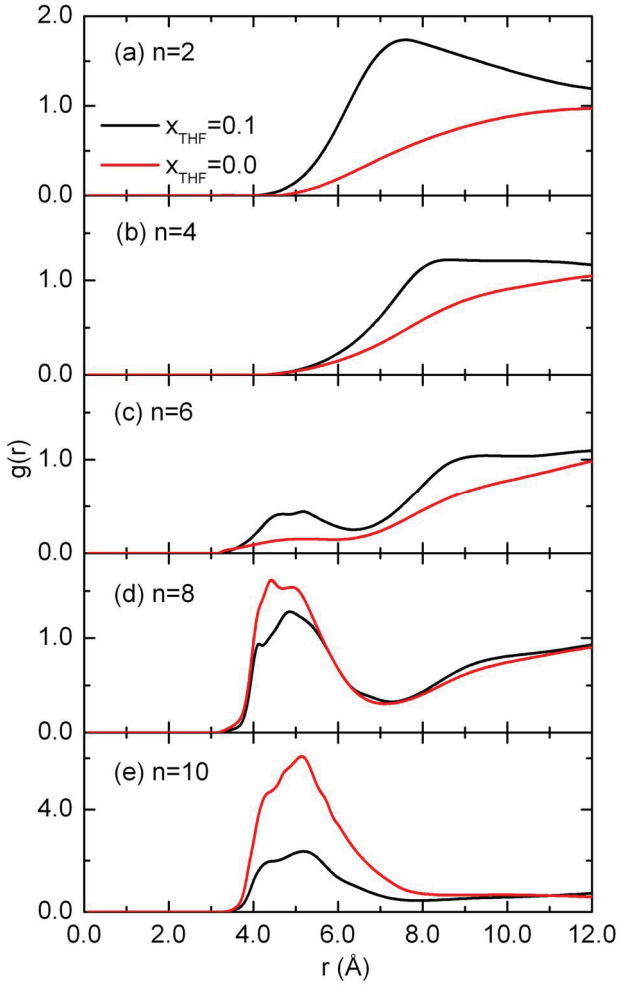

Figure 7.6. Structural properties of THF/water and water solutions containing alkyl diammonium chlorides of varying alkyl chain length, $[H_3N(CH_2)_nNH_3]Cl_2$. Dication-dication RDFs with the distance between the central carbons as the intermolecular coordinate (averaged over both central carbons of the alkyl chain) for a) n = 2, b) n = 4, c) n = 6, d) n = 8 and e) n = 10. Obtained from MD simulations of ~0.5 M salt solutions performed with the OG7 force field at 298.15 K and 1 atm.

The THF–THF RDFs (Figure 7.5b) indicate that addition of dications with short alkyl chains to the mixture increases the local ordering and number of nearest-neighbor of THF molecules (5.5 for n = 2) relative to the ion-free THF/water mixture, reflecting increased interactions between THF molecules as a result of ion-induced phase separation for shorter, well-hydrated, dications. The number of nearest-neighbor of THF molecules decreases and converges towards that of the ion-free mixture (4.8) with increased alkyl

chain length (4.5 for n = 10), suggesting that longer dications do not induce significant phase separation. The THF–water RDF, shown in Figure 7.5c, indicates that addition of shorter dications (n = 2, 4) decreases the probability of finding water molecules around THF, relative to the ion-free THF/water mixture, while the addition of longer dications (n = 6, 8 and 10) increases it. This reflects the decreased hydration of THF molecules as a consequence of salting out upon addition of shorter dications, while addition of longer dications in fact enhances the mixing of THF and water.

The dication–dication RDFs in Figure 7.6 indicate that addition of THF molecules to the aqueous solution containing short dications increases the probability of finding the dications closer to one another. This is obviously not due to direct association of the dications, as the RDFs tend to be broad and do not show much structure for short dications (e.g. n = 2, Figure 7.6a), but might simply reflect the higher concentration of ions in the water-rich phase (consistent with the enhanced aggregation of THF molecules and phase separation discussed above). With increased alkyl chain length, a pronounced peak emerges around 5 Å in the RDF, reflecting the increased aggregation of the longer dications discussed in Section 3.2, but addition of THF molecules decreases the aggregation of the dications because of their increased interactions with THF molecules which displace to some extent their hydrophobic association (e.g. n = 10, Figure 7.6e).

To further characterize the extent of dication-THF interactions, the PMF between diammonium dications of varying alkyl chain length and THF were evaluated. The

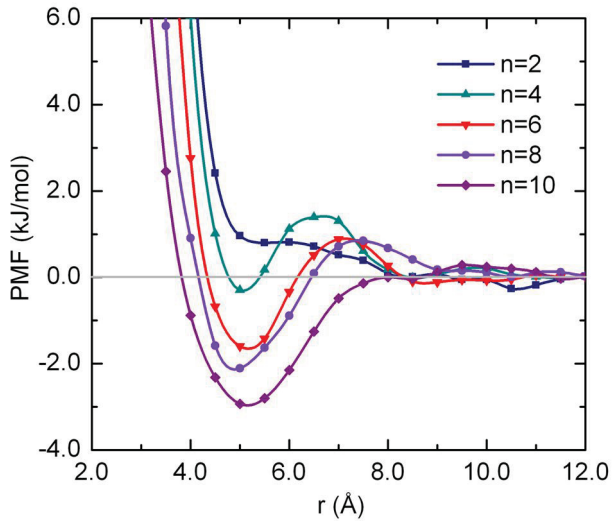

Figure 7.7. PMF between diammonium dications of varying alkyl chain length and THF, with the distance between the centers of mass of the dication and THF as the intermolecular coordinate. Obtained from MD simulations performed with the OG7 force field at 298.15 K and 1 atm at infinite dilution.

PMFs, shown in Figure 7.7, indicate that aggregation of THF molecules around dications is not thermodynamically favorable for the smallest dication (n = 2), while it is for all other longer dications. In fact, aggregation of THF molecules around the dications becomes increasingly more favorable with increasing alkyl chain length, as suggested by the increasingly deeper minima observed in the PMFs. These minima emerge around 5 Å, a distance typical of hydrophobic interactions, because of a weak, stabilizing, interaction between the dication alkyl chain and the hydrophobic THF domain. The stabilization free energies for this weak interaction are 1.6, 2.1 and 2.9 kJ/mol for dications with n = 6, 8 and 10, respectively.

Two representative sample snapshots of MD simulations of THF/water mixtures containing the shortest and the longest dications are shown in Figure 7.8, in order to

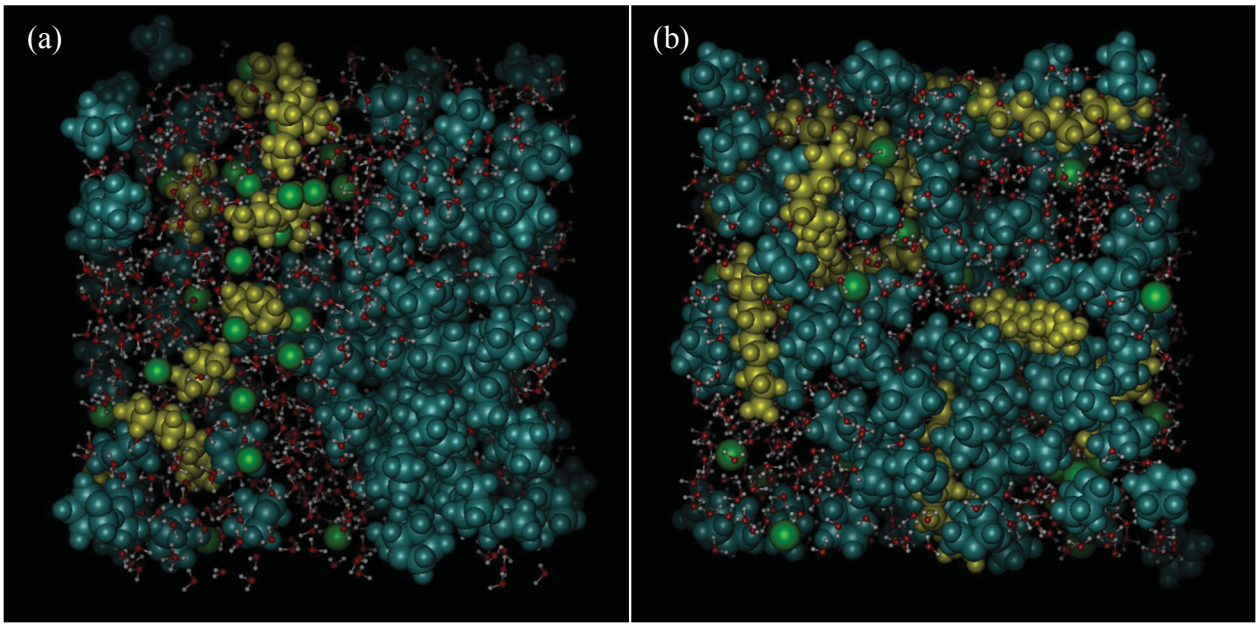

Figure 7.8. Representative sample snapshots of THF/water mixtures containing a) $[H_3N(CH_2)_2NH_3]Cl_2$ and b) $[H_3N(CH_2)_{10}NH_3]Cl_2$. The water oxygens are shown in red, the water hydrogens in white, the THFs in cyan, the dications in yellow and the chlorides in green. Obtained from MD simulations of ~0.5 M salt solutions with $x_{THF} = 0.1$ performed with the OG7 force field at 298.15 K and 1 atm.

visually summarize the discussion of the MD results. As inferred from these snapshots, the THF and water phases are completely separated into two distinct layers in the presence of the short dications, while the mixture containing the longer dications exhibits a more uniform distribution of THF and water molecules reflecting better phase mixing. It should be noted that the THF/water mixture is inhomogeneous such that, at low water mole fractions, water form "pools" in the organic phase instead of being homogeneously mixed with THF, as previously reported.[239] Likewise, at high water mole fractions, THF molecules form organic aggregates which might be considered as the "island" counterparts of the aforementioned water "pools". The simulation results indicate that such aggregates may be stabilized by long, partially solvated, dications, preventing

macroscopic THF/water phase separation despite the inhomogeneous mixing observed at the nanoscale level.[239]

7.4. Conclusions

The hydration of α,ω-alkyl diammonium chlorides and their effect on the salting out of THF molecules from the aqueous phase in THF/water mixtures have been investigated with molecular dynamics simulations. A modified OPLS force field was first validated on the basis of its ability to reproduce experimental properties for THF solutions and THF/water mixtures, and employed subsequently for all simulations. The present results indicate that shorter dications (with alkyl chains containing 2 and 4 carbon atoms) tend to be fully hydrated, while longer ions (with alkyl chains containing 6, 8 and 10 carbon atoms) only undergo partial hydration and tend to either reside at the water interface or aggregate with the hydrophobic domains of available organic solutes. Structural and thermodynamic analysis of the simulation results for ionic THF/water mixtures demonstrate that dications with short alkyl chains do not interact significantly with THF molecules and rather reside in a water-rich phase. In contrast, for longer dications, interactions between the dication alkyl chain and THF molecules significantly increase with alkyl chain length. Such interactions could stabilize small organic aggregates in the aqueous phase and accordingly cause better mixing of the phases. This work supports the hypothesis that the hydration extent of ions plays a key role in stabilizing or destabilizing organic solutes in aqueous systems. While partial hydration of dications with longer chains may facilitate their aggregation with available organic solutes via hydrophobic interactions, complete hydration of dications with shorter chains prevents such

interactions and addition of these ions to the mixture causes phase separation. This highlights the role of the *direct* interactions between organic molecules and ions concurrently to the traditional *indirect* mechanism based on ion hydration in the salting-out of organic molecules from aqueous phases.

Chapter 8

Conclusions and Outlook

The primary objective of this work was to provide accurate and efficient computational methods to investigate the hydration of ions in clusters and solutions with a particular emphasize on their hydration extent and its relation to their specific effects in aqueous systems. In this respect, the density-functional tight-binding model with third-order extension, referred to as DFTB3 – which is an approximate quantum-chemistry approach based on density-functional theory (DFT) – has been extended, comprehensively validated, and employed in molecular dynamics (MD) simulations to investigate the hydration of the anions of the Hofmeister series in aqueous clusters. Furthermore, the hydration of α,ω-alkyl diammonium cations and their effect on organic/water phase separation, in light of their hydration extent, has been investigated by performing extensive simulations with empirical force fields which were carefully adapted and validated for this purpose.

The procedure for generating DFTB3 parameters for the halogen atoms and their interaction with hydrogen and oxygen has been discussed in Chapter 2 of this thesis. The newly generated parameters were validated on the basis of the hydration properties of chloride, bromide and iodide anions in clusters containing up to four water molecules. Comparison of the structural and energetic properties as well as the harmonic vibrational frequencies obtained from DFTB3 calculations with the results of high-level *ab initio* quantum chemistry revealed that, despite the approximate nature of the DFTB3 model, it predicts the hydration properties of halide–water clusters with reliable accuracy. This is due in particular to the treatment of the charge fluctuations self-consistently in this model; the partial atomic charges predicted by DFTB3 were found to be in a good agreement with those obtained from *ab initio* quantum-chemistry calculations.

The newly parameterized DFTB3 model was employed in MD simulations to investigate the hydration behavior of halides in clusters containing up to 48 water molecules. The simulation results, which are presented and discussed in Chapter 3, revealed that fluoride is enclosed by a tight sphere of water molecules and therefore remains fully hydrated inside the aqueous cluster, while larger halides prefer to lie asymmetrically hydrated at the cluster surface. This difference may be attributed to the ion–water binding energy, which in the case of fluoride is about twice as large as that for the larger halides. Moreover, it was observed that at higher temperatures, at which entropic effects are more pronounced, interior hydration becomes more favorable. Accordingly, we conclude that strong ion–water interactions and entropic effects promote interior hydration for fluoride while weaker ion–water interactions and larger size and polarizability result in partial hydration of larger halide anions at the cluster surface. The first-principles-based results obtained in this work confirm the predictions of MD simulations with empirical force fields performed previously.[28] Furthermore, these results are expected to be used as a reference for future investigations.

The efficiency and accuracy of the newly parameterized DFTB3 model inspire further applications of this model for investigating ion hydration. Oxychlorine ($ClO_{1\text{-}4}^-$) anions are appropriate paradigms for this purpose as they have attracted considerable attention in the recent years due to their presence in the environment.[240-243] These investigations might also provide further insight into the determinants of the hydration extent of ions as the charge, size and polarizability of oxychlorine anions change systematically by increasing the number of oxygen atoms. In fact, experimental investigations have demonstrated that the surface propensity of oxychlorine anions

increases from ClO^- to ClO_4^-.[188] It is worth mentioning that preliminary calculations have demonstrated the ability of DFTB3 to predict low-energy conformers of small water clusters containing these anions compared to the results of accurate *ab initio* quantum-chemistry calculations. Analogous investigations might be conducted to characterize the hydration behavior of $BrO_{1\text{-}4}^-$ and $IO_{1\text{-}4}^-$ anions.

The accuracy of DFTB models in predicting the structural and energetic properties as well as the harmonic vibrational frequencies of clusters containing the polyatomic anions of the Hofmeister series has been comprehensively benchmarked in Chapter 4. Comparison of DFTB results with those obtained from high-level *ab initio* quantum-chemistry calculations demonstrated the accuracy of DFTB3 with deviations comparable to those observed for halide anions. Overall, the results presented in Chapters 2–4 suggest that DFTB3 model is a reliable method for describing ion–water interactions for a broad range of anions.

In light of the accuracy of the DFTB3 model, the hydration behavior of the polyatomic anions of the Hofmeister series has been investigated by DFTB3-MD simulations in Chapter 5. Analogous to what was observed for the halide series, the carbonate, sulfate and hydrogen phosphate anions – with strong ion–water binding energies – were found to be surrounded by a tight sphere of water molecules and accordingly adopt interior hydration inside the water clusters. However, acetate, nitrate, perchlorate and thiocyanate were found to be only partially hydrated at the cluster surface, similarly to the larger halide anions. Close inspection of the simulation results revealed that the singly-charged anions posses partial *hydrophobic* character as a result of charge delocalization on their terminal atoms. This interesting feature might be further

examined by a systematic decomposition of the ion–water interaction energies into electrostatic, polarization and charge transfer components, according for instance to the scheme developed by Kitaura and Morokuma.[244] Comparison of the interaction energy components for a broad range of ions might facilitate understanding of the hydration extent of ions in light of the nature of their interaction with water molecules.

According to the results obtained in this work, we conclude that the binding energy, charge density and polarizability of ions are key factors in ultimately determining the extent of their hydration. It is worth mentioning that the ion–water binding energy seems to be the dominant factor as our results demonstrated a correlation between the hydration extent of ions and the strength of their ion–water binding energies. Moreover, a qualitative correlation was observed between the hydration extent of the ions and their ordering in the Hofmeister series. This highlights the importance of the hydration extent in explaining the mechanism of the Hofmeister effect.

The relationship between the hydration extent of ions and their specific effect was investigated for α,ω-alkyl diammonium cations. These ions were chosen in part because they allow a systematic adjustment of their hydration extent by varying the alkyl chain length. The results of our comprehensive MD simulations in water clusters, which are presented in Chapter 6, indicated that the surface-solvated structures are stabilized in the case of longer dications. As presented in Chapter 7, it was also found that the longer dications interact with the hydrophobic domain of tetrahydrofuran (THF) molecules in THF/water mixtures and stabilize mixing, whereas smaller dications, which prefer to be fully hydrated in the aqueous phase, were found to promote phase separation. These findings provide evidence for a possible correlation between the hydration extent of ions

and their salting-in and salting-out behavior in aqueous solutions. In this respect, we suggest that the DFTB3 model could be implemented in quantum mechanics/molecular mechanics simulations to extend the investigation conducted in Chapter 7 to the anions of the Hofmeister series. This will provide a transferable approach that could be used to perform affordable first-principles-based simulations for solutions. Moreover, according to the results obtained in Chapters 6 and 7, another possible way to extend this work is to investigate the impact of the position of hydrophilic groups on the hydration and solubility of organic molecules and macromolecules in aqueous systems. As mentioned in Chapter 7, it has been shown experimentally that the presence of hydrophobic groups in the alkyl chain of dications has significant effects on their hydration behavior.[207] It is worth mentioning that molecular simulations may be used to guide the design of new switchable solvents.

The methodology presented in this work could also be used to investigate the effect of ions on a variety of cluster properties. In particular, the effect of ions on the melting temperature and evaporation rate of water clusters as a function of cluster size could be investigated by DFTB3-MD simulations. Such investigations might provide information about the extent of interaction of hydrated ions with water molecules and therefore provide insight into the extent of ionic effects on the water hydrogen-bond structure. The results of these investigations could also shed some light onto the effects of ions on the stability of the atmospheric ionic water clusters.

In summary, the results obtained in this work demonstrate that kosmotropic anions tend to be fully hydrated while chaotropic anions prefer partial hydration at interfaces. Our results also highlight the importance of the hydration extent, along with

the effect of ions on water structure, in explaining specific ion effects in aqueous solutions. The methodology developed in this work is expected to be broadly applied in future investigations of ion hydration.

References

(1) Curtius, J.; Lovejoy, E. R.; Froyd, K. D. *Space Sci. Rev.* **2006**, *125*, 159-167.
(2) Hirsikko, A.; Nieminen, T.; Gagne, S.; Lehtipalo, K.; Manninen, H. E.; Ehn, M.; Horrak, U.; Kerminen, V. M.; Laakso, L.; McMurry, P. H.; Mirme, A.; Mirme, S.; Petaja, T.; Tammet, H.; Vakkari, V.; Vana, M.; Kulmala, M. *Atmos. Chem. Phys.* **2011**, *11*, 767-798.
(3) Pawar, S. D.; Murugavel, P.; Gopalakrishnan, V. *J. Earth Syst. Sci.* **2011**, *120*, 843-850.
(4) Von Hippel, P. H.; Schleich, T. *Accounts Chem. Res.* **1969**, *2*, 257-265.
(5) Baldwin, R. L. *Biophys. J.* **1996**, *71*, 2056-2063.
(6) Chi, E. Y.; Krishnan, S.; Randolph, T. W.; Carpenter, J. F. *Pharm. Res.* **2003**, *20*, 1325-1336.
(7) Shukla, D.; Schneider, C. P.; Trout, B. L. *J. Am. Chem. Soc.* **2011**, *133*, 18713-18718.
(8) Mercer, S. M.; Jessop, P. G. *Chemsuschem* **2010**, *3*, 467-470.
(9) Kumar, A. *Chem. Rev.* **2001**, *101*, 1-19.
(10) Asmis, K. R.; Neumark, D. M. *Accounts Chem. Res.* **2012**, *45*, 43-52.
(11) Lisy, J. M. *J. Chem. Phys.* **2006**, *125*, 132302.
(12) Meot-Ner, M. *Chem. Rev.* **2005**, *105*, 213-284.
(13) Baer, M. D.; Mundy, C. J. *J. Phys. Chem. Lett.* **2011**, *2*, 1088-1093.
(14) O'Brien, J. T.; Williams, E. R. *J. Am. Chem. Soc.* **2012**, *134*, 10228-10236.
(15) Wyttenbach, T.; Bowers, M. T. *Chem. Phys. Lett.* **2009**, *480*, 1-16.
(16) Wyttenbach, T.; Liu, D. F.; Bowers, M. T. *Int. J. Mass Spectrom.* **2005**, *240*, 221-232.
(17) Lo Nostro, P.; Ninham, B. W. *Chem. Rev.* **2012**, *112*, 2286-2322.
(18) Zhang, Y. J.; Cremer, P. S. *Curr. Opin. Chem. Biol.* **2006**, *10*, 658-663.
(19) Kunz, W.; Henle, J.; Ninham, B. W. *Curr. Opin. Colloid Interface Sci.* **2004**, *9*, 19-37.
(20) Hofmeister, F. *Arch. Exp. Pathol. Pharmacol.* **1888**, *24*, 247-260.
(21) Collins, K. D.; Washabaugh, M. W. *Q. Rev. Biophys.* **1985**, *18*, 323-422.
(22) Cacace, M. G.; Landau, E. M.; Ramsden, J. J. *Q. Rev. Biophys.* **1997**, *30*, 241-277.
(23) Marcus, Y. *Chem. Rev.* **2009**, *109*, 1346-1370.
(24) Omta, A. W.; Kropman, M. F.; Woutersen, S.; Bakker, H. J. *Science* **2003**, *301*, 347-349.
(25) Tobias, D. J.; Hemminger, J. C. *Science* **2008**, *319*, 1197-1198.
(26) Zhang, Y. J.; Cremer, P. S. *Annu. Rev. Phys. Chem.* **2009**, *61*, 63-83.
(27) Langmuir, I. *J. Am. Chem. Soc.* **1917**, *39*, 1848-1906.
(28) Jungwirth, P.; Tobias, D. J. *Chem. Rev.* **2006**, *106*, 1259-1281.
(29) Finlayson-Pitts, B. J. *Phys. Chem. Chem. Phys.* **2009**, *11*, 7760-7779.
(30) Kebarle, P. *Annu. Rev. Phys. Chem.* **1977**, *28*, 445-476.
(31) Arshadi, M.; Yamdagni, R.; Kebarle, P. *J. Phys. Chem.* **1970**, *74*, 1475-1482.
(32) Blades, A. T.; Klassen, J. S.; Kebarle, P. *J. Am. Chem. Soc.* **1995**, *117*, 10563-10571.
(33) Blades, A. T.; Klassen, J. S.; Kebarle, P. *J. Am. Chem. Soc.* **1996**, *118*, 12437-12442.
(34) Klassen, J. S.; Blades, A. T.; Kebarle, P. *J. Am. Chem. Soc.* **1994**, *116*, 12075-12076.

(35) Blades, A. T.; Kebarle, P. *J. Phys. Chem. A* **2005**, *109*, 8293-8298.
(36) Roscioli, J. R.; Diken, E. G.; Johnson, M. A.; Horvath, S.; McCoy, A. B. *J. Phys. Chem. A* **2006**, *110*, 4943-4952.
(37) Wang, X.-B.; Yang, X.; Nicholas, J. B.; Wang, L.-S. *Science* **2001**, *294*, 1322-1325.
(38) Yang, X.; Wang, X.-B.; Wang, L.-S. *J. Phys. Chem. A* **2002**, *106*, 7607-7616.
(39) Wang, X.-B.; Yang, X.; Wang, L.-S.; Nicholas, J. B. *J. Chem. Phys.* **2002**, *116*, 561-570.
(40) Masamura, M. *J. Mol. Strct. (THEOCHEM)* **1999**, *466*, 85-93.
(41) Xantheas, S. S.; Dunning, T. H. *J. Phys. Chem.* **1994**, *98*, 13489-13497.
(42) Lambrecht, D. S.; Clark, G. N. I.; Head-Gordon, T.; Head-Gordon, M. *J. Phys. Chem. A* **2011**, *115*, 11438-11454.
(43) Pathak, A. K.; Maity, D. K. *J. Phys. Chem. A* **2009**, *113*, 13443-13447.
(44) Pathak, A. K.; Mukherjee, T.; Maity, D. K. *J. Phys. Chem. A* **2008**, *112*, 3399-3408.
(45) Schonfeld, P.; Montero, L.; Fabian, J. *Biophys. J.* **2005**, *89*, 1504-1515.
(46) Pye, C. C.; Walker, V. E. J. *J. Phys. Chem. A* **2011**, *115*, 13007-13015.
(47) Salvador, P.; Curtis, J. E.; Tobias, D. J.; Jungwirth, P. *Phys. Chem. Chem. Phys.* **2003**, *5*, 3752-3757.
(48) Jungwirth, P.; Curtis, J. E.; Tobias, D. J. *Chem. Phys. Lett.* **2003**, *367*, 704-710.
(49) Perera, L.; Berkowitz, M. L. *J. Chem. Phys.* **1991**, *95*, 1954-1963.
(50) Perera, L.; Berkowitz, M. L. *J. Chem. Phys.* **1992**, *96*, 8288-8294.
(51) Perera, L.; Berkowitz, M. L. *J. Chem. Phys.* **1993**, *99*, 4236-4237.
(52) Dang, L. X.; Rice, J. E.; Caldwell, J.; Kollman, P. A. *J. Am. Chem. Soc.* **1991**, *113*, 2481-2486.
(53) Dang, L. X.; Garrett, B. C. *J. Chem. Phys.* **1993**, *99*, 2972-2977.
(54) Koch, D. M.; Peslherbe, G. H. *Chem. Phys. Lett.* **2002**, *359*, 381-389.
(55) Jungwirth, P.; Tobias, D. J. *J. Phys. Chem. B* **2001**, *105*, 10468-10472.
(56) Jungwirth, P.; Tobias, D. J. *J. Phys. Chem. B* **2002**, *106*, 6361-6373.
(57) Ghosal, S.; Hemminger, J. C.; Bluhm, H.; Mun, B. S.; Hebenstreit, E. L. D.; Ketteler, G.; Ogletree, D. F.; Requejo, F. G.; Salmeron, M. *Science* **2005**, *307*, 563-566.
(58) Elstner, M.; Porezag, D.; Jungnickel, G.; Elsner, J.; Haugk, M.; Frauenheim, T.; Suhai, S.; Seifert, G. *Phys. Rev. B* **1998**, *58*, 7260-7268.
(59) Porezag, D.; Frauenheim, T.; Kohler, T.; Seifert, G.; Kaschner, R. *Phys. Rev. B* **1995**, *51*, 12947-12957.
(60) Slater, J. C.; Koster, G. F. *Phys. Rev.* **1954**, *94*, 1498-1524.
(61) Gaus, M.; Cui, Q.; Elstner, M. *J. Chem. Theory Comput.* **2011**, *7*, 931-948.
(62) Elstner, M.; Frauenheim, T.; Kaxiras, E.; Seifert, G.; Suhai, S. *Phys. Stat. Sol. B* **2000**, *217*, 357-376.
(63) Aradi, B.; Hourahine, B.; Frauenheim, T. *J. Phys. Chem. A* **2007**, *111*, 5678-5684.
(64) Jorgensen, W. L.; Maxwell, D. S.; TiradoRives, J. *J. Am. Chem. Soc.* **1996**, *118*, 11225-11236.
(65) Chang, T. M.; Dang, L. X. *Chem. Rev.* **2006**, *106*, 1305-1322.
(66) Netz, R. R.; Horinek, D. *Annu. Rev. Phys. Chem.* **2012**, *63*, 401-418.
(67) Levin, Y. *Phys. Rev. Lett.* **2009**, *102*, 147803.
(68) Caleman, C.; Hub, J. S.; van Maaren, P. J.; van der Spoel, D. *Proc. Natl. Acad. Sci. U.S.A.* **2011**, *108*, 6838-6842.

(69) Nguyen, T.-N. V.; Hughes, S. R.; Peslherbe, G. H. *J. Phys. Chem. B* **2008**, *112*, 621-635.
(70) Hernandez de la Pena, L.; Peslherbe, G. H. *J. Phys. Chem. B* **2010**, *114*, 5404-5411.
(71) Sremaniak, L. S.; Perera, L.; Berkowitz, M. L. *Chem. Phys. Lett.* **1994**, *218*, 377-382.
(72) Vazdar, M.; Pluharova, E.; Mason, P. E.; Vacha, R.; Jungwirth, P. *J. Phys. Chem. Lett.* **2012**, *3*, 2087-2091.
(73) Elstner, M.; Cui, Q.; Munih, P.; Kaxiras, E.; Frauenheim, T.; Karplus, M. *J. Comput. Chem.* **2003**, *24*, 565-581.
(74) Frauenheim, T.; Seifert, G.; Elstner, M.; Hajnal, Z.; Jungnickel, G.; Porezag, D.; Suhai, S.; Scholz, R. *Phys. Stat. Sol. B* **2000**, *217*, 41-62.
(75) Frauenheim, T.; Seifert, G.; Elstner, M.; Niehaus, T.; Kohler, C.; Amkreutz, M.; Sternberg, M.; Hajnal, Z.; Di Carlo, A.; Suhai, S. *J. Phys. Condens. Matter* **2002**, *14*, 3015-3047.
(76) Witek, H. A.; Morokuma, K. *J. Comput. Chem.* **2004**, *25*, 1858-1864.
(77) Hazebroucq, S.; Picard, G. S.; Adamo, C.; Heine, T.; Gemming, S.; Seifert, G. *J. Chem. Phys.* **2005**, *123*, 134510.
(78) Zheng, G. S.; Irle, S.; Morokuma, K. *Chem. Phys. Lett.* **2005**, *412*, 210-216.
(79) Kruger, T.; Elstner, M.; Schiffels, P.; Frauenheim, T. *J. Chem. Phys.* **2005**, *122*, 114110.
(80) Köhler, C.; Frauenheim, T. *Surf. Sci.* **2006**, *600*, 453-460.
(81) Choi, T. H.; Jordan, K. D. *J. Phys. Chem. B* **2010**, *114*, 6932-6936.
(82) Goyal, P.; Elstner, M.; Cui, Q. *J. Phys. Chem. B* **2011**, *115*, 6790-6805.
(83) Gaus, M.; Goez, A.; Elstner, M. *J. Chem. Theory Comput.* **2013**, *9*, 338-354.
(84) Yang, Y.; Yu, H.; York, D.; Elstner, M.; Cui, Q. *J. Chem. Theory Comput.* **2008**, *4*, 2067-2084.
(85) Moreira, N. H.; Dolgonos, G.; Aradi, B.; da Rosa, A. L.; Frauenheim, T. *J. Chem. Theory Comput.* **2009**, *5*, 605-614.
(86) Dolgonos, G.; Aradi, B.; Moreira, N. H.; Frauenheim, T. *J. Chem. Theory Comput.* **2010**, *6*, 266-278.
(87) Sarkar, S.; Pal, S.; Sarkar, P.; Rosa, A. L.; Frauenheim, T. *J. Chem. Theory Comput.* **2011**, *7*, 2262-2276.
(88) Grundkotter-Stock, B.; Bezugly, V.; Kunstmann, J.; Cuniberti, G.; Frauenheim, T.; Niehaus, T. A. *J. Chem. Theory Comput.* **2012**, *8*, 1153-1163.
(89) Elstner, M. *Theor. Chem. Acc.* **2006**, *116*, 316-325.
(90) Elstner, M.; Frauenheim, T.; McKelvey, J.; Seifert, G. *J. Phys. Chem. A* **2007**, *111*, 5607-5608.
(91) Yang, Y.; Yu, H. B.; York, D.; Cui, Q.; Elstner, M. *J. Phys. Chem. A* **2007**, *111*, 10861-10873.
(92) Perdew, J. P.; Burke, K.; Ernzerhof, M. *Phys. Rev. Lett.* **1996**, *77*, 3865-3868.
(93) Adamo, C.; Barone, V. *J. Chem. Phys.* **1999**, *110*, 6158-6170.
(94) Stephens, P. J.; Devlin, F. J.; Chabalowski, C. F.; Frisch, M. J. *J. Phys. Chem.* **1994**, *98*, 11623-11627.
(95) Becke, A. D. *J. Chem. Phys.* **1993**, *98*, 5648-5652.
(96) Lee, C. T.; Yang, W. T.; Parr, R. G. *Phys. Rev. B* **1988**, *37*, 785-789.

(97) Francl, M. M.; Pietro, W. J.; Hehre, W. J.; Binkley, J. S.; Gordon, M. S.; DeFrees, D. J.; Pople, J. A. *J. Chem. Phys.* **1982**, *77*, 3654-3665.
(98) Rassolov, V. A.; Ratner, M. A.; Pople, J. A.; Redfern, P. C.; Curtiss, L. A. *J. Comput. Chem.* **2001**, *22*, 976-984.
(99) Glukhovtsev, M. N.; Pross, A.; McGrath, M. P.; Radom, L. *J. Chem. Phys.* **1995**, *103*, 1878-1885.
(100) Feller, D. *J. Comput. Chem.* **1996**, *17*, 1571-1586.
(101) Schuchardt, K. L.; Didier, B. T.; Elsethagen, T.; Sun, L.; Gurumoorthi, V.; Chase, J.; Li, J.; Windus, T. L. *J. Chem. Inf. Model.* **2007**, *47*, 1045-1052.
(102) Woon, D. E.; Dunning, T. H. *J. Chem. Phys.* **1993**, *98*, 1358-1371.
(103) Peterson, K. A.; Figgen, D.; Goll, E.; Stoll, H.; Dolg, M. *J. Chem. Phys.* **2003**, *119*, 11113-11123.
(104) Peterson, K. A.; Shepler, B. C.; Figgen, D.; Stoll, H. *J. Phys. Chem. A* **2006**, *110*, 13877-13883.
(105) Lee, H. M.; Kim, K. S. *J. Chem. Phys.* **2001**, *114*, 4461-4471.
(106) Masamura, M. *J. Chem. Phys.* **2003**, *118*, 6336-6347.
(107) Köhler, C.; Frauenheim, T.; Hourahine, B.; Seifert, G.; Sternberg, M. *J. Phys. Chem. A* **2007**, *111*, 5622-5629.
(108) Møller, C.; Plesset, M. S. *Phys. Rev.* **1934**, *46*, 618-622.
(109) Boys, S. F.; Bernardi, F. *Mol. Phys.* **1970**, *19*, 553-566.
(110) Huber, K. P.; Herzberg, G. *Molecular Spectra and Molecular Structure. IV. Constants of Diatomic Molecules*; Van Nostrand Reinhold Company: New York, 1979.
(111) Deeley, C. M.; Mills, I. M. *J. Mol. Spectrosc.* **1985**, *114*, 368-376.
(112) Casper, B.; Mack, H. G.; Muller, H. S. P.; Willner, H.; Oberhammer, H. *J. Phys. Chem.* **1994**, *98*, 8339-8342.
(113) Linstrom, P. J.; Mallard, W. G. *NIST Chemistry WebBook, NIST Standard Reference Database Number 69*, National Institute of Standards and Technology, http://webbook.nist.gov, (retrieved October 2012).
(114) Koga, Y.; Takeo, H.; Kondo, S.; Sugie, M.; Matsumura, C.; McRae, G. A.; Cohen, E. A. *J. Mol. Spectrosc.* **1989**, *138*, 467-481.
(115) Ozeki, H.; Saito, S. *J. Chem. Phys.* **2004**, *120*, 5110-5116.
(116) Horvath, S.; McCoy, A. B.; Elliott, B. M.; Weddle, G. H.; Roscioli, J. R.; Johnson, M. A. *J. Phys. Chem. A* **2010**, *114*, 1556-1568.
(117) Ayotte, P.; Nielsen, S. B.; Weddle, G. H.; Johnson, M. A.; Xantheas, S. S. *J. Phys. Chem. A* **1999**, *103*, 10665-10669.
(118) Singh, U. C.; Kollman, P. A. *J. Comput. Chem.* **1984**, *5*, 129-145.
(119) Besler, B. H.; Merz, K. M.; Kollman, P. A. *J. Comput. Chem.* **1990**, *11*, 431-439.
(120) Hu, H.; Lu, Z.; Yang, W. *J. Chem. Theory Comput.* **2007**, *3*, 1004-1013.
(121) Garrett, B. C. *Science* **2004**, *303*, 1146-1147.
(122) Hu, J. H.; Shi, Q.; Davidovits, P.; Worsnop, D. R.; Zahniser, M. S.; Kolb, C. E. *J. Phys. Chem.* **1995**, *99*, 8768-8776.
(123) Stern, A. C.; Baer, M. D.; Mundy, C. J.; Tobias, D. J. *J. Chem. Phys.* **2013**, *138*, 114709.
(124) Tobias, D. J.; Jungwirth, P.; Parrinello, M. *J. Chem. Phys.* **2001**, *114*, 7036-7044.
(125) Torrie, G. M.; Valleau, J. P. *J. Comput. Chem.* **1977**, *23*, 187-199.

(126) Kumar, S.; Rosenberg, J. M.; Bouzida, D.; Swendsen, R. H.; Kollman, P. A. *J. Comput. Chem.* **1995**, *16*, 1339-1350.
(127) Gelman-Constantin, J.; Carignano, M. A.; Szleifer, I.; Marceca, E. J.; Corti, H. R. *J. Chem. Phys.* **2010**, *133*, 024506.
(128) Douady, J.; Calvo, F.; Spiegelman, F. *Eur. Phys. J. D* **2009**, *52*, 47-50.
(129) Burnham, C. J.; Petersen, M. K.; Day, T. J. F.; Iyengar, S. S.; Voth, G. A. *J. Chem. Phys.* **2006**, *124*, 024327.
(130) A. Grossfield, "WHAM: the weighted histogram analysis method", version 2.0.6, http://membrane.urmc.rochester.edu/content/wham.
(131) Sugita, Y.; Okamoto, Y. *Chem. Phys. Lett.* **1999**, *314*, 141-151.
(132) Earl, D. J.; Deem, M. W. *Phys. Chem. Chem. Phys.* **2005**, *7*, 3910-3916.
(133) Wood, R. H.; Yezdimer, E. M.; Sakane, S.; Barriocanal, J. A.; Doren, D. J. *J. Chem. Phys.* **1999**, *110*, 1329-1337.
(134) Dunning, T. H. *J. Chem. Phys.* **1989**, *90*, 1007-1023.
(135) Santra, B.; Michaelides, A.; Scheffler, M. *J. Chem. Phys.* **2007**, *127*, 184104.
(136) Zhao, Y.; Truhlar, D. G. *J. Chem. Theory Comput.* **2005**, *1*, 415-432.
(137) Pople, J. A.; Headgordon, M.; Raghavachari, K. *J. Chem. Phys.* **1987**, *87*, 5968-5975.
(138) Egorov, A. V.; Brodskaya, E. N.; Laaksonen, A. *Synth. React. Inorg. Met.-Org. Chem.* **2008**, *38*, 62-68.
(139) Lindemann, F. A. *Phys. Z* **1910**, *11*, 609.
(140) Bosma, W. B.; Rhodes, M. M. *J. Chem. Phys.* **2002**, *117*, 9286-9292.
(141) Kuo, J. L.; Ciobanu, C. V.; Ojamae, L.; Shavitt, I.; Singer, S. J. *J. Chem. Phys.* **2003**, *118*, 3583-3588.
(142) Nguyen, Q. C.; Ong, Y. S.; Soh, H.; Kuo, J.-L. *J. Phys. Chem. A* **2008**, *112*, 6257-6261.
(143) Ninham, B. W.; Lo Nostro, P. *Molecular Forces and Self Assembly*; Cambridge University Press: Cambridge, 2010.
(144) Kunz, W. *Curr. Opin. Colloid Interface Sci.* **2010**, *15*, 34-39.
(145) Kunz, W.; Henle, J.; Ninham, B. W. *Curr. Opin. Colloid Interface Sci.* **2004**, *9*, 19-37.
(146) Kunz, W.; Lo Nostro, P.; Ninham, B. W. *Curr. Opin. Colloid Interface Sci.* **2004**, *9*, 1-18.
(147) Clark, T. *J. Mol. Struct. THEOCHEM* **2000**, *530*, 1-10.
(148) Bredow, T.; Jug, K. *Theor. Chem. Acc.* **2005**, *113*, 1-14.
(149) Yu, H.; Cui, Q. *J. Chem. Phys.* **2007**, *127*, 234504.
(150) Han, W. G.; Elstner, M.; Jalkanen, K. J.; Frauenheim, T.; Suhai, S. *Int. J. Quantum Chem.* **2000**, *78*, 459-479.
(151) Cui, Q.; Elstner, M.; Kaxiras, E.; Frauenheim, T.; Karplus, M. *J. Phys. Chem. B* **2001**, *105*, 569-585.
(152) Elstner, M.; Jalkanen, K. J.; Knapp-Mohammady, M.; Frauenheim, T.; Suhai, S. *Chem. Phys.* **2001**, *263*, 203-219.
(153) Niehaus, T. A.; Elstner, M.; Frauenheim, T.; Suhai, S. *J. Mol. Struct. THEOCHEM* **2001**, *541*, 185-194.
(154) Zhou, H. Y.; Tajkhorshid, E.; Frauenheim, T.; Suhai, S.; Elstner, M. *Chem. Phys.* **2002**, *277*, 91-103.

(155) Elstner, M.; Frauenheim, T.; Suhai, S. *J. Mol. Struct. THEOCHEM* **2003**, *632*, 29-41.
(156) Sattelmeyer, K. W.; Tirado-Rives, J.; Jorgensen, W. L. *J. Phys. Chem. A* **2006**, *110*, 13551-13559.
(157) Otte, N.; Scholten, M.; Thiel, W. *J. Phys. Chem. A* **2007**, *111*, 5751-5755.
(158) Gaussian 09, Revision B.01, Frisch, M. J.; Trucks, G. W.; Schlegel, H. B.; Scuseria, G. E.; Robb, M. A.; Cheeseman, J. R.; Scalmani, G.; Barone, V.; Mennucci, B.; Petersson, G. A.; Nakatsuji, H.; Caricato, M.; Li, X.; Hratchian, H. P.; Izmaylov, A. F.; Bloino, J.; Zheng, G.; Sonnenberg, J. L.; Hada, M.; Ehara, M.; Toyota, K.; Fukuda, R.; Hasegawa, J.; Ishida, M.; Nakajima, T.; Honda, Y.; Kitao, O.; Nakai, H.; Vreven, T.; Montgomery, Jr., J. A.; Peralta, J. E.; Ogliaro, F.; Bearpark, M.; Heyd, J. J.; Brothers, E.; Kudin, K. N.; Staroverov, V. N.; Kobayashi, R.; Normand, J.; Raghavachari, K.; Rendell, A.; Burant, J. C.; Iyengar, S. S.; Tomasi, J.; Cossi, M.; Rega, N.; Millam, J. M.; Klene, M.; Knox, J. E.; Cross, J. B.; Bakken, V.; Adamo, C.; Jaramillo, J.; Gomperts, R.; Stratmann, R. E.; Yazyev, O.; Austin, A. J.; Cammi, R.; Pomelli, C.; Ochterski, J. W.; Martin, R. L.; Morokuma, K.; Zakrzewski, V. G.; Voth, G. A.; Salvador, P.; Dannenberg, J. J.; Dapprich, S.; Daniels, A. D.; Farkas, Ö.; Foresman, J. B.; Ortiz, J. V.; Cioslowski, J.; Fox, D. J. Gaussian, Inc., Wallingford CT, 2009.
(159) Sinha, P.; Boesch, S. E.; Gu, C. M.; Wheeler, R. A.; Wilson, A. K. *J. Phys. Chem. A* **2004**, *108*, 9213-9217.
(160) Su, J. T.; Xu, X.; Goddard, W. A. *J. Phys. Chem. A* **2004**, *108*, 10518-10526.
(161) Curtiss, L. A.; Frurip, D. J.; Blander, M. *J. Chem. Phys.* **1979**, *71*, 2703-2711.
(162) Meotner, M. *J. Am. Chem. Soc.* **1988**, *110*, 3854-3858.
(163) Lee, N.; Keesee, R. G.; Castleman, A. W. *J. Chem. Phys.* **1980**, *72*, 1089-1094.
(164) Robertson, W. H.; Price, E. A.; Weber, J. M.; Shin, J. W.; Weddle, G. H.; Johnson, M. A. *J. Phys. Chem. A* **2003**, *107*, 6527-6532.
(165) Goebbert, D. J.; Garand, E.; Wende, T.; Bergmann, R.; Meijer, G.; Asmis, K. R.; Neumark, D. M. *J. Phys. Chem. A* **2009**, *113*, 7584-7592.
(166) Wang, X. B.; Yang, X.; Wang, L. S.; Nicholas, J. B. *J. Chem. Phys.* **2002**, *116*, 561-570.
(167) Algaer, E. A.; van der Vegt, N. F. A. *J. Phys. Chem. B* **2011**, *115*, 13781-13787.
(168) Onorato, R. M.; Otten, D. E.; Saykally, R. J. *Proc. Natl. Acad. Sci. U.S.A.* **2009**, *106*, 15176-15180.
(169) Wang, C.; Ge, Y.; Mortensen, J.; Westh, P. *J. Phys. Chem. B* **2011**, *115*, 9955-9961.
(170) Okabe, K.; Matsumiya, N.; Mano, H. *Sep. Purif. Technol.* **2007**, *57*, 242-249.
(171) Finlayson-Pitts, B. J.; Pitts, J. N. *Chemistry of the Uper and Lower Atmosphere*; Academic Press: San Diego, 2000.
(172) Yu, Y.; Ezell, M. J.; Zelenyuk, A.; Imre, D.; Alexander, L.; Ortega, J.; Thomas, J. L.; Gogna, K.; Tobias, D. J.; D'Anna, B.; Harmon, C. W.; Johnson, S. N.; Finlayson-Pitts, B. J. *Phys. Chem. Chem. Phys.* **2008**, *10*, 3063-3071.
(173) Wingen, L. M.; Moskun, A. C.; Johnson, S. N.; Thomas, J. L.; Roeselova, M.; Tobias, D. J.; Kleinman, M. T.; Finlayson-Pitts, B. J. *Phys. Chem. Chem. Phys.* **2008**, *10*, 5668-5677.
(174) Richards, N. K.; Wingen, L. M.; Callahan, K. M.; Nishino, N.; Kleinman, M. T.; Tobias, D. J.; Finlayson-Pitts, B. J. *J. Phys. Chem. A* **2011**, *115*, 5810-5821.

(175) Drisdell, W. S.; Saykally, R. J.; Cohen, R. C. *J. Phys. Chem. C* **2010**, *114*, 11880-11885.
(176) Laver, D. R.; Lenz, G. K. E.; Dulhunty, A. F. *J. Physiol. London* **2001**, *535*, 715-728.
(177) Xu, Y.; Szep, S.; Lu, Z. *Proc. Natl. Acad. Sci. U.S.A.* **2009**, *106*, 20515-20519.
(178) Gibb, C. L. D.; Gibb, B. C. *J. Am. Chem. Soc.* **2011**, *133*, 7344-7347.
(179) Jungwirth, P.; Winter, B. *Annu. Rev. Phys. Chem.* **2008**, *59*, 343-366.
(180) Gopalakrishnan, S.; Jungwirth, P.; Tobias, D. J.; Allen, H. C. *J. Phys. Chem. B* **2005**, *109*, 8861-8872.
(181) Petersen, P. B.; Saykally, R. J.; Mucha, M.; Jungwirth, P. *J. Phys. Chem. B* **2005**, *109*, 10915-10921.
(182) Minofar, B.; Vacha, R.; Wahab, A.; Mahiuddin, S.; Kunz, W.; Jungwirth, P. *J. Phys. Chem. B* **2006**, *110*, 15939-15944.
(183) Dang, L. X.; Chang, T. M.; Roeselova, M.; Garrett, B. C.; Tobias, D. J. *J. Chem. Phys.* **2006**, *124*, 066101.
(184) Minofar, B.; Jungwirth, P.; Das, M. R.; Kunz, W.; Mahiuddin, S. *J. Phys. Chem. C* **2007**, *111*, 8242-8247.
(185) Thomas, J. L.; Roeselova, M.; Dang, L. X.; Tobias, D. J. *J. Phys. Chem. A* **2007**, *111*, 3091-3098.
(186) Du, H.; Liu, J.; Ozdemir, O.; Nguyen, A. V.; Miller, J. D. *J. Colloid Interface Sci.* **2008**, *318*, 271-277.
(187) Miller, Y.; Thomas, J. L.; Kemp, D. D.; Finlayson-Pitts, B. J.; Gordon, M. S.; Tobias, D. J.; Gerber, R. B. *J. Phys. Chem. A* **2009**, *113*, 12805-12814.
(188) Ottosson, N.; Vacha, R.; Aziz, E. F.; Pokapanich, W.; Eberhardt, W.; Svensson, S.; Ohrwall, G.; Jungwirth, P.; Bjorneholm, O.; Winter, B. *J. Chem. Phys.* **2009**, *131*, 124706.
(189) Baer, M. D.; Kuo, I. F. W.; Bluhm, H.; Ghosal, S. *J. Phys. Chem. B* **2009**, *113*, 15843-15850.
(190) Pasalic, H.; Roeselova, M.; Lischka, H. *J. Phys. Chem. B* **2011**, *115*, 1807-1816.
(191) Zhou, J.; Santambrogio, G.; Bruemmer, M.; Moore, D. T.; Meijer, G.; Neumark, D. M.; Asmis, K. R. *J. Chem. Phys.* **2006**, *125*, 111102.
(192) Mason, P. E.; Cruickshank, J. M.; Neilson, G. W.; Buchanan, P. *Phys. Chem. Chem. Phys.* **2003**, *5*, 4686-4690.
(193) Herce, D. H.; Perera, L.; Darden, T. A.; Sagui, C. *J. Chem. Phys.* **2005**, *122*, 024513.
(194) Vrbka, L.; Mucha, M.; Minofar, B.; Jungwirth, P.; Brown, E. C.; Tobias, D. J. *Curr. Opin. Colloid Interface Sci.* **2004**, *9*, 67-73.
(195) Rajamani, S.; Truskett, T. M.; Garde, S. *Proc. Natl. Acad. Sci. U.S.A.* **2005**, *102*, 9475-9480.
(196) Collins, K. D. *Methods* **2004**, *34*, 300-311.
(197) Pankewitz, T.; Lagutschenkov, A.; Niedner-Schatteburg, G.; Xantheas, S. S.; Lee, Y. T. *J. Chem. Phys.* **2007**, *126*, 074307.
(198) Karthikeyan, S.; Singh, J. N.; Park, M.; Kumar, R.; Kim, K. S. *J. Chem. Phys.* **2008**, *128*, 244304.
(199) Bruge, F.; Bernasconi, M.; Parrinello, M. *J. Chem. Phys.* **1999**, *110*, 4734-4736.

(200) Jiang, J. C.; Chang, H. C.; Lee, Y. T.; Lin, S. H. *J. Phys. Chem. A* **1999**, *103*, 3123-3135.
(201) Kim, K. Y.; Cho, U. I.; Boo, D. W. *Bull. Korean Chem. Soc.* **2001**, *22*, 597-604.
(202) Kim, K. Y.; Han, W. H.; Cho, U. I.; Lee, Y. T.; Boo, D. W. *Bull. Korean Chem. Soc.* **2006**, *27*, 2028-2036.
(203) Morrell, T. E.; Shields, G. C. *J. Phys. Chem. A* **2010**, *114*, 4266-4271.
(204) Pickard, F. C.; Dunn, M. E.; Shields, G. C. *J. Phys. Chem. A* **2005**, *109*, 4905-4910.
(205) Gronert, S. *Int. J. Mass Spectrom.* **1999**, *185*, 351-357.
(206) Lee, S. W.; Freivogel, P.; Schindler, T.; Beauchamp, J. L. *J. Am. Chem. Soc.* **1998**, *120*, 11758-11765.
(207) Mercer, S. M.; Robert, T.; Dixon, D. V.; Chen, C. S.; Ghoshouni, Z.; Harjani, J. R.; Jahangiri, S.; Peslherbe, G. H.; Jessop, P. G. *Green Chem.* **2012**, *14*, 832-839.
(208) Demireva, M.; O'Brien, J. T.; Williams, E. R. *J. Am. Chem. Soc.* **2012**, *134*, 11216-11224.
(209) Yang, X.; Fu, Y. J.; Wang, X. B.; Slavicek, P.; Mucha, M.; Jungwirth, P.; Wang, L. S. *J. Am. Chem. Soc.* **2004**, *126*, 876-883.
(210) Minofar, B.; Mucha, M.; Jungwirth, P.; Yang, X.; Fu, Y. J.; Wang, X. B.; Wang, L. S. *J. Am. Chem. Soc.* **2004**, *126*, 11691-11698.
(211) Neria, E.; Fischer, S.; Karplus, M. *J. Chem. Phys.* **1996**, *105*, 1902-1921.
(212) Zhao, Y. L.; Meot-Ner, M.; Gonzalez, C. *J. Phys. Chem. A* **2009**, *113*, 2967-2974.
(213) de Lima, G. F.; Duarte, H. A.; Pliego, J. R. *J. Phys. Chem. B* **2010**, *114*, 15941-15947.
(214) Trzesniak, D.; Kunz, A.-P. E.; van Gunsteren, W. F. *Chemphyschem* **2007**, *8*, 162-169.
(215) Phillips, J. C.; Braun, R.; Wang, W.; Gumbart, J.; Tajkhorshid, E.; Villa, E.; Chipot, C.; Skeel, R. D.; Kale, L.; Schulten, K. *J. Comput. Chem.* **2005**, *26*, 1781-1802.
(216) Thalladi, V. R.; Nusse, M.; Boese, R. *J. Am. Chem. Soc.* **2000**, *122*, 9227-9236.
(217) Mishra, M. K.; Varughese, S.; Ramamurty, U.; Desiraju, G. R. *J. Am. Chem. Soc.* **2013**, *135*, 8121-8124.
(218) McDevit, W. F.; Long, F. A. *J. Am. Chem. Soc.* **1952**, *74*, 1773-1777.
(219) Pegram, L. M.; Wendorff, T.; Erdmann, R.; Shkel, I.; Bellissimo, D.; Felitsky, D. J.; Record, M. T. *Proc. Natl. Acad. Sci. U.S.A.* **2010**, *107*, 7716-7721.
(220) Karlstrom, G. *Phys. Chem. Chem. Phys.* **2003**, *5*, 3238-3246.
(221) Yang, X.; Kiran, B.; Wang, X. B.; Wang, L. S.; Mucha, M.; Jungwirth, P. *J. Phys. Chem. A* **2004**, *108*, 7820-7826.
(222) Girard, S.; Muller-Plathe, F. *Mol. Phys.* **2003**, *101*, 779-787.
(223) Martinez, L.; Andrade, R.; Birgin, E. G.; Martinez, J. M. *J. Comput. Chem.* **2009**, *30*, 2157-2164.
(224) Berendsen, H. J. C.; Postma, J. P. M.; Vangunsteren, W. F.; Dinola, A.; Haak, J. R. *J. Chem. Phys.* **1984**, *81*, 3684-3690.
(225) Jorgensen, W. L.; Madura, J. D.; Swenson, C. J. *J. Am. Chem. Soc.* **1984**, *106*, 6638-6646.
(226) Walser, R.; Mark, A. E.; van Gunsteren, W. F.; Lauterbach, M.; Wipff, G. *J. Chem. Phys.* **2000**, *112*, 10450-10459.
(227) Tanaka, H.; Gubbins, K. E. *J. Chem. Phys.* **1992**, *97*, 2626-2634.

(228) Kumar, S.; Bouzida, D.; Swendsen, R. H.; Kollman, P. A.; Rosenberg, J. M. *J. Comput. Chem.* **1992**, *13*, 1011-1021.
(229) Marcus, Y. *The Properties of Solvents*; Wiley: Chichester, 1998.
(230) Glew, D. N.; Watts, H. *Can. J. Chem.* **1973**, *51*, 1993-1940.
(231) Morcom, K. W.; Smith, R. W. *Trans. Faraday Soc.* **1970**, *66*, 1073-1080.
(232) Faller, R.; Schmitz, H.; Biermann, O.; Muller-Plathe, F. *J. Comput. Chem.* **1999**, *20*, 1009-1017.
(233) Briggs, J. M.; Matsui, T.; Jorgensen, W. L. *J. Comput. Chem.* **1990**, *11*, 958-971.
(234) Damm, W.; Frontera, A.; TiradoRives, J.; Jorgensen, W. L. *J. Comput. Chem.* **1997**, *18*, 1955-1970.
(235) Rappe, A. K.; Casewit, C. J.; Colwell, K. S.; Goddard, W. A.; Skiff, W. M. *J. Am. Chem. Soc.* **1992**, *114*, 10024-10035.
(236) Verlinde, C. L.; Deranter, C. J.; Blaton, N. M.; Peeters, O. M. *Acta Crystallogr., Sect. B: Struct. Sci* **1989**, *45*, 107-112.
(237) Wensink, E. J. W.; Hoffmann, A. C.; van Maaren, P. J.; van der Spoel, D. *J. Chem. Phys.* **2003**, *119*, 7308-7317.
(238) Bowron, D. T.; Finney, J. L.; Soper, A. K. *J. Am. Chem. Soc.* **2006**, *128*, 5119-5126.
(239) Bragg, A. E.; Kanu, G. U.; Schwartz, B. J. *J. Phys. Chem. Lett.* **2011**, *2*, 2797-2804.
(240) Kang, N. G.; Anderson, T. A.; Jackson, W. A. *Anal. Chim. Acta* **2006**, *567*, 48-56.
(241) Kang, N.; Jackson, W. A.; Dasgupta, P. K.; Anderson, T. A. *Sci. Total Environ.* **2008**, *405*, 301-309.
(242) Rao, B.; Anderson, T. A.; Redder, A.; Jackson, W. A. *Environ. Sci. Technol.* **2010**, *44*, 2961-2967.
(243) Rao, B.; Estrada, N.; McGee, S.; Mangold, J.; Gu, B.; Jackson, W. A. *Environ. Sci. Technol.*, *46*, 11635-11643.
(244) Kitaura, K.; Morokuma, K. *Int. J. Quantum Chem.* **1976**, *10*, 325-340.